Doctoral Dissertation
博士論文

Quantum metrology with superpositions of macroscopically distinct states

(マクロに異なる量子状態の重ね合わせを用いた量子計測)

A Dissertation Submitted for the Degree of Doctor of Philosophy
December 2019
令和元年 12 月博士（理学）申請

Department of Physics, Graduate School of Science, The University of Tokyo
東京大学理学系研究科物理学専攻

Mamiko TATSUTA

龍田真美子

Abstract

In this thesis, a general relationship between the sensitivity in quantum metrology and a superposition of macroscopically distinct states is shown. The goal of quantum metrology is to estimate a target parameter as precisely as possible by exploiting quantum systems. The uncertainty of the estimation is bound by the standard quantum limit for separable states, while quantum mechanics allows a better uncertainty that is bound by the Heisenberg limit. Both limits depend on the degrees of freedom N, e.g. number of spins, of the probe system, showing different scalings. How the uncertainty scales with N is an important factor for judging the utility of a given sensor.

We show that all the generalized cat states, superposition of macroscopically distinct states characterized by an index named q, achieve the ultimate scaling when used in quantum metrology. Index q identifies superposition of macroscopically distinct states by extracting the quantum coherence between macroscopically distinct states. The index can be used for both pure and mixed states, and even a mixed state with a small purity can be identified as a generalized cat state. We show that in the ideal case where noise is absent, every generalized state achieves the Heisenberg scaling uncertainty. Furthermore, we consider a realistic independent dephasing that generally degrades the performance of a sensor and show that generalized cat states still beat the standard quantum limit, achieving the ultimate scaling available in the presence of such dephasing. As an example, we discuss a generalized cat state with an exponentially small purity. We propose a theoretical recipe to generate such a state from a thermal equilibrium state. We numerically examine how much the sensitivity will be if this generalized cat state is realized in a silicon substrate and show that the state is indeed advantageous compared to a separable state sensor. A realistic protocol to create the state using a superconducting flux qubit and nitrogen-vacancy ensembles in diamond is also analyzed, and we numerically observe the emergence of a metrologically useful state. Revealing that a wide variety of states can be metrologically useful, this work broadens the potential application of quantum metrology.

Acknowledgements

I sincerely thank my advisor Professor Shimizu for discussions, advice, encouragements, and the photos of his cats. I thank the coauthor of [1], Yuichiro Matsuzaki, very much for bright ideas and all the care. I also thank other students in the lab. I would also like to dedicate my sincere gratitude to members of Coro Letizia, the female choir of the University of Tokyo, for providing me all the joy through my nine years in the university. I thank my family for always supporting me. I thank my fiance Ryusuke Hamazaki for all the help.

Publication list

This thesis is based on the following works.

- Quantum metrology with generalized cat states, Mamiko Tatsuta, Yuichiro Matsuzaki, and Akira Shimizu, Physical Review A **100**, 032318 Published 13 September 2019 [1]
- Conversion of thermal equilibrium states into superpositions of macroscopically distinct states, Mamiko Tatsuta and Akira Shimizu, Physical Review A **97**, 012124 Published 24 January 2018 [2]

Contents

Chapter 1

Introduction

1.1 Overview

Quantum metrology is one of the most major applications of quantum technology. It pursues high-precision measurement using quantum systems. Having theoretical roots in classical estimation theory, it was quantum-mechanically formulated by Helstrom and Holevo from late 1960's [3–5]. Among various sensors such as electric field sensors [6] and thermometers [7], application of magnetic field sensors is particularly wide. In medical sites, the technology of magnetic resonance imaging (MRI) plays a crucial role in diagnosing disease and injury. Thanks to the superconducting quantum interference device (SQUID) [8], magnetoencephalography [9], the imaging of the activity of brain by measuring the magnetic field within, is possible nowadays. In geology, sensitive magnetic field is necessary for paleomagnetism [10], a study of the Earth's magnetic field billions of years ago encoded in ancient rocks. And of course, sensitive magnetic field sensor is essential in fundamental studies of physics [11, 12]. To obtain better sensitivity with better spatial resolution, numbers of works have been devoted [13–30]. Among numerous types of magnetometers [31–33], a qubit-based sensing with Ramsey-type protocol is popular as done in, for example, atomic magnetometers [34–36], a superconducting flux qubit [37, 38] or nitrogen-vacancy (NV) centers [39–42]. In this thesis we consider such magnetometers.

It is known that quantum superposition states greatly enhance the sensitivity in quantum metrology. For example, through Ramsey-type sensing, the renowned Greenberger-Horne-Zeilinger (GHZ) state, i.e., a superposition of all up state and all down state in a spin-$1/2$ system,

$$|\mathrm{GHZ}\rangle = \frac{1}{\sqrt{2}}|\uparrow\rangle^{\otimes N} + \frac{1}{\sqrt{2}}|\downarrow\rangle^{\otimes N}, \tag{1.1}$$

is known to achieve the ultimate sensitivity bound by quantum mechanics. The ultimate sensitivity

bound by quantum mechanics is called Heisenberg scaling, while classical sensors and quantum sensors using separable states are bound by the standard quantum limit. Since the GHZ state, the representative of Schrödinger's cat state, which is more precisely a superposition of macroscopically distinct states, enhances the sensitivity, it is likely that more general types of superpositions of macroscopically distinct states show advantageous sensitivity if used as a sensor. However, it was not generally known what type of superposition is useful, although several examples of metrologically useful states were investigated [16, 27].

Superposition of macroscopically distinct states, also known as Schrödinger's cat state, is a peculiar state quantum mechanics offers [43] and has attracted much attention [44–70] since its proposal by Schrödinger in 1930's. However, the term superposition of macroscopically distinct states has ambiguity. For example, consider a product state of an eigenstate of $\hat{\sigma}_x$, i.e., $|+\rangle^{\otimes N}$, where N is the number of spins. Even though it is no more than a polarized state, and thus does not show the sensitivity as good as the GHZ state, when we change the basis to the eigenstates of $\hat{\sigma}_z$, macroscopically different states $|\uparrow\rangle^{\otimes N}$ and $|\downarrow\rangle^{\otimes N}$ are superposed[1]. These two states are actually superposed with other macroscopically non-distinct states, and the weight of $|\uparrow\rangle^{\otimes N}$ and $|\downarrow\rangle^{\otimes N}$ are exponentially small, thus not functioning as a sensor as good as the GHZ state.

$$|+\rangle = \left(\frac{|\uparrow\rangle + |\downarrow\rangle}{\sqrt{2}}\right)^{\otimes N} \tag{1.2}$$

$$= \frac{1}{2^{N/2}}|\uparrow\rangle^{\otimes N} + \frac{1}{2^{N/2}}\sum_{i=1}^{N}(|\uparrow\rangle^{\otimes i-1}|\downarrow\rangle|\uparrow\rangle^{\otimes N-i} + |\downarrow\rangle^{\otimes i-1}|\uparrow\rangle|\downarrow\rangle^{\otimes N-i})$$

$$+ \frac{1}{2^{N/2}}\sum_{i=1}^{N}\sum_{j(\neq i)}\sigma_x^j(|\uparrow\rangle^{\otimes i-1}|\downarrow\rangle|\uparrow\rangle^{\otimes N-i} + |\downarrow\rangle^{\otimes i-1}|\uparrow\rangle|\downarrow\rangle^{\otimes N-i}) + \cdots + \frac{1}{2^{N/2}}|\downarrow\rangle^{\otimes N} \tag{1.3}$$

This example tells us that a quantum state being a superposition is just a matter of the choice of the local basis, and that the choice of local basis is important when discussing cat states that appear in the systems with large degrees of freedom. Another example accompanied with the ambiguity that is different from the choice of the basis is discussed in Chapter 3. To exclude such confusing cases and correctly detect cat states, some criteria were proposed [50, 53, 57, 71–74]. Among them, we use an index called q [50] for the following reason. While other criteria for cat states are for only, e.g., superposition of two states [72] or pure states [53] or defined from the viewpoint of applicational sense [57, 74], index q simply quantifies the coherence of macroscopically distinct states for both pure and mixed states. Surprisingly, q identifies quite a wide variety of states

[1] Throughout this thesis, we denote $|\uparrow\rangle$ and $|\downarrow\rangle$ as the eigenstates of $\hat{\sigma}_z$ with eigenvalues $+1$ and -1, respectively.

including a mixed state with exponentially low purity, which is counter-intuitive to be recognized as a cat state. If all the generalized cat states are proven to show high sensitivity, the possibility of quantum metrology will be greatly expanded.

In this thesis, we show that all the states with $q = 2$, i.e., superposition of macroscopically distinct states, show the sensitivity with the same scaling as the ultimate scaling. More specifically, we show the Heisenberg scaling when we use the states with $q = 2$ in the ideal case where there is no noise. Also, even when we consider a realistic noise, states with $q = 2$ can beat the standard quantum limit and achieves the ultimate scaling achieved by best quantum sensors. We also propose a theoretical recipe to generate a generalized cat state with exponentially low purity, which achieves the ultimate scaling sensitivity as well. We numerically estimate the sensitivity of such a generalized cat state if realized in a silicon substrate, and indeed see a better sensitivity than a separable state sensor. Finally, we discuss a realistic setup with a hybrid system of NV centers in diamond and a superconducting flux qubit, and numerically observe the emergence of a metrologically useful state. Proving that all the generalized cat states show improvement in the sensitivity and proposing a protocol to create one, this work offers a novel approach for high-precision measurements.

1.2 Organization of this thesis

This thesis is organized as follows. In Chapter 2, we review the quantum metrology, starting with the basic sensing protocol which we call Ramsey-type. We explain the classical and quantum limits of the sensitivity of sensors. An experimental method for quantum sensing is also presented exemplifying with the nitrogen-vacancy centers in diamond. In Chapter 3, we review the indices p and q that characterize the superpositions of macroscopically distinct states and introduce a term *generalized cat state* by using q. Examples of nontrivial generalized cat states are also given. In Chapter 4 and 5, we analyze how generalized cat states are useful in quantum metrology. In Chapter 4 we prove that generalized cat states can achieve the Heisenberg scaling, the ultimate scaling in the absence of noise. In Chapter 5 we consider realistic noise, i.e., independent dephasing. We prove that by considering non-Markovian dephasing, generalized cat states beat the classical limit. In Chapter 6 we show a recipe to generate a generalized cat state in finite temperature. A generalized cat state can be generated from a thermal equilibrium state by a single global projective measurement. We study its features such as it has exponentially low purity and discuss the sensitiv-

ity of the sensor using the generalized cat state. In Chapter 7 we discuss a possible physical system that could demonstrate the ideas discussed in Chapter 6. We consider NV centers, which has a long coherence time, coupled to a superconducting flux qubit. In this setup, a global measurement with high resolution required in the recipe in Chapter 6 is expected to be relatively easily implemented. We examine whether a metrologically useful state is obtainable by repetitive measurements by the flux qubit. In Chapter 8 we summarize the thesis.

Chapter 2

Review of quantum metrology

In this chapter we review quantum metrology, magnetic field sensing in particular. We especially focus on qubit-based magnetic field sensors, and explain the basic protocol and the limits of the sensitivity. To grasp the experimental intuition, magnetometry using nitrogen-vacancy (NV) centers is discussed. Brief reviews of other two kinds of sensitivity-record-competing magnetometers are also given.

For simplicity, we consider sensing a DC magnetic field. For AC magnetic field sensing, one needs to apply π pulse to the probe spins during the interaction with the target field. Otherwise the accumulated phase, which is encoded with the information of the target field, cancels out during the time evolution.

2.1 Ramsey interferometry

One of the most common sensing protocols is called Ramsey interferometry, in which a superposition state is used to acquire the information of the target parameter. The sensing protocol is the following in principle, corresponding to Fig. 2.1. In the rest of this thesis, we call the measurement protocol that is basically the same as this one as "Ramsey-type" sensing.

Step 1 Prepare probe spins in a state that is suitable for sensing, e.g. $(|\uparrow\rangle + |\downarrow\rangle)/\sqrt{2}$. (for more information, see table 2.1.)

Step 2 Let the probe spins evolve for time t_{int} in the presence of the target magnetic field. We assume the spins interact with the target field via the interaction Hamiltonian is described as

$$\hat{H}_0 = \omega \hat{M}_z = \omega \sum_{i=1}^{N} \hat{\sigma}_z, \tag{2.1}$$

where ω is the Zeeman frequency shift of the spins. Our aim is to estimate ω. Through time evolution, sensor spins acquire the phase that is dependent on the target parameter, e.g. $e^{-i\omega t_{\rm int}}$ for $|\uparrow\rangle$.

Step 3 Readout by, e.g., projecting to the initial state. The probability of the final state being equal to the initial state is $|\frac{\langle\uparrow|+\langle\downarrow|}{\sqrt{2}}\frac{e^{-i\omega t_{\rm int}}|\uparrow\rangle+e^{i\omega t_{\rm int}}|\downarrow\rangle}{\sqrt{2}}|^2=\cos^2(\omega t_{\rm int})$.

Step 4 Repeat the Steps 1 to 3 for $T/t_{\rm int}$ times, where T is the total measurement time.

We have assumed the time to perform the initialization and the readout can be made sufficiently short, i.e., much shorter than the interaction time $t_{\rm int}$ so the number of repetition can be considered as $T/t_{\rm int}$.

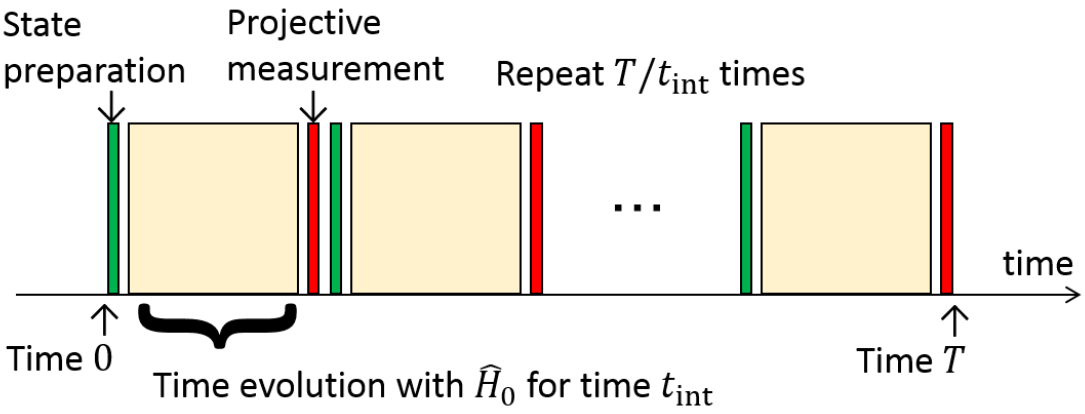

Figure 2.1: The basic protocol of the Ramsey-type sensing. In the green part, the sensor is initialized. In the yellow part, the sensor state evolves freely with time, accumulating the phase. In the red part, readout is done.

The sensitivity depends on what kind of states are prepared as the initial state. In Table 2.1, we take a separable state and the GHZ state as the initial state and compare the states of the sensor spins at each Step in the Ramsey-type protocol.

Procedure	Separable state (equivalent to using a single spin sensor for N times)	GHZ state
Step 1, initialization	For each spin, $\|\phi(t=0)\rangle := \frac{\|\uparrow\rangle+\|\downarrow\rangle}{\sqrt{2}}$	$\|\psi(0)\rangle := \frac{\|\uparrow\rangle^{\otimes N}+\|\downarrow\rangle^{\otimes N}}{\sqrt{2}}$
Step 2, time evolution	$\|\phi(t=t_{\rm int})\rangle = \frac{e^{-i\omega t_{\rm int}}\|\uparrow\rangle+e^{i\omega t_{\rm int}}\|\downarrow\rangle}{\sqrt{2}}$	$\|\psi(t=t_{\rm int})\rangle = \frac{e^{-i\omega N t_{\rm int}}\|\uparrow\rangle^{\otimes N}+e^{i\omega N t_{\rm int}}\|\downarrow\rangle^{\otimes N}}{\sqrt{2}}$
Step 3, readout	$\|\langle\phi(0)\|\phi(t_{\rm int})\rangle\|^2 = \cos^2(\omega t_{\rm int})$	$\|\langle\psi(0)\|\psi(t_{\rm int})\rangle\|^2 = \cos^2 N\omega t_{\rm int}$
Uncertainty	$\frac{1}{2\sqrt{N}t_{\rm int}}$ (for one spin, $\frac{1}{2t_{\rm int}}$)	$\frac{1}{2Nt_{\rm int}}$

Table 2.1: The flow of Ramsey interferometry with a separable state and the GHZ state with N spins. The uncertainty is for the case where $T/t_{\rm int} = 1$. For simplicity, we here consider the case where the readout process is extracting the probability of the final state being equal to the initial state. In practice, measurement of $\hat{\sigma}_y$ is often done for sensors with a single spin. Note that a sensor with N spins in a separable state is equivalent to using a sensor with a single spin for N times.

2.2 Sensitivity

Now we describe the uncertainty of the sensing protocol given above. The uncertainty $\delta\omega$ of the target parameter ω is

$$\delta\omega = \frac{\sqrt{P(1-P)}}{\left|\frac{dP}{d\omega}\right|}\frac{1}{\sqrt{T/t_{\rm int}}}, \tag{2.2}$$

where P denotes the probability that the projection described by $\hat{\mathscr{P}}$ occurs at the readout process. In this thesis we consider the case that the readout is done by a projective measurement. If the sensor state is initially $\hat{\rho}(t=0)$, then

$$P = {\rm Tr}(\hat{\rho}(t=t_{\rm int})\hat{\mathscr{P}}). \tag{2.3}$$

The numerator of $\delta\omega$ is the dispersion of P, and the denominator is the steepness of P as a function of ω. As depicted in Fig. 2.2, the uncertainty of ω depends on

$$\delta P = \frac{\sqrt{{\rm Tr}(\hat{\rho}(t_{\rm int})\hat{\mathscr{P}}^2) - [{\rm Tr}(\hat{\rho}(t_{\rm int})\hat{\mathscr{P}})]^2}}{\sqrt{T/t_{\rm int}}} \tag{2.4}$$

because of the error propagation formula. Note that the factor $\sqrt{T/t_{\rm int}}$ comes from the central limit theorem.

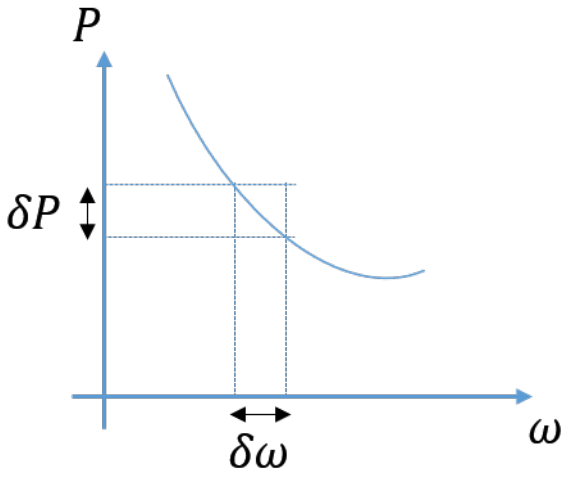

Figure 2.2: The schematic to intuitively see the relation between $\delta\omega$ and δP. The probability P depends on ω, and it has statistical fluctuation δP because of the finite number of measurements.

Note that in this thesis we use both the terms *sensitivity* and *uncertainty* to discuss how good the sensor is. Uncertainty is the inverse of the sensitivity. The smaller the uncertainty $\delta\omega$ is, the better sensor it is.

2.3 Standard quantum limit and Heisenberg limit

The uncertainties of the sensors are known to be bound by two limits: Standard quantum limit (SQL) and Heisenberg limit. The SQL is the best sensitivity achievable by classical sensors, and quantum sensors using separable states are also bound by the SQL. With a single readout measurement using N spins, the SQL is expressed as

$$\delta\omega \propto \frac{1}{\sqrt{N}}. \tag{2.5}$$

Some also call it as shot-noise limit.

Heisenberg limit is the ultimate sensitivity quantum states can offer. With a single readout measurement using N spins, the Heisenberg limit is expressed as

$$\delta\omega \propto \frac{1}{N}. \tag{2.6}$$

If more complex measurement protocols are adopted, other scalings may appear [75,76]. However, in the standard Ramsey-type sensing, this scaling is the ultimate. Since how $\delta\omega$ scales with N is important theoretically, we focus more on the $1/N$ part instead of the prefactors. To emphasize that we are looking at the scaling, we say a state achieves the Heisenberg scaling if $\delta\omega \propto 1/N$.

2.4 Magnetic field sensing with NV centers in diamond

Let us see how the Ramsey-type sensing is done in experiments by considering NV centers in diamond.

An NV center [40] has spin-1, i.e., $|0\rangle$ ($m_s = 0$ state) and $|\pm 1\rangle$ ($m_s = \pm 1$ state). When the external magnetic field is zero, $m_s = \pm 1$ states are degenerate, but $m_s = 0$ state and $m_s = \pm 1$ states are apart by about 2.87 GHz. To split the degenerate $m_s = \pm 1$ states and to set the NV's quantization axis, which we call z axis, a controllable magnetic field B_0 is applied (Fig. 2.3).

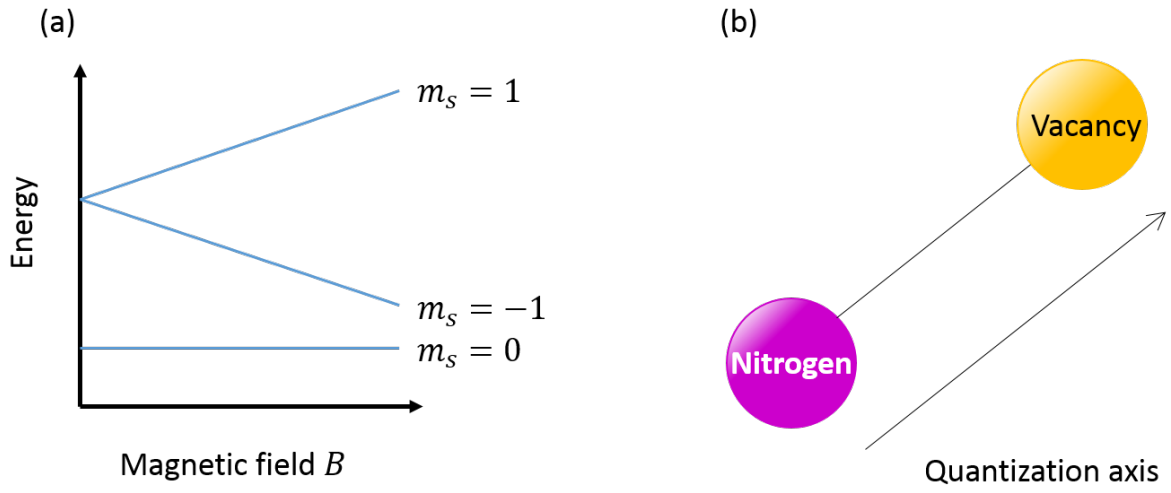

Figure 2.3: (a) Change of energy level (Zeeman splitting) of a NV center in the presence of magnetic field. (b) NV's quantization axis.

With a finite magnetic field B_0 along the NV's quantization axis, the energy of $|1\rangle$ state and $|-1\rangle$ state splits as (Zeeman effect)

$$g\mu_B B_0(|1\rangle\langle 1| - |-1\rangle\langle -1|), \tag{2.7}$$

where g is the g-factor and μ_B is the Bohr magneton. This energy change induced by the magnetic field is what is measured in NV magnetometry.

In a standard setup, magnetic field sensing using uncorrelated NV centers is done through either taking an electron spin resonance (ESR) spectroscopy or Ramsey pulse sequence. Here we focus on how Ramsey sequence is done. Since $|0\rangle$ state can be easily read out, the transitions involving the $|0\rangle$ state, i.e., either $|0\rangle \leftrightarrow |1\rangle$ or $|0\rangle \leftrightarrow |-1\rangle$, are often used through a microwave transition. Their resonance frequencies differ, therefore by correctly choosing the frequency of the microwave

to control the transition, NV spin can be considered as effectively spin-$1/2$. Here we exemplify with $|0\rangle \leftrightarrow |1\rangle$ case. In this section we define $\hat{s}_z := |1\rangle\langle 1| - |0\rangle\langle 0|$ and $\hat{s}_x := |1\rangle\langle 0| + |0\rangle\langle 1|$.

1. Initialization

   NV has a feature that it can be initialized to $|0\rangle$ state by applying green laser (532 nm) for sufficiently long time. Since all the NVs in the diamond will be initialized to $|0\rangle$, the initialization procedure is often called polarization. The prepared $|0\rangle$ state can be brought into a superposition state $(|0\rangle + |1\rangle)/\sqrt{2}$ by a microwave $\pi/2$ pulse. The appropriate microwave frequency and the pulse duration is determined by sweeping the frequency and measuring the Rabi nutation beforehand.

2. Phase accumulation

   The sum of the target unknown magnetic field B' and the known magnetic field B_0 will operate on NV as

   $$g\mu_{\mathrm{B}}(B_0 + B')\hat{s}_z =: g\mu_{\mathrm{B}}B\hat{s}_z. \tag{2.8}$$

   After the free evolution in the target magnetic field for time t_{int}, the state becomes $(|0\rangle + e^{-ig\mu_{\mathrm{B}}Bt_{\mathrm{int}}}|1\rangle)/\sqrt{2}$.

3. Readout

   To read out, another $\pi/2$ is applied so the state becomes

   $$\frac{1 + e^{-ig\mu_{\mathrm{B}}Bt_{\mathrm{int}}}}{2}|0\rangle + \frac{1 - e^{-ig\mu_{\mathrm{B}}Bt_{\mathrm{int}}}}{2}|1\rangle. \tag{2.9}$$

   Finally, the same green laser is applied to see the population in $|0\rangle$ state. The NVs in $|0\rangle$ state emit photons when the laser is applied. Hence by recording the fluorescence at the initialization, the population in $|0\rangle$ state at the readout gives the fluorescence contrast which is theoretically $\cos^2(g\mu_{\mathrm{B}}Bt_{\mathrm{int}}/2)$. Hence B can be estimated.

The smallest uncertainty achieved by NV ensembles is $150\mathrm{fT}/\sqrt{\mathrm{Hz}}$ with the spatial resolution $100\mu\mathrm{m}$ [39], at the time of writing this thesis. Note that the spatial resolution means the size within which the sensor can distinguish the existence of the signal. An example is shown in Fig. 2.4.

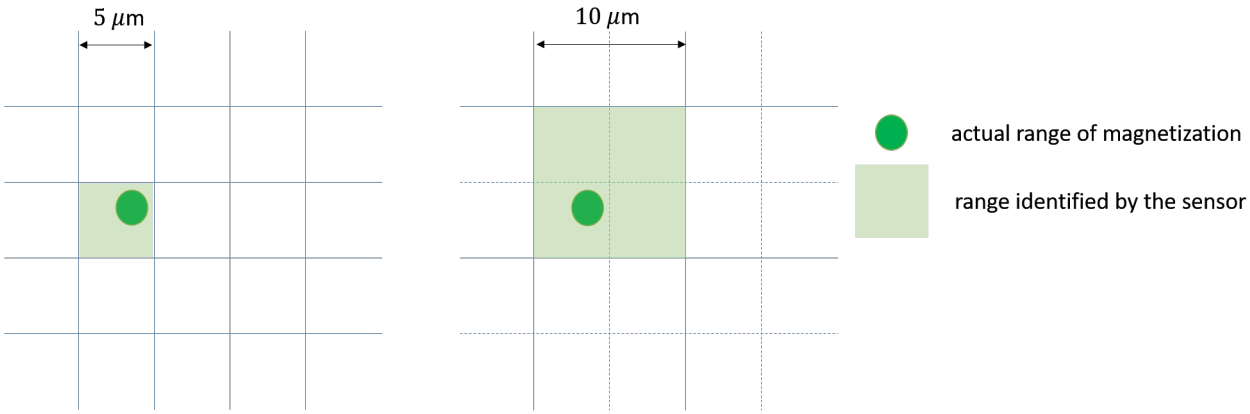

Figure 2.4: Schematic explanation of spatial resolution. Suppose that the dark green dot is the actual range of magnetic field. A magnetometer with 5μm spatial resolution can determine the location of the magnetic field in the accuracy of the bright green range of the left figure. If the spatial resolution is 10μm, the bright green box is larger, meaning the location is less accurately determined, as depicted in the right figure.

The smaller the spatial resolution is, the more details we can find. For instance, detection of the magnetization of a single spin requires high spatial resolution in addition to high sensitivity.

2.5 Various sensors

There are other types of magnetic field sensors [31–33, 36, 77]. The following two have especially high sensitivity.

2.5.1 SQUID

The superconducting quantum interference device (SQUID) is a superconducting loop with Josephson junctions. It is sensitive to the magnetic flux penetrating the loop, hence it can be used as a magnetic field sensor.

Here is the best sensitivity that has been achieved with SQUID at the time of writing this thesis, with the spatial resolution and the temperature of the system as follows [77].

- Sensitivity: 270 fT/$\sqrt{\text{Hz}}$
- Spatial resolution: 6.3×10^{-8} cm^2
- Temperature: 290 mK

Also, as we will see later, a similar superconducting loop can be regarded as a qubit system by considering the clockwise and counter-clockwise current states as the two degrees of freedom. It is called superconducting flux qubit and is also a useful, i.e., sensitive and easy to control, magnetometer.

2.5.2 SERF

A spin-exchange relaxation free (SERF) magnetometer is one of the optically-pumped atomic magnetometers operating at high temperature (the probe cell needs to be heated about 200°C) and low magnetic field [35, 36, 78]. In a glass cell, which works as the probe, potassium gas is enclosed. The initialization and the readout is done optically. The key feature of this sensor is that the spin exchange relaxation is suppressed by making the density of the potassium gas sufficiently low and operating in weak magnetic field. Suppression of spin exchange relaxation implies the long coherence time, making it possible to do the measurement for a long time, resulting in high sensitivity.

Here is the best sensitivity that has been achieved at the time of writing this thesis, with the spatial resolution and the temperature of the system as follows.

- Sensitivity: 160 aT/$\sqrt{\text{Hz}}$
- Spatial resolution: 0.45 cm^3
- Temperature: up to 420°C

Chapter 3

Generalized cat state

In this chapter, we introduce the notion "generalized cat state." It is a superposition of macroscopically distinct states characterized by the index named q [50]. We first clarify what macroscopically distinct states are, and review the indices p and q. The former characterizes superposition of macroscopically distinct states for pure states, and the latter covers both pure and mixed states. We take a look at some examples to see how these criteria are important.

3.1 Motivation

Quantum physics allows two or more states to be superposed for microscopic systems, and in 1935 Schrödinger raised a question whether superposition can occur in a macroscopic scale. This famous paradox of Schrödinger's cat has been an intriguing topic since then. In spin systems, the following state is recognized as a "cat" state.

$$\frac{1}{\sqrt{2}}|\uparrow\rangle^{\otimes N}+\frac{1}{\sqrt{2}}|\downarrow\rangle^{\otimes N}, \tag{3.1}$$

This is called the Greenberger-Horne-Zeilinger (GHZ) state. It is obviously a superposition of macroscopically distinct states when $N \gg 1$, for $|\uparrow\rangle^{\otimes N}$ having $+N$ magnetization and $|\downarrow\rangle^{\otimes N}$ having $-N$ magnetization along z axis. Fundamental interest and possible application to quantum technology such as computation [79–87] and metrology [11, 12, 88–92] have driven the intense research of the GHZ state, and it is realized with up to 18 spins [93].

However, the GHZ state is not the only state worthwhile to be called a cat state. For example, no one doubts the following being a superposition of macroscopically distinct states, i.e., a cat

state.

$$\frac{1}{\sqrt{2}}|\downarrow\rangle|\uparrow\rangle^{\otimes N-1}+\frac{1}{\sqrt{2}}|\uparrow\rangle|\downarrow\rangle^{\otimes N-1} \tag{3.2}$$

We expect there are countless kinds of cat-like states. However, we must also note that the notion "superposition of macroscopically distinct states" is ambiguous. For instance, is this a cat state?

$$|biased\rangle=\sqrt{\frac{1}{N}}|\uparrow\rangle^{\otimes N}+\sqrt{1-\frac{1}{N}}|\downarrow\rangle^{\otimes N} \tag{3.3}$$

When we consider macroscopic N, i.e., $N\to\infty$, $|biased\rangle$ asymptotically becomes $|\downarrow\rangle^{\otimes N}$, which is no longer a superposition of $\hat{M}_z=+N$ state and $\hat{M}_z=-N$ state. To distinguish these confusing non-cat states, we need a criterion. Below we consider two criteria: index p and index q. The former is for pure states, and the latter is for mixed states. Using q, we define the term "generalized cat state."

3.2 What is "macroscopically distinct states?"

Let us first clarify what "macroscopically distinct states" are. It is reasonable to consider two states as macroscopically distinct if they have macroscopically different values of some "macroscopic observable." Two states $|state1\rangle$ and $|state2\rangle$ are macroscopically distinct states if $\hat{A}$ is a macroscopic observable and

$$|\langle state1|\hat{A}|state1\rangle-\langle state2|\hat{A}|state2\rangle|=\text{macroscopic}. \tag{3.4}$$

According to thermodynamics and statistical mechanics, additive observables are macroscopic observables [94]. Here, additive observable $\hat{A}$ is the sum of local observables $\hat{a}(i)$, where i labels the components, e.g. spins:

$$\hat{A}=\sum_{i=1}^{N}\hat{a}(i), \tag{3.5}$$

where N is the degrees of freedom such as number of spins. The precise expression of the local observable $\hat{a}(i)$ is

$$\hat{1}^{\otimes i-1}\otimes\hat{a}(i)\otimes\hat{1}^{\otimes N-i}, \tag{3.6}$$

and we assume this $\hat{a}(i)$ in the direct product does not depend on N. Throughout this thesis, we assume N to be large, i.e., macroscopic, but finite. Therefore, $|state1\rangle$ and $|state2\rangle$ are macroscopically distinct if

$$|\langle state1|\hat{A}|state1\rangle - \langle state2|\hat{A}|state2\rangle| = \Theta(N) \tag{3.7}$$

for an additive observable $\hat{A}$. For example, $|\uparrow^{\otimes N}\rangle$ and $|\downarrow^{\otimes N}\rangle$ are macroscopically distinct because

$$|\langle\uparrow^{\otimes N}|\hat{M}_z|\uparrow^{\otimes N}\rangle - \langle\downarrow^{\otimes N}|\hat{M}_z|\downarrow^{\otimes N}\rangle| = 2N, \tag{3.8}$$

where $\hat{M}_z = \sum_{i=1}^{N}\hat{\sigma}_z(i)$ and $\hat{\sigma}_z(i)$ operates on ith spin. We also assume

$$\|\hat{a}(i)\| = \Theta(1), \tag{3.9}$$

hence

$$\|\hat{A}\| = \Theta(N) \tag{3.10}$$

throughout this thesis, where $\|\hat{O}\|$ denotes an operator norm of $\hat{O}$.

Note that for a function f of N, we say

$$f = \Theta(N^k) \tag{3.11}$$

if

$$\frac{f}{N^k} \to \text{constant} > 0 \quad (N \to \infty). \tag{3.12}$$

If $f = \Theta(N^k)$ then $f = O(N^k)$, but the inverse is not necessarily true.

3.3 Index p

For pure states, the index p can correctly detect the superposition of macroscopically distinct states. It is defined as follows.

Definition:
For a pure state ψ, p is defined as

$$\max_{\hat{A}} \langle\psi|(\Delta\hat{A})^2|\psi\rangle = \Theta(N^p), \tag{3.13}$$

where $\Delta\hat{A} = \hat{A} - \langle\psi|\hat{A}|\psi\rangle$.

Ref. [53] indicates that if $p = 2$, then $|\psi\rangle$ is a superposition of macroscopically distinct states. In

other words, if $|\psi\rangle$ contains only macroscopically non-distinct states, the fluctuation $\hat{A} - \langle\psi|\hat{A}|\psi\rangle$ is not large, i.e., merely $o(N^2)$. Note that the index p has a property that $1 \leq p \leq 2$. The maximum $p = 2$ means anomalously large fluctuation. The same idea is discussed in other works as well [57, 73].

Good thing about the index p is that it is directly related to the stability against noises and measurements [45]. It is indicated to be necessary for speedup of quantum computation [85]. Also, it is efficiently calculable through variance-covariance method [53].

However, we cannot detect the existence of superposition of macroscopically distinct states in mixed states by using p. For example, the following mixture of $p = 2$ states is not a superposition of macroscopically distinct states.

$$\begin{aligned}&\frac{1}{2}\left(\frac{|\uparrow\rangle^{\otimes N} + |\downarrow\rangle^{\otimes N}}{\sqrt{2}}\right)\left(\frac{\langle\uparrow|^{\otimes N} + \langle\downarrow|^{\otimes N}}{\sqrt{2}}\right) + \frac{1}{2}\left(\frac{|\uparrow\rangle^{\otimes N} - |\downarrow\rangle^{\otimes N}}{\sqrt{2}}\right)\left(\frac{\langle\uparrow|^{\otimes N} - \langle\downarrow|^{\otimes N}}{\sqrt{2}}\right)\\ &= \frac{1}{2}\left(|\uparrow\rangle^{\otimes N}\langle\uparrow|^{\otimes N} + |\downarrow\rangle^{\otimes N}\langle\downarrow|^{\otimes N}\right)\end{aligned} \tag{3.14}$$

The fluctuation of $\hat{M}_z$ of this state is N^2, but it is obviously no more than a classical mixture.

3.4 Index q

3.4.1 Definition

To detect superpositions of macroscopically distinct states in mixed states, we introduce the index q. It is defined as follows.

Definition:
For a density matrix $\hat{\rho}$, q is defined as

$$\max\left\{\max_{\hat{A},\hat{\eta}} \mathrm{Tr}\left[\hat{\rho}\hat{C}_{\hat{A}\hat{\eta}}\right], N\right\} = \Theta(N^q), \tag{3.15}$$

where

$$\hat{C}_{\hat{A}\hat{\eta}} = [\hat{A}, [\hat{A}, \hat{\eta}]]. \tag{3.16}$$

$\hat{A}$ is an additive observable and $\hat{\eta}$ is a projection operator.

Ref. [50] says if $q = 2$, then $\hat{\rho}$ contains superpositions of macroscopically distinct states with significant ratio. The outer maximization is to make $1 \leq q \leq 2$.

An intuitive reason why $q = 2$ means the existence of superpositions of macroscopically distinct states is as follows. Using the eigenvalue and the eigenstate of $\hat{A}$, i.e.,

$$\hat{A}\,|A,\nu\rangle = A\,|A,\nu\rangle\,, \tag{3.17}$$

where ν labels the degeneracy, we have

$$\mathrm{Tr}(\hat{\rho}\hat{C}_{\hat{A}\hat{\eta}}) = \sum_{A,\nu}\langle A,\nu|\hat{\rho}\sum_{A,\nu}|A',\nu'\rangle\,\langle A',\nu'|\,(\hat{A}^2\hat{\eta} - 2\hat{A}\hat{\eta}\hat{A} + \hat{\eta}\hat{A}^2)|A,\nu\rangle \tag{3.18}$$

$$= \sum_{A,\nu,A',\nu'}(A-A')^2\,\langle A,\nu|\hat{\rho}|A',\nu'\rangle\,\langle A',\nu'|\hat{\eta}|A,\nu\rangle\,. \tag{3.19}$$

The three factors $\langle A,\nu|\hat{\rho}|A',\nu'\rangle$, $(A-A')^2$ and $\langle A',\nu'|\hat{\eta}|A,\nu\rangle\,(\leq 1)$ in the summand in (3.19) cooperate well to detect the superposition of macroscopically distinct states. The term $\langle A,\nu|\hat{\rho}|A',\nu'\rangle$ is the quantum coherence between $|A,\nu\rangle$ and $|A',\nu'\rangle$, something we expect cats to have nonvanishing values for $|A-A|' = \Theta(N)$. The term $(A-A')^2$ provides a large weight to the coherence terms of macroscopically distinct states. Since we maximize with $\hat{\eta}$, we can regard the term $\langle A',\nu'|\hat{\eta}|A,\nu\rangle\,(\leq 1)$ as an adjuster of the signs of the important coherent terms. Therefore we can see that if $\hat{\rho}$ has $q = 2$, then there are significant quantity of $\langle A,\nu|\hat{\rho}|A',\nu'\rangle$ with $(A-A')^2 = \Theta(N^2)$.

To support the above explanation, let us consider the GHZ state. The density operator of the GHZ state has the form

$$|\mathrm{GHZ}\rangle\,\langle\mathrm{GHZ}| = \begin{pmatrix} 1/2 & 0 & \cdots & 0 & 1/2 \\ 0 & 0 & & & 0 \\ \vdots & & \ddots & & \vdots \\ 0 & & & 0 & 0 \\ 1/2 & 0 & \cdots & 0 & 1/2 \end{pmatrix} \tag{3.20}$$

with nonzero elements in every corner of the matrix. In this case, one of the coherence term $\langle A,\nu|\hat{\rho}|A',\nu'\rangle$ with macroscopic $A-A'$ is this:

$$\langle\downarrow|^{\otimes N}\,(|\mathrm{GHZ}\rangle\,\langle\mathrm{GHZ}|)\,|\uparrow\rangle^{\otimes N} = \begin{pmatrix} 0 \\ \vdots \\ 0 \\ 1 \end{pmatrix}^T \begin{pmatrix} 1/2 & 0 & \cdots & 0 & 1/2 \\ 0 & 0 & & & 0 \\ \vdots & & \ddots & & \vdots \\ 0 & & & 0 & 0 \\ 1/2 & 0 & \cdots & 0 & 1/2 \end{pmatrix} \begin{pmatrix} 1 \\ 0 \\ \vdots \\ 0 \end{pmatrix}$$

Another approach to understand the meaning of $\hat{\eta}$ is to consider a trace norm. For details, see Sec. 4.3.

3.4.2 Properties

Index q has several reasonable properties as follows.

1. Separable states have $q = 1$.

2. If $\hat{\rho}$ is pure, then

$$p = 2 \Leftrightarrow q = 2, \tag{3.21}$$

$$q = 1 \Rightarrow p = 1, \tag{3.22}$$

$$p = 1 \Rightarrow q \leq 1.5. \tag{3.23}$$

   An example of a pure state with $q = 1.5$ and $p = 1$ is $|biased\rangle$ in Sec. 3.1. For this state, we obtain $\max_{\hat{\eta}} \mathrm{Tr}(|biased\rangle \langle biased| [\hat{M}_z, [\hat{M}_z, \hat{\eta}]]) = 4N\sqrt{N-1}$ since $[\hat{M}_z, [\hat{M}_z, |biased\rangle \langle biased|]] = 4N\sqrt{N-1}(|\uparrow\rangle^{\otimes N} \langle\downarrow|^{\otimes N} + |\downarrow\rangle^{\otimes N} \langle\uparrow|^{\otimes N})$. The proof of $q \leq 1.5$ for arbitrary pure states with $p = 1$ are given in Appendix A.

3. Classical mixture can decrease q. An example is given in (3.14), that is,

$$\frac{1}{2}\left(\frac{|\uparrow\rangle^{\otimes N} + |\downarrow\rangle^{\otimes N}}{\sqrt{2}}\right)\left(\frac{\langle\uparrow|^{\otimes N} + \langle\downarrow|^{\otimes N}}{\sqrt{2}}\right) + \frac{1}{2}\left(\frac{|\uparrow\rangle^{\otimes N} - |\downarrow\rangle^{\otimes N}}{\sqrt{2}}\right)\left(\frac{\langle\uparrow|^{\otimes N} - \langle\downarrow|^{\otimes N}}{\sqrt{2}}\right)$$
$$= \frac{1}{2}\left(|\uparrow\rangle^{\otimes N} \langle\uparrow|^{\otimes N} + |\downarrow\rangle^{\otimes N} \langle\downarrow|^{\otimes N}\right). \tag{3.24}$$

   Because of mixing, $q = 2$ states became a separable state with $q = 1$.

4. Classical mixture does not increase q. Suppose we can decompose $\hat{\rho}$ as

$$\hat{\rho} = \sum_i \lambda_i \hat{\rho}_i. \tag{3.25}$$

   Since

$$\max_{\hat{A},\hat{\eta}} \mathrm{Tr}\left(\hat{\rho}\hat{C}_{\hat{A},\hat{\eta}}\right) \leq \sum_i \lambda_i \max_{\hat{A}_i,\hat{\eta}_i} \mathrm{Tr}\left(\hat{\rho}_i \hat{C}_{\hat{A}_i,\hat{\eta}_i}\right), \tag{3.26}$$

   we find that the state $\hat{\rho}_i$'s q, which we denote as q_i, satisfies

$$q \leq \max_i \{q_i\}. \tag{3.27}$$

5. If $\hat{\rho}$ has $q = 2$, then in every decomposition there exists a state(s) with $q = 2$. That is, when

$$\hat{\rho} = \sum_i \lambda_i \hat{\rho}_i = \sum_i \lambda_i' \hat{\rho}_i' = \cdots, \tag{3.28}$$

where $0 \leq \lambda_i \leq 1$ and $\sum_i \lambda_i = 1$ and similarly for λ_i', then there exists a state with $q = 2$ in each of $\{\hat{\rho}_i\}_i$, $\{\hat{\rho}_i'\}_i$, $\cdots$.

6. If $\hat{\rho}$ has $q = 2$, there exists a pure state(s) with $p = 2$ in every *pure-states* decomposition. That is, when

$$\hat{\rho} = \sum_i \lambda_i |\psi_i\rangle\langle\psi_i| = \sum_i \lambda_i' |\psi_i'\rangle\langle\psi_i'| = \cdots, \tag{3.29}$$

where $0 \leq \lambda_i \leq 1$ and $\sum_i \lambda_i = 1$ and similarly for λ_i', then there exists a pure state with $p = 2$ in each of $\{|\psi_i\rangle\}_i$, $\{|\psi_i'\rangle\}_i$, $\cdots$. Here, the pure states in the decomposition are not necessarily orthogonal to each other, e.g., we do *not* assume $\langle\psi_i|\psi_j\rangle = 0$ for $i \neq j$.

7. If $\hat{\rho}$ has $q = 2$, then in every pure-state decomposition pure states with $p = 2$ should be contained with a significant weight, i.e.,

$$\sum_{i \,\in\, p=2} \lambda_i = \Theta(1).$$

This is a *necessary* condition for $q = 2$.

8. A *sufficient* condition for $q = 2$ is as follows. For an additive operator $\hat{A}$, suppose that pure states $|\psi_1\rangle$, $|\psi_2\rangle$, $\cdots$ satisfy

$$\langle\psi_i|\psi_j\rangle = \delta_{i,j} \text{ for } i, j = 1, 2, \cdots, \tag{3.30}$$

$$\langle\psi_i|\hat{A}|\psi_j\rangle = 0 \text{ for } i \neq j, \tag{3.31}$$

$$\langle\psi_i|(\Delta_i\hat{A})^2|\psi_i\rangle = \Theta(N^2) \text{ for } i \leq \Lambda, \tag{3.32}$$

$$\langle\psi_i|(\Delta_i\hat{A})^2|\psi_i\rangle < \Theta(N^2) \text{ for } i > \Lambda, \tag{3.33}$$

where $\Delta_i\hat{A} \equiv \hat{A} - \langle\psi_i|\hat{A}|\psi_i\rangle$ and Λ is a positive integer. Consider a classical mixture of these states, $\hat{\rho} = \sum_i \lambda_i |\psi_i\rangle\langle\psi_i|$, where $0 \leq \lambda_i \leq 1$ and $\sum_i \lambda_i = 1$. If

$$\sum_{i \leq \Lambda} \lambda_i = \Theta(1), \tag{3.34}$$

then any such a mixture has $q = 2$.

Also, the superposition may be superposition of more than three states. For example, we can prove the following state has $q = 2$.

$$\frac{|\uparrow\uparrow\uparrow\cdots\uparrow\rangle + |\downarrow\uparrow\uparrow\cdots\uparrow\rangle + |\downarrow\downarrow\uparrow\cdots\uparrow\rangle + \cdots + |\downarrow\downarrow\downarrow\cdots\downarrow\rangle}{\sqrt{N+1}}. \tag{3.35}$$

Intuitively, it is a superposition of states with $M_z = \Theta(N)$ and $M_z = -\Theta(N)$.

3.5 Generalized cat state

We call a state $\hat{\rho}$ with $q = 2$ a generalized cat state. From the property 2, generalized cat state automatically includes both pure and mixed states.

If there exists an additive observable and a projection operator such that

$$\mathrm{Tr}(\hat{\rho}\hat{C}_{\hat{A},\hat{\eta}}) = \Theta(N^2), \tag{3.36}$$

then $q = 2$ is guaranteed. Let us call such $\hat{\rho}$ a *generalized cat state of* $\hat{A}$.

We also call $\max_{\hat{A},\hat{\eta}} \mathrm{Tr}(\hat{\rho}\hat{C}_{\hat{A},\hat{\eta}}) =: \langle C\rangle$ as "catness" in short. The coefficient of N^2 term in the catness quantifies how much cat is contained in a state. For example,

$$|\mathrm{GHZ}\rangle\langle\mathrm{GHZ}| \tag{3.37}$$

has $\langle C\rangle = 2N^2$ while

$$\frac{1}{2}|\mathrm{GHZ}\rangle\langle\mathrm{GHZ}| + \frac{1}{2}\frac{\hat{1}}{2^N} \tag{3.38}$$

has $\langle C\rangle = N^2$. We can see that there is more weight of the superpositions of macroscopically distinct states in the former than the latter. The larger the $\langle C\rangle / N^2$ is, the more weight the cat has.

3.6 Example

Let us give an interesting example of a mixed generalized cat state. Suppose $|k\rangle$ is a product state with k spins being $|\uparrow\rangle$ and $N-k$ spins being $|\downarrow\rangle$, and $|\bar{k}\rangle$ is a product state with k spins being $|\downarrow\rangle$ and $N-k$ spins being $|\uparrow\rangle$. (We do not care whether, e.g., $|k=1\rangle$ takes the configuration $|\uparrow\rangle|\downarrow\rangle^{\otimes N-1}$ or $|\downarrow\rangle|\uparrow\rangle|\downarrow\rangle^{\otimes N-2}$ or others.) Let us define their superposition as

$$|k\text{−}\mathrm{GHZ}\rangle := \frac{|k\rangle + |\bar{k}\rangle}{\sqrt{2}}.$$

For $k = 0$ and $k = N$, $|k{-}\mathrm{GHZ}\rangle$ is exactly the GHZ state, meaning $q = 2$. Undoubtedly, $|k{-}\mathrm{GHZ}\rangle$ with $k = 1$ or $k = 2$ or $k = 3$ should also have $q = 2$. For this $|k{-}\mathrm{GHZ}\rangle$, the following *mixture* also has $q = 2$:

$$\frac{3}{N}\sum_{k=1}^{N/3} |k{-}\mathrm{GHZ}\rangle\langle k{-}\mathrm{GHZ}| \tag{3.39}$$

What is interesting is that the weight of each $|k{-}\mathrm{GHZ}\rangle\langle k{-}\mathrm{GHZ}|$ is only $\Theta(1/N)$. (3.39) having $q = 2$ implies that a mixture of "similar cats" can have $q = 2$.

As can be seen, q identifies a wide variety of states as a "cat" state. Then the question is, are all the generalized cat states as useful as the GHZ state in metrology? In the upcoming Chapters 4 and 5, we answer this question.

3.7 Other criteria

For pure states, detection of cat states by a large fluctuation of an additive observable is considered in other contexts as well [57, 73].

For mixed states, other quantities are also considered to detect macroscopic quantumness, as reviewed in [71]. However, how they relate to q remained an open question, though q reasonably characterizes superposition of macroscopically distinct states by picking up the coherence.

As we will see later, there are advantages in considering q. First, it is quite reliable as a criterion for detecting a superposition of macroscopically distinct states. While other criteria attempts to characterize "macroscopic quantumness" instead of the superposition of macroscopically distinct states, what q quantifies is the coherence itself. Second, when we consider q, projection operators always come along. This directly connects to metrology, clarifying what kind of measurement is sufficient for obtaining the ultimate scaling sensitivity. Even for pure states that do not require q for just identifying a cat, q is more useful than p for this reason. Third, we can see the dynamical aspect because the index q is related to the equation of motion. This feature is especially significant when we consider a noisy environment.

Chapter 4

Heisenberg scaling sensitivity in the absence of noise

In this chapter, we discuss the sensitivity of a magnetic field sensor with generalized cat states in the absence of noise. We show that in such an ideal case, the sensitivity achieves the Heisenberg scaling. We also show how to derive the projection operator that lets us achieve the Heisenberg scaling for a given generalized cat state. Advantages of using q is also discussed by referring to the quantum Fisher information.

4.1 Overview

As we have seen in the previous two chapters, the sensitivity of quantum metrology is enhanced by using some special superposition states such as the GHZ state, and generalized cat states are superposition of macroscopically distinct states in various forms including mixed states with small purities. Though generalized cat states are defined quite reasonably, it is nontrivial whether all the states identified as generalized cat states are of use in metrology, since it covers a wide range of states. Answering this question will broaden the possibility of quantum metrology. To begin with, we consider the ideal case where there is no noise. In such a case the renowned GHZ state is known to achieve the Heisenberg scaling sensitivity. We will discuss whether the other generalized cat states can also achieve such a scaling.

4.2 Sensitivity of a magnetic field sensor with a generalized cat state

Since we are discussing the ideal case without noise, we may assume the Hamiltonian to be

$$\hat{H}_0(\omega) = \omega\hat{A}, \tag{4.1}$$

where ω is the Zeeman frequency shift that we want to estimate. For simplicity, we omit other terms in Hamiltonian even if present. Note that $\|\hat{A}\| = \Theta(N)$ because $\hat{A}$ is an additive observable, i.e., the sum of local spin operators. We consider using a generalized cat state $\hat{\rho}$ satisfying

$$\mathrm{Tr}(\hat{\rho}[\hat{A},[\hat{A},\hat{\eta}]) = \Theta(N^2). \tag{4.2}$$

to estimate ω.

Following the Ramsey-type protocol, we let $\hat{\rho}$ evolve for time t_{int} to obtain

$$\hat{\rho}(t_{\mathrm{int}}) = e^{-i\omega\hat{A}t}\hat{\rho}e^{i\omega\hat{A}t}. \tag{4.3}$$

To this $\hat{\rho}(t_{\mathrm{int}})$, we read out through a projection $\hat{\eta}$. Then the probability of the projection $\hat{\eta}$ being done is

$$P_0 = \mathrm{Tr}(\hat{\eta}e^{-i\omega\hat{A}t}\hat{\rho}e^{i\omega\hat{A}t}), \tag{4.4}$$

where the subscript "0" denotes the case where noise is absent. The uncertainty of ω measured by the generalized cat state $\hat{\rho}$ is

$$\delta\omega = \frac{\sqrt{P_0(1-P_0)}}{\left|\frac{dP_0}{d\omega}\right|}\frac{1}{\sqrt{T/t_{\mathrm{int}}}}. \tag{4.5}$$

Since P_0 does not exceed 1, $\delta\omega \leq \frac{1}{\left|\frac{dP_0}{d\omega}\right|}\frac{1}{\sqrt{T/t_{\mathrm{int}}}}$. Hence let us evaluate $\left|\frac{dP_0}{d\omega}\right|$.

Using the Baker-Hausdorff formula, we can easily show

$$\hat{\rho}(t_{\mathrm{int}}) = e^{-i\omega t_{\mathrm{int}}}\hat{\rho}e^{i\omega\hat{A}t_{\mathrm{int}}} = \sum_{k=0}^{\infty}\frac{(-i\omega\hat{A}t_{\mathrm{int}})^k}{k!}[\hat{A},\hat{\rho}]_k, \tag{4.6}$$

where

$$[\hat{A},\hat{\rho}]_{k+1} := [\hat{A},[\hat{A},\hat{\rho}]_k], \tag{4.7}$$

$$[\hat{A},\hat{\rho}]_0 := \hat{\rho}. \tag{4.8}$$

Using the cyclicity of the trace, we have

$$P_0 = \mathrm{Tr}\left(\hat{\rho}\sum_{k=0}^{\infty}\frac{(-i\omega t_{\mathrm{int}})^k}{k!}[\hat{A},\hat{\eta}]_k\right), \tag{4.9}$$

$$\frac{dP_0}{d\omega} = \mathrm{Tr}\left(\hat{\rho}\sum_{k=1}^{\infty}\frac{(-it_{\mathrm{int}})(-i\omega t_{\mathrm{int}})^{k-1}}{(k-1)!}[\hat{A},\hat{\eta}]_k\right). \tag{4.10}$$

Therefore,

$$\begin{aligned}\left|\frac{dP_0}{d\omega}\right| \geq \left|\left|\omega t_{\mathrm{int}}^2\mathrm{Tr}(\hat{\rho}[\hat{A},[\hat{A},\hat{\eta}]])\right| - \left|it_{\mathrm{int}}\mathrm{Tr}(\hat{\rho}[\hat{A},\hat{\eta}])\right|\right| \\ -2t_{\mathrm{int}}\|\hat{A}\|(e^{2\omega t_{\mathrm{int}}\|\hat{A}\|}-1-2\omega t_{\mathrm{int}}\|\hat{A}\|).\end{aligned} \tag{4.11}$$

4.2.1 Derivation of the Heisenberg scaling sensitivity

In the following, we show that with an appropriately-tuned $\omega t_{\mathrm{int}}N$, the right-hand side of (4.11) scales as $\Theta(N^{-1})$ and thus $\delta\omega$ achieves the Heisenberg scaling, when the initial state ρ is a generalized cat state satisfying (4.2). As we will discuss later, the parameter to be measured can be tuned to be in a certain required range by applying a known field corresponding to ω_0 in addition to the unknown ω. In the following we denote the total frequency $\omega+\omega_0$, which is appropriately tuned, simply as ω. Below we denote

$$x := \omega t_{\mathrm{int}}N. \tag{4.12}$$

First of all, we take

$$x = \Theta(N^0) \tag{4.13}$$

throughout this thesis. We will show that for appropriately tuned x, the following holds.

$$\begin{aligned}f :&= \left|\left|\frac{xt_{\mathrm{int}}}{N}\mathrm{Tr}(\hat{\rho}[\hat{A},[\hat{A},\hat{\eta}]])\right| - \left|it_{\mathrm{int}}\mathrm{Tr}(\hat{\rho}[\hat{A},\hat{\eta}])\right|\right| - 2t_{\mathrm{int}}\|\hat{A}\|(e^{2x\frac{\|\hat{A}\|}{N}}-1-2x\frac{\|\hat{A}\|}{N}) && (4.14)\\ &\geq \Theta(x^2t_{\mathrm{int}}N). && (4.15)\end{aligned}$$

To make it easier to see, we denote

$$v_1 := \frac{1}{N}\left|\mathrm{Tr}(\hat{\rho}[\hat{A},\hat{\eta}])\right|, \tag{4.16}$$

$$v_2 := \frac{1}{N^2}\left|\mathrm{Tr}(\hat{\rho}[\hat{A},[\hat{A},\hat{\eta}]])\right|, \tag{4.17}$$

$$f_1 := |xt_{\mathrm{int}}Nv_2 - t_{\mathrm{int}}Nv_1|, \tag{4.18}$$

$$f_2 := 2t_{\mathrm{int}}\|\hat{A}\|(e^{2x\frac{\|\hat{A}\|}{N}}-1-2x\frac{\|\hat{A}\|}{N}). \tag{4.19}$$

Hence

$$f = f_1 - f_2. \tag{4.20}$$

For a given set of $\{\hat{\rho}, \hat{A}, \hat{\eta}\}$, which gives (4.2), we can arbitrarily take a positive constant k_1 such that

$$k_1 \leq \frac{v_2}{2}. \tag{4.21}$$

We also take another positive constant k_2 as follows. First, take an arbitrary positive N-independent value c. Then we define a positive c-dependent value k_c as

$$k_c := \frac{2\|\hat{A}\|(e^{2c\frac{\|\hat{A}\|}{N}} - 1 - 2c\frac{\|\hat{A}\|}{N})}{Nc^2}. \tag{4.22}$$

We vary c to maximize $\min(c, \frac{k_1}{2k_c})$ and take k_2 as

$$k_2 := \max_c \min(c, \frac{k_1}{2k_c}). \tag{4.23}$$

We fix c as the value that maximizes $\min(c, \frac{k_1}{2k_c})$[1]. Since

$$h(x) := \frac{2\|\hat{A}\|(e^{2\frac{\|\hat{A}\|}{N}x} - 1 - 2\frac{\|\hat{A}\|}{N}x)}{Nx^2} \tag{4.24}$$

is an increasing function of x, for $x \leq c$, $h(x) \leq h(c)$. Hence for all x that satisfies $x \leq k_2$, the inequality

$$f_2 \leq k_c t_{\rm int} N x^2 \tag{4.25}$$

holds. Using k_2 to determine the appropriate range of x, we can show (4.15) as follows.

If $2v_1/v_2 \leq k_2$, then we tune x to satisfy

$$\frac{2v_1}{v_2} \leq x \leq k_2. \tag{4.26}$$

Since $x \geq \frac{2v_1}{v_2}$, we have

$$\begin{aligned} f_1 &= x t_{\rm int} N v_2 - t_{\rm int} N v_1 && (4.27)\\ &\geq t_{\rm int} N (x v_2 - \frac{x v_2}{2}) && (4.28)\\ &= \frac{1}{2} x t_{\rm int} N v_2 && (4.29)\\ &\geq k_1 x t_{\rm int} N. && (4.30) \end{aligned}$$

[1]The reason we maximized with c is to make the range of x wide. The derivation of the Heisenberg scaling does not require the maximization. Hence, if maximization is difficult, one can arbitrarily fix c as $c' = \Theta(N^0)$ and take $k_2 = \min(c', \frac{k_1}{2k_{c'}})$.

Combining this with (4.20) and (4.25), we have

$$f \geq k_1 x \cdot t_{\text{int}} N - k_c x^2 t_{\text{int}} N = x t_{\text{int}} N (k_1 - k_c x). \tag{4.31}$$

Since $x \leq k_2 \leq \frac{k_1}{2k_c}$, i.e., $k_1 \geq 2k_c x$, we have

$$f \geq k_c x^2 t_{\text{int}} N, \tag{4.32}$$

proving (4.15). Hence (4.11) is bound as

$$\left| \frac{dP_0}{d\omega} \right| \geq f \geq k_c x^2 t_{\text{int}} N, \tag{4.33}$$

which gives us

$$\delta\omega \leq \frac{1}{k_c x^2 t_{\text{int}} N} \frac{1}{\sqrt{T/t_{\text{int}}}}. \tag{4.34}$$

Hence the Heisenberg scaling is obtained.

If $2v_1/v_2 > k_2$, then we tune x to satisfy

$$0 < x \leq \min(k_2, \frac{2v_1}{3v_2}). \tag{4.35}$$

Note that the lower bound $x > 0$ comes from the condition $x = \Theta(N^0)$. Since $x \leq \frac{2v_1}{3v_2}$, we obtain $f_1 = t_{\text{int}} N(v_1 - x v_2) \geq k_1 x t_{\text{int}} N$, the same bound as (4.30), from a similar calculation. Similarly with the case $2v_1/v_2 \leq k_2$, combining the bound of f_1 with (4.25), we obtain (4.31)-(4.34), which allows the Heisenberg scaling.

Therefore, generalized cat states can achieve the Heisenberg scaling sensitivity.

4.2.2 The order of ω and $\delta\omega$

To obtain the Heisenberg scaling $\delta\omega \propto N^{-1}$, the interaction time t_{int} needs to be $\Theta(N^0)$. Then the assumption $\omega t_{\text{int}} N = \Theta(N^0)$ requires $\omega = \Theta(N^{-1})$. Such ω is realizable by appropriately tuning ω_0 as indicated in the next subsection, but the following question rises: Is $\delta\omega = \Theta(N^{-1})$ significant when we already know $\omega = \Theta(N^{-1})$? To answer the question, we would first like to remark the following point: $\delta\omega \propto \omega$ is nothing special in actual sensors such as electric current testers. It is normal that a sensor with small $\delta\omega$ has a small range, i.e., can handle only smaller ω. All we need is $\delta\omega \ll \omega$, which is satisfied, e.g., when $\delta\omega = 1/N$ and $\omega = 100/N$.

This requirement $\delta\omega \ll \omega$ can always be achieved by means of taking T sufficiently long. The total measurement time T can be increased by simply increasing the number of repetition T/t_{int}.

Note that we assumed $\delta\omega_0 \ll \delta\omega$. Practically, $\delta\omega_0$ can be reduced as much as required, i.e., smaller than $\delta\omega$ of a given N, beforehand. For a given magnetic field generator, such as a magnet, one should measure its magnetic field strength $\propto \omega_0$ by using some magnetic field sensor repeatedly. Whatever the used magnetic field sensor is, $\delta\omega_0$ can be reduced as the the number of repetition is increased. Hence $\delta\omega_0$ can be made as small as we wish.

4.2.3 Discussion on the conditions of x

In the previous subsection, we obtained the Heisenberg scaling sensitivity by assuming that x is tuned in a certain range. Let us denote the range as $l \leq x \leq u$, for simplicity. In this subsection, we discuss how can this condition imposed on $x = \omega t_{\rm int} N$ be satisfied practically.

In many practical cases, we know that the target parameter ω is around zero[2] and has the absolute value smaller than a certain ω^*, i.e, $|\omega| \leq \omega^*$. Using this ω^*, we can clarify how to satisfy the conditions. A sensor normally has a dynamic range ω_r that restricts the measurable upper limit of the absolute value of the target parameter. As the sensitivity becomes better, the dynamic range usually becomes narrower for typical sensors. Hence it is important to appropriately set ω_r to obtain small enough $\delta\omega$. Since we are provided with ω^* such that $|\omega| \leq \omega^*$, we know we should take $\omega_r \geq \omega^*$ so the target ω is within the range. Here we take $\omega_r = \omega^*$. With such ω_r, the condition $l \leq x \leq u$ can be dealt with and thus the generalized cat state sensor can be fully exploited by tuning N and $t_{\rm int}$ as follows: First, tune $Nt_{\rm int}$ so that $u - l = 2\omega_r t_{\rm int} N$. Then, add a known field $\omega_0 = l + \omega_r t_{\rm int} N$. Then the total field $\omega_{\rm tot} = \omega_0 + \omega$ satisfies $l \leq \omega_{\rm tot} t_{\rm int} N \leq u$.

4.3 Calculation of the index q for fixed $\hat{A}$

As we have seen, states with $q = 2$ are useful in metrology. However, there is no general method to calculate the index q for a given mixed state $\hat{\rho}$. The difficulty lies in the maximization with both $\hat{\eta}$ and $\hat{A}$. However, once $\hat{A}$ is given, it is possible to choose $\hat{\eta}$ to maximize $\mathrm{Tr}(\hat{\rho}[\hat{A},[\hat{A},\hat{\eta}]])$. For this purpose, we need to find candidates of $\hat{A}$. Candidates of $\hat{A}$ can be found by, for example, maximizing the fluctuation $\mathrm{Tr}(\hat{\rho}(\Delta\hat{A})^2)$. Such maximization can be performed by the variance-covariance method [53].

[2]Or, we can add ω_0 and make $\omega_t = \omega + \omega_0$ to be around zero and measure ω_t.

For a fixed $\hat{A}$, the definition of the index q can be expressed differently as follows.

$$\Theta(N^q) = \max\{N, \max_{\hat{\eta}} \mathrm{Tr}\left(\hat{\rho}\left[\hat{A},\left[\hat{A},\hat{\eta}\right]\right]\right)\} \tag{4.36}$$

$$= \max\{N, \frac{1}{2}\|[\hat{A},[\hat{A},\hat{\rho}]]\|_1\} \tag{4.37}$$

Here, $\|\hat{X}\|_1$ is a trace norm:

$$\|\hat{X}\|_1 = \mathrm{Tr}(\sqrt{\hat{X}^\dagger \hat{X}}) \tag{4.38}$$

$$= \sum_n |e_n|, \tag{4.39}$$

$$\hat{X} = \sum_n e_n |n\rangle \langle n|. \tag{4.40}$$

This re-expression can be understood from the cyclicity of the trace

$$\mathrm{Tr}\left(\hat{\rho}\left[\hat{A},\left[\hat{A},\hat{\eta}\right]\right]\right)\} = \mathrm{Tr}\left(\hat{\eta}\left[\hat{A},\left[\hat{A},\hat{\rho}\right]\right]\right) \tag{4.41}$$

and the fact that

$$\mathrm{Tr}\left(\left[\hat{A},\left[\hat{A},\hat{\rho}\right]\right]\right) = 0. \tag{4.42}$$

Maximization of $\mathrm{Tr}\left(\hat{\eta}\left[\hat{A},\left[\hat{A},\hat{\rho}\right]\right]\right)$ requires $\hat{\eta}$ to be the projection onto the subspace spanned by the eigenstates of $\left[\hat{A},\left[\hat{A},\hat{\rho}\right]\right]$ with positive eigenvalues. That is the half of the trace norm because the total of the eigenvalues is zero in this case.

Since numerical methods to calculate the eigenvalues of a given observable are well established, this formula helps us to numerically calculate the index q.

In other words, we can construct the projection $\hat{\eta}$ that makes the given $\hat{\rho}$ achieve its best sensitivity by diagonalizing $[\hat{A},[\hat{A},\hat{\rho}]]$. The maximizing $\hat{\eta}$ is

$$\hat{\eta} = \sum_{e_n>0} |n\rangle \langle n|. \tag{4.43}$$

Note that in the context of quantum metrology, the observable $\hat{A}$ is often fixed for judging the utility of a given state. It is because quantum metrology aims to estimate the parameter associated with a certain fixed observable.

4.3.1 Example

Let us calculate the index q of a mixed state

$$\hat{\rho}_{ex} := \frac{1}{N}\sum_{\lambda=1}^{N} |\psi_\lambda\rangle \langle\psi_\lambda|, \tag{4.44}$$

where $|\psi_\lambda\rangle$ is a GHZ-like state differing by the λth spin:

$$|\psi_\lambda\rangle := \frac{1}{\sqrt{2}}|\downarrow\rangle^{\otimes(\lambda-1)}|\uparrow\rangle|\downarrow\rangle^{\otimes(N-\lambda)} + \frac{1}{\sqrt{2}}|\uparrow\rangle^{\otimes(\lambda-1)}|\downarrow\rangle|\uparrow\rangle^{\otimes(N-\lambda)} \quad (\lambda = 1,2,...,N) \tag{4.45}$$

For simplicity, use use the following notation.

$$|\Uparrow\rangle_\lambda := |\uparrow\rangle^{\otimes(\lambda-1)}|\downarrow\rangle|\uparrow\rangle^{\otimes(N-\lambda)}, \tag{4.46}$$

$$|\Downarrow\rangle_\lambda := |\downarrow\rangle^{\otimes(\lambda-1)}|\uparrow\rangle|\downarrow\rangle^{\otimes(N-\lambda)} \tag{4.47}$$

Since the GHZ state is a generalized cat state of $\hat{M}_z$, we can guess this $\hat{\rho}_{\rm ex}$ could also be a generalized cat state of $\hat{M}_z$. Therefore we take $\hat{A} = \hat{M}_z$ and see how $\|[\hat{M}_z,[\hat{M}_z,\hat{\rho}_{ex}]]\|_1$ scales. The eigenstates of $[\hat{M}_z,[\hat{M}_z,\hat{\rho}_{ex}]]$ are $|\psi_\lambda\rangle$'s, and the eigenvalues are all positive because

$$[\hat{M}_z,[\hat{M}_z,\hat{\rho}_{ex}]] = \hat{M}_z^2\hat{\rho}_{\rm ex} - 2\hat{M}_z\hat{\rho}_{\rm ex}\hat{M}_z + \hat{\rho}_{\rm ex}\hat{M}_z^2 \tag{4.48}$$

$$= 2(N-2)^2(\hat{\rho}_{\rm ex} - \overline{\hat{\rho}_{\rm ex}}), \tag{4.49}$$

$$= 2(N-2)^2\frac{1}{N}\sum_{\lambda=1}^{N}\left(|\Uparrow\rangle_\lambda\langle\Downarrow|_\lambda + |\Downarrow\rangle_\lambda\langle\Uparrow|_\lambda .\right), \tag{4.50}$$

where

$$\overline{\hat{\rho}_{ex}} := \frac{1}{N}\sum_{\lambda=1}^{N}|\overline{\psi_\lambda}\rangle\langle\overline{\psi_\lambda}|, \tag{4.51}$$

$$|\overline{\psi_\lambda}\rangle := \frac{1}{\sqrt{2}}(|\Uparrow\rangle_\lambda - |\Downarrow\rangle_\lambda) \quad (\lambda = 1,2,...,N). \tag{4.52}$$

Therefore,

$$\|[\hat{M}_z,[\hat{M}_z,\hat{\rho}_{ex}]]\|_1 = 2(N-2)^2\frac{1}{N}\times N = 2(N-2)^2 = \Theta(N^2), \tag{4.53}$$

providing $q = 2$. The maximizing $\hat{\eta}$ is derived as $N\hat{\rho}_{\rm ex}$. Hence the mixed state $\hat{\rho}_{ex}$ can achieve the ultimate scaling in measuring $\hat{M}_z$ with a projection $\hat{\eta} = N\hat{\rho}_{\rm ex}$ after Ramsey-type protocol.

4.4 Relation with the quantum Fisher information

In quantum metrology, the quantum Fisher information (QFI) is one of the most important quantity, for it gives the lower bound of the uncertainty. A famous Cramer-Rao bound

$$\delta\omega \geq \frac{1}{\sqrt{\rm QFI}} \tag{4.54}$$

holds regardless the details of the measurement. Since we have shown

$$\delta\omega \leq \Theta(N^{-1}) \tag{4.55}$$

for generalized cat states, we now know

$$\mathrm{QFI} \geq \Theta(N^2) \tag{4.56}$$

for generalized cat states.

From the reasoning that the improvement of the sensitivity over the SQL should be caused by the *macroscopic* quantum effect rather than the accumulation of microscopic quantum effects, the QFI is also considered as a measure of macroscopicity of quantum states [57]. The QFI of a quantum state $\hat{\rho} = \sum_{i=1}^{2^N} \pi_i |i\rangle\langle i|$ which is subjected to the time-independent Hamiltonian $\hat{H}$ is

$$\mathscr{F}(\hat{\rho}, \hat{H}) = 2 \sum_{i,j=1}^{2^N} \frac{(\pi_i - \pi_j)^2}{\pi_i + \pi_j} |\langle i|\hat{H}|j\rangle|^2, \tag{4.57}$$

where the sum is taken over only $\pi_i + \pi_j > 0$ terms. From the observations that separable states have $\mathscr{F} \leq 4N$ and the GHZ state has $\mathscr{F} \leq 4N^2$ for the Hamiltonian $\hat{H} = \sum_{i=1}^{N} \hat{h}(i)$ with $\|\hat{h}(i)\| = 1$, Fröwis and Dür proposed the QFI as a measure of macroscopicity.

For a pure state $|\psi\rangle\langle\psi|$, the QFI becomes

$$\begin{aligned}
\mathscr{F}(|\psi\rangle\langle\psi|, \hat{H}) &= 2 \sum_i \left(\sum_{j(\neq i)} \frac{(\pi_i - \pi_j)^2}{\pi_i + \pi_j} |\langle i|\hat{H}|j\rangle|^2 + \sum_{j=i} \frac{(\pi_i - \pi_i)^2}{\pi_i + \pi_i} |\langle i|\hat{H}|i\rangle|^2 \right) && (4.58) \\
&= 2 \left(\sum_{j(\neq\psi)} \frac{(1-0)^2}{1+0} |\langle\psi|\hat{H}|j\rangle|^2 + \sum_{i(\neq\psi)} \sum_{j(\neq i)} \frac{(0-\pi_j)^2}{0+\pi_j} |\langle i|\hat{H}|i\rangle|^2 \right) && (4.59) \\
&= 2 \left(\sum_j |\langle\psi|\hat{H}|j\rangle|^2 - |\langle\psi|\hat{H}|\psi\rangle|^2 + \sum_{i(\neq\psi)} \frac{(0-1)^2}{0+1} |\langle i|\hat{H}|\psi\rangle|^2 \right) && (4.60) \\
&= 4(\langle\psi|\hat{H}^2|\psi\rangle - \langle\psi|\hat{H}|\psi\rangle^2), && (4.61)
\end{aligned}$$

coinciding with the four times of the energy fluctuation

$$\langle\psi|(\Delta\hat{H})^2|\psi\rangle\,. \tag{4.62}$$

For pure states, $\|[\hat{H}, [\hat{H}, |\psi\rangle\langle\psi|]]\|_1 \geq 2\langle\psi|(\Delta\hat{H})^2|\psi\rangle$. Hence the relation between q and the QFI is clear even though they are defined from different aspects of physics.

However, the relation of these two measures was an open question for mixed states. It means the characterization of quantum macroscopicity could still have ambiguity. So, clarifying the relation (4.56) for generalized cat states has some significance.

In addition, there are clear advantages in considering generalized cat states. As summarized in Table (4.1), the QFI provides the lower bound of the uncertainty $\delta\omega$, i.e., $\delta\omega \geq 1/\sqrt{\mathrm{QFI}}$; the Cramer-Rao inequality. Although the equality is satisfied by *some* optimal POVM measurement, such a measurement is generally unknown for mixed states, and even if it is somehow found, it could be very complicated. Hence, practically, the QFI gives $\delta\omega > 1/\sqrt{\mathrm{QFI}}$, which does not ensure the ultimate scaling even when QFI$=\Theta(N^2)$.

On the other hand, generalized cat states guarantee the ultimate scalings, $\delta\omega \leq 1/\Theta(N)$ (or $\delta\omega \leq 1/\Theta(N^{3/4})$ in the presence of noise, as we will see in next chapter), providing the upper bound. This inequality is satisfied by a known simple measurement: Ramsey-type protocol and reading out with the projection $\hat{\eta}$ which we know. That is, the way of achieving the ultimate scaling sensitivity is explicitly given.

Quantum Fisher Information	Generalized Cat State
$\delta\omega \geq \frac{1}{\sqrt{\mathrm{QFI}}}$	$\delta\omega \leq \frac{1}{\Theta(N)}$
equality achieved by some unknown POVM	equality achieved with a known measurement
the POVM could be complicated	a simple Ramsey-type protocol can be used

Table 4.1: Comparison between QFI and generalized cat state.

Chapter 5

The ultimate sensitivity in the presence of noise

In this chapter, we consider the case where there is independent dephasing. In reality, dephasing is one of the inevitable source of the degradation of the sensitivity. The weight of the off-diagonal terms that show quantum coherence of macroscopically distinct states are diminished because of the dephasing, which makes it non-trivial whether the generalized cat states are useful or not with the realistic environment. Here we show that even in the presence of independent non-Markovian dephasing, the realistic noise for the most of the solid-state systems, generalized cat states achieves the ultimate scaling sensitivity.

5.1 Noise model

First of all, we restrict our discussion to independent dephasing by which each spin dephases without affecting others. The noise we consider is the following:

$$\sum_{l=1}^{N} \lambda f_l(t) \hat{a}(l), \tag{5.1}$$

where λ is the amplitude of the noise, and $f_l(t)$ satisfies

$$\overline{f_l(t)} = 0, \tag{5.2}$$

$$\overline{f_l(t) f_{l'}(t')} = \exp(-|t-t'|/\tau_c)\delta_{l,l'}, \tag{5.3}$$

where the overline denotes the average over the ensemble of the noise, and τ_c is the the correlation time of the environment.

5.1.1 Markovian dephasing

In the case where $\tau_c \ll t_{\text{int}}$, the dephasing process is Markovian. In the presence of Markovian dephasing, it is known that even the GHZ state, the most ideal cat state, does not show the superiority than separable sensors. The enhancement of sensitivity disappears, and SQL becomes the ultimate scaling [17]. It is because under the effect of the Markovian independent dephasing with the GHZ state, the weight of the off-diagonal terms changes as $\exp(-tN/T_2^*)$, while the phase accumulation is $\exp(i\omega tN)$. Here, T_2^* is the coherence time of a single spin, determined by the amplitude of the noise, i.e., $T_2^* \propto 1/\lambda$. To make use of the GHZ state, we need $t_{\text{int}} \leq T_2^*$. However, with any t_{int}, the decay of the off-diagonal term is not slower than the advantageous phase accumulation, hence the entanglement does not improve the sensitivity.

5.1.2 Non-Markovian dephasing

By assuming non-Markovian dephasing, we obtain a different result. Previous works [14,16,24,27, 28,30,95] showed that the GHZ state can actually beat the SQL in the presence of non-Markovian dephasing. The uncertainty is proven to scale as

$$\delta\omega \propto \frac{1}{N^{3/4}}, \tag{5.4}$$

beating the SQL by the factor $\Theta(N^{1/4})$. Furthermore, Refs. [96, 97] showed this is the ultimate scaling in the presence of dephasing. The key is to take t_{int} in the so-called Zeno regime, i.e., $t_{\text{int}} \ll \tau_c$. With non-Markovian decay, the metrologically useful off-diagonal terms in the GHZ state decay as $\exp(-(t/T_2^*)^2 N)$, which is quadratic in the early stage of decoherence. This slow dephasing provides us the chance to beat the SQL. Depicted in Fig. 5.1 is the schematic of the the slow decay of the coherence, i.e., the weight of the metrologically useful off-diagonal terms for non-Markovian noise and the faster decay induced by Markovian noise.

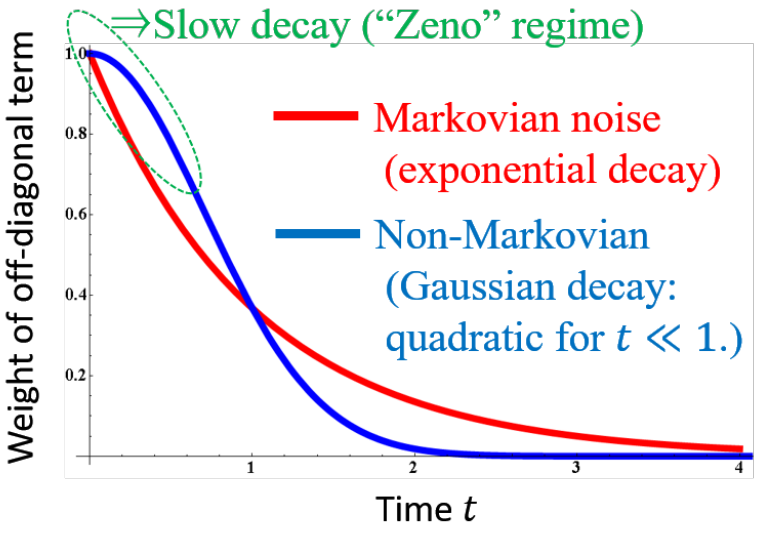

Figure 5.1: In the early stage of dephasing, more coherence, i.e., the weight of the off-diagonal term, remains for non-Markovian dephasing than Markovian dephasing.

In addition to this advantage, non-Marovian dephasing is more realistic than Markovian dephasing, although Markovian noise model is easy to handle and thus thoroughly studied. In most of the solid-state systems such as NV centers, the noise is non-Markovian [98]. An evidence of this is the usage of echo sequence. Echo sequence is a technique in magnetic resonance where one applies π pulse in the midst of the free induction decay and obtains a signal back again. This is possible because the environment “remembers the past,” i.e., non-Markovian.

In spite of such potential improvement of quantum metrology, the previous studies were focusing on some specific states such as the GHZ state and spin squeezed states. A question whether there are any other metrologically useful quantum states or not still remained open. Moreover, although pure states are assumed to be preparable as a sensor state in most of the previous researches, sensor states prepared in experiments may be mixed. In order to understand the full potential of quantum metrology, investigation of the sensitivities of other, nontrivial and non-ideal, quantum states is crucial. Therefore we analyze the sensitivity of generalized cat state sensors in the presence of non-Markovian independent dephasing.

5.2 Sensitivity of generalized cat states

5.2.1 If one spin dephases

To begin with, we consider the case in which only one spin among N spins is subjected to the decoherence. This artificial setup helps us understand the natural N-spin dephasing case. The Hamiltonian is expressed as

$$\hat{H}_0 + \hat{H}_{\rm int1}(t), \tag{5.5}$$

where

$$\hat{H}_0 = \omega \sum_{l=1}^{N} \hat{a}(l) = \omega \hat{A}, \tag{5.6}$$

$$\hat{H}_{\rm int1}(t) = \lambda f_l(t) \hat{a}(l). \tag{5.7}$$

Here we consider the non-Markovian dephasing by assuming $\tau_c \gg t_{\rm int}$. Hence, we approximate $\exp(-|t-t'|/\tau_c) \simeq 1$, which simplifies the upcoming calculation.

We let a generalized cat state $\hat{\rho}$ evolve for time $t_{\rm int}$ to become $\hat{\rho}(t_{\rm int})$. In the interaction picture,

$$\hat{\rho}^I(t) = e^{i\hat{H}_0 t} \hat{\rho}(t) e^{-i\hat{H}_0 t}, \tag{5.8}$$

$$\frac{d\hat{\rho}^I(t)}{dt} = -i[\hat{H}_{\rm int1}(t), \hat{\rho}^I(t)]. \tag{5.9}$$

By integrating, we have

$$\hat{\rho}^I(t_{\rm int}) = \hat{\rho}(0) + \sum_{n=1}^{\infty} (-i\lambda)^n \int_0^{t_{\rm int}} \int_0^{t_1} \cdots \int_0^{t_{n-1}} dt_1 dt_2 \cdots dt_n [\hat{H}_{\rm int1}(t_1), [\hat{H}_{\rm int1}(t_2), \cdots [\hat{H}_{\rm int1}(t_n), \hat{\rho}(0)]]]. \tag{5.10}$$

Taking the average over the ensemble of the noise, we obtain

$$\hat{\rho}^I(t_{\rm int}) - \hat{\rho}(0) = \sum_{n=1}^{\infty} (-i\lambda)^n \overline{f_l(t_1) f_l(t_2) \cdots f_l(t_n)} \int_0^{t_{\rm int}} \int_0^{t_1} \cdots \int_0^{t_{n-1}} dt_1 dt_2 \cdots dt_n [\hat{a}(l), \hat{\rho}(0)]_n. \tag{5.11}$$

We can decompose $\overline{f_l(t_1) f_l(t_2) \cdots f_l(t_n)}$ into

$$\overline{f_l(t_1) f_l(t_2) \cdots f_l(t_{2n})} = \sum_{all\, combination} \overline{f(t'_1) f(t'_2)}\, \overline{f(t'_3) f(t'_4)} \cdots \overline{f(t'_{2n-1}) f(t'_{2n})} \tag{5.12}$$

$$= (2n-1)(2n-3) \cdots 3 \cdot 1 = (2n-1)!! \tag{5.13}$$

and

$$\overline{f_l(t_1)f_l(t_2)\cdots f_l(t_{2n+1})} = \sum_{all\,combination} \overline{f(t_1')f(t_2')}\,\overline{f(t_3')f(t_4')}\cdots\overline{f(t_{2n-1}')f(t_{2n}')}\,\overline{f(t_{2n+1}')} \tag{5.14}$$

$$= 0 \tag{5.15}$$

since we we assume $\overline{f_j(t)f_k(t')} = \delta_{j,k}$ and the $m(>2)$th cumulants are zero for Gaussian noise. Therefore, we obtain

$$\hat{\rho}^I(t_{\rm int}) - \hat{\rho}(0) = \sum_{n=1}^{\infty}(-i\lambda)^{2n}(2n-1)!!\int_0^{t_{\rm int}}\int_0^{t_1}\cdots\int_0^{t_{n-1}} dt_1 dt_2\cdots dt_{2n}[\hat{a}(l),\hat{\rho}(0)]_{2n} \tag{5.16}$$

$$= \sum_{n=1}^{\infty}(-\lambda^2)^n(2n-1)!!t_{\rm int}^n\frac{1}{(2n)!}[\hat{a}(l),\hat{\rho}(0)]_{2n} \tag{5.17}$$

$$= \sum_{n=1}^{\infty}(-\lambda^2 t_{\rm int})^n\frac{1}{2^n n!}[\hat{a}(l),\hat{\rho}(0)]_{2n}. \tag{5.18}$$

The commutation can be simplified by assuming $\hat{a}(l)^2 = \hat{1}$, which holds for $\pm\hat{\sigma}_{x,y,z}$. Hence,

$$[\hat{a}(l),\hat{\rho}(0)]_{2n} = \frac{2^{2n}}{2}(\hat{\rho}(0) - \hat{a}(l)\hat{\rho}(0)\hat{a}(l)) \tag{5.19}$$

Then we obtain

$$\hat{\rho}^I(t_{\rm int}) - \hat{\rho}(0) = \sum_{n=1}^{\infty}(-\lambda^2 t_{\rm int})^n\frac{1}{2^n n!}\frac{2^{2n}}{2}(\hat{\rho}(0) - \hat{a}(l)\hat{\rho}(0)\hat{a}(l)) \tag{5.20}$$

$$= \frac{1}{2}\sum_{n=1}^{\infty}\frac{(-2\lambda^2 t_{\rm int})^n}{n!}(\hat{\rho}(0) - \hat{a}(l)\hat{\rho}(0)\hat{a}(l)) \tag{5.21}$$

$$= \frac{1}{2}\sum_{n=0}^{\infty}\frac{(-2\lambda^2 t_{\rm int})^n}{n!}(\hat{\rho}(0) - \hat{a}(l)\hat{\rho}(0)\hat{a}(l)) - (\frac{\hat{\rho}(0) - \hat{a}(l)\hat{\rho}(0)\hat{a}(l)}{2}) \tag{5.22}$$

$$= \frac{e^{-2\lambda^2 t_{\rm int}}}{2}(\hat{\rho}(0) - \hat{a}(l)\hat{\rho}(0)\hat{a}(l)) - \frac{\hat{\rho}(0) - \hat{a}(l)\hat{\rho}(0)\hat{a}(l)}{2}. \tag{5.23}$$

Therefore, in the case where only l-th spin dephases, the sensor state $\hat{\rho}$ evolves into

$$\hat{\rho}^I(t_{\rm int}) = \hat{\rho}(0) + \frac{e^{-2\lambda^2 t_{\rm int}} - 1}{2}\hat{\rho}(0) + \frac{1 - e^{-2\lambda^2 t_{\rm int}}}{2}\hat{a}(l)\hat{\rho}(0)\hat{a}(l) \tag{5.24}$$

$$= \frac{1 + e^{-2\lambda^2 t_{\rm int}}}{2}\hat{\rho}(0) + \frac{1 - e^{-2\lambda^2 t_{\rm int}}}{2}\hat{a}(l)\hat{\rho}(0)\hat{a}(l). \tag{5.25}$$

This is the formula for the case in which a single spin dephases by non-Markovian independent noise. We use this formula to examine the case for the case where N spin dephases.

5.2.2 If N spins dephase

Now we consider the case where all of the N spins dephase. In this case the Hamiltonian is

$$\hat{H}_0 + \hat{H}_{\rm int}(t), \tag{5.26}$$

$$\hat{H}_{\rm int}(t) = \sum_{l=1}^{N} \lambda f_l(t) \hat{a}(l). \tag{5.27}$$

As we have seen in the previous subsection, dephasing of lth spin corresponds to changing $\hat{\rho}$ into

$$\varepsilon_l[\hat{\rho}] := \frac{1+e^{-2\lambda^2 t_{\rm int}}}{2}\hat{\rho}(0) + \frac{1-e^{-2\lambda^2 t_{\rm int}}}{2}\hat{a}(l)\hat{\rho}(0)\hat{a}(l). \tag{5.28}$$

When N spins dephase, the state becomes

$$\hat{\rho}(t_{\rm int})^I = \varepsilon_N[\varepsilon_{N-1}\cdots\varepsilon_1[\hat{\rho}(0)]] \tag{5.29}$$

$$= \left(\frac{1+e^{-\lambda^2 t_{\rm int}^2}}{2}\right)^N \hat{\rho}(0) + \left(\frac{1+e^{-\lambda^2 t_{\rm int}^2}}{2}\right)^{N-1}\left(\frac{1-e^{-\lambda^2 t_{\rm int}^2}}{2}\right)\sum_{j=1}^{N}\hat{a}(j)\hat{\rho}(0)\hat{a}(j) + \cdots$$

$$+ \left(\frac{1-e^{-\lambda^2 t_{\rm int}^2}}{2}\right)^N \hat{a}_N\hat{a}_{N-1}\cdots\hat{a}_1\hat{\rho}(0)\hat{a}_1\cdots\hat{a}_{N-1}\hat{a}_N, \tag{5.30}$$

$$\tag{5.31}$$

Going back to the Schrödinger picture, we have

$$\hat{\rho}(t_{\rm int}) = e^{-i\hat{H}_0 t_{\rm int}}\left(\left(\frac{1+e^{-\lambda^2 t_{\rm int}^2}}{2}\right)^N \hat{\rho}(0) + \left(\frac{1+e^{-\lambda^2 t_{\rm int}^2}}{2}\right)^{N-1}\left(\frac{1-e^{-\lambda^2 t_{\rm int}^2}}{2}\right)\sum_{j=1}^{N}\hat{a}(j)\hat{\rho}(0)\hat{a}(j) + \cdots\right.$$

$$\left. + \left(\frac{1-e^{-\lambda^2 t_{\rm int}^2}}{2}\right)^N \hat{a}_N\hat{a}_{N-1}\cdots\hat{a}_1\hat{\rho}(0)\hat{a}_1\cdots\hat{a}_{N-1}\hat{a}_N\right)e^{i\hat{H}_0 t_{\rm int}} \tag{5.32}$$

Here, $\left(\frac{1+e^{-\lambda^2 t_{\rm int}^2}}{2}\right)^N e^{-i\hat{H}_0 t_{\rm int}}\hat{\rho}(0)e^{i\hat{H}_0 t_{\rm int}}$ in $\hat{\rho}(t_{\rm int})$ is what we obtain when the generalized cat state evolves in the presence of the target magnetic field without noise, only with a diminished weight $\left(\frac{1+e^{-\lambda^2 t_{\rm int}^2}}{2}\right)^N$. We have already studied in the previous chapter that this state shows the ultimate scaling sensitivity. To examine the effect of the other terms in $\hat{\rho}(t_{\rm int})$, we denote $\hat{\rho}' := \hat{\rho}(t_{\rm int}) - \left(\frac{1+e^{-\lambda^2 t_{\rm int}^2}}{2}\right)^N e^{-i\hat{H}_0 t_{\rm int}}\hat{\rho}(0)e^{i\hat{H}_0 t_{\rm int}}$. To make it short, sometimes we call $e^{-i\hat{H}_0 t_{\rm int}}\hat{\rho}(0)e^{i\hat{H}_0 t_{\rm int}}$ the "original" generalized cat state to distinguish from $\hat{\rho}'$. Applying the triangle inequality to the

denominator of $\delta\omega$, we obtain

$$\sqrt{T/t_{\rm int}}\left|\frac{d{\rm Tr}(\hat{\eta}\hat{\rho}(t_{\rm int}))}{d\omega}\right| \geq \sqrt{T/t_{\rm int}}(\left|\frac{d{\rm Tr}(\hat{\eta}e^{-i\omega\hat{A}t_{\rm int}}\hat{\rho}(0)e^{i\omega\hat{A}t_{\rm int}})}{d\omega}\right|\left(\frac{1+e^{-\lambda^2 t_{\rm int}^2}}{2}\right)^N - \left|\frac{d{\rm Tr}(\hat{\eta}\hat{\rho}')}{d\omega}\right|). \tag{5.33}$$

Since

$$|{\rm Tr}(\hat{\rho}[\hat{A},\hat{\eta}]_k)| \leq 2^k\|\hat{A}\|^k, \tag{5.34}$$

the second term can be evaluated as follows.

$$\left|\frac{d{\rm Tr}(\hat{\rho}'\hat{\eta})}{d\omega}\right| \tag{5.35}$$

$$= \left|\frac{d}{d\omega}\sum_{k=0}^{\infty}\frac{(i\omega t_{\rm int})^k}{k!}{\rm Tr}(\rho_0'[\hat{A},\hat{\eta}]_k)\right| \tag{5.36}$$

$$\leq 2\|\hat{A}\|t_{\rm int}e^{2\omega t_{\rm int}\|\hat{A}\|}\|\rho_0'\| \tag{5.37}$$

$$= 2\|\hat{A}\|t_{\rm int}e^{2\omega t_{\rm int}\|\hat{A}\|}\times\|\left(\frac{1+e^{-\lambda^2 t_{\rm int}^2}}{2}\right)^{N-1}\left(\frac{1-e^{-\lambda^2 t_{\rm int}^2}}{2}\right)\sum_{j=1}^{N}\hat{a}(j)\hat{\rho}(0)\hat{a}(j)+$$
$$\cdots+\left(\frac{1-e^{-\lambda^2 t_{\rm int}^2}}{2}\right)^N\hat{a}_N\hat{a}_{N-1}\cdots\hat{a}_1\hat{\rho}(0)\hat{a}_1\cdots\hat{a}_{N-1}\hat{a}_N\| \tag{5.38}$$

$$= 2\|\hat{A}\|t_{\rm int}e^{2\omega t_{\rm int}\|\hat{A}\|}\left(\left(\frac{1+e^{-\lambda^2 t_{\rm int}^2}}{2}\right)^{N-1}\left(\frac{1-e^{-\lambda^2 t_{\rm int}^2}}{2}\right)\binom{N}{1}+\cdots+\left(\frac{1-e^{-\lambda^2 t_{\rm int}^2}}{2}\right)^N\binom{N}{N}\right) \tag{5.39}$$

$$= 2\|\hat{A}\|t_{\rm int}e^{2\omega t_{\rm int}\|\hat{A}\|}\left(1-\left(\frac{1+e^{-\lambda^2 t_{\rm int}^2}}{2}\right)^N\right). \tag{5.40}$$

Hence we have

$$\sqrt{T/t_{\rm int}}\left|\frac{d{\rm Tr}(\hat{\eta}\hat{\rho}(t_{\rm int}))}{d\omega}\right|$$
$$\geq \sqrt{T/t_{\rm int}}\left(\left|\frac{dP}{d\omega}\right|\left(\frac{1+e^{-\lambda^2 t_{\rm int}^2}}{2}\right)^N - 2\|\hat{A}\|t_{\rm int}e^{2\omega t_{\rm int}\|\hat{A}\|}\left(1-\left(\frac{1+e^{-\lambda^2 t_{\rm int}^2}}{2}\right)^N\right)\right). \tag{5.41}$$

Recall that the first term is already evaluated in the previous chapter:

$$\left|\frac{dP}{d\omega}\right| \geq k_c(\omega tN)^2 N t_{\rm int} > 0. \tag{5.42}$$

We assume that the right-hand side of (5.41) is positive, which means that the weight of the original generalized cat state is sufficiently large. Then we have

$$\begin{aligned}&\delta\omega_{\mathrm{deph}}\sqrt{T}\\&\leq (N\sqrt{t_{\mathrm{int}}})^{-1}\left[k_c(\omega t_{\mathrm{int}}N)^2\left(\frac{1+e^{-2\lambda^2 t_{\mathrm{int}}^2}}{2}\right)^N-2e^{2\omega t_{\mathrm{int}}\|\hat{A}\|}\frac{\|\hat{A}\|}{N}\left(1-\left(\frac{1+e^{-2\lambda^2 t_{\mathrm{int}}^2}}{2}\right)^N\right)\right]^{-1}.\end{aligned}\tag{5.43}$$

To see how small this uncertainty is, we must optimize it by changing t_{int}. Regarding the first factor of the right-hand side, i.e., $(N\sqrt{t_{\mathrm{int}}})^{-1}$, the larger the interaction time t_{int} is, the smaller the factor becomes, i.e., the better uncertainty we get. However, larger t_{int} makes the weight $\left(\frac{1+e^{-2\lambda^2 t_{\mathrm{int}}^2}}{2}\right)^N\leq 1$ of the original generalized cat state smaller, resulting in the degradation of the uncertainty. To find the optimal scaling, we take $t_{\mathrm{int}}\propto\frac{N^\varepsilon}{\sqrt{N}}$, where ε is a constant to be determined. Actually,

$$\frac{d}{d\varepsilon}\left(\frac{1+e^{-2\lambda^2/N^{1-2\varepsilon}}}{2}\right)^N=-2\lambda^2N^{2\varepsilon}\log(N)e^{-2\lambda^2N^{2\varepsilon-1}}\left(\frac{1+e^{-2\lambda^2N^{2\varepsilon-1}}}{2}\right)^{N-1},\tag{5.44}$$

meaning $\left(\frac{1+e^{-2\lambda^2 t_{\mathrm{int}}^2}}{2}\right)^N$ is a decreasing function of ε for $N>1$. In particular, it decreases to zero for $N\gg 1$ for $\varepsilon>0$, while remaining finite for $\varepsilon=0$. Regarding $\varepsilon<0$, it is not optimal because while $\left(\frac{1+e^{-2\lambda^2 t_{\mathrm{int}}^2}}{2}\right)^N$ does stay finite, the first factor of (5.43), i.e., $(N\sqrt{t_{\mathrm{int}}})^{-1}\propto(N^{\frac{3}{4}+\frac{\varepsilon}{2}})^{-1}$, shows a metrologically better scaling for larger ε. Hence the right-hand side of (5.43) takes the optimal scaling at $\varepsilon=0$, i.e., $t_{\mathrm{int}}\propto\sqrt{N^{-1}}$. This scaling is reasonable from the view point of the coherence time. With T_2^* as the coherence time of a single spin, the coherence time of N-spin system is $T_2^*/\sqrt{N}$. It is not likely to obtain the best sensitivity if the interaction time t_{int} greatly exceeds the coherence time of the total system. Also note that we need $t_{\mathrm{int}}\propto(\omega N t_{\mathrm{int}})^2$ to make the right-hand side of (5.43) positive.

With such t_{int}, the uncertainty is bounded as

$$\delta\omega_{\mathrm{deph}}\sqrt{T}\leq\Theta(N^{-3/4}).\tag{5.45}$$

This scaling is known to be the ultimate according to the previous works [96,97]. It beats the SQL by a factor of $N^{1/4}$, even though the system is under the effect of dephasing. Again, in addition to the ultimate scaling, the value of the upper bound of $\delta\omega_{\mathrm{deph}}$ can be made as small as required by taking sufficiently large T.

From this result, we see that all the generalized cat states achieve the ultimate scaling sensitivity when used as a sensor. Since generalized cat states include highly mixed states, this fact greatly broadens the possibility of quantum metrology.

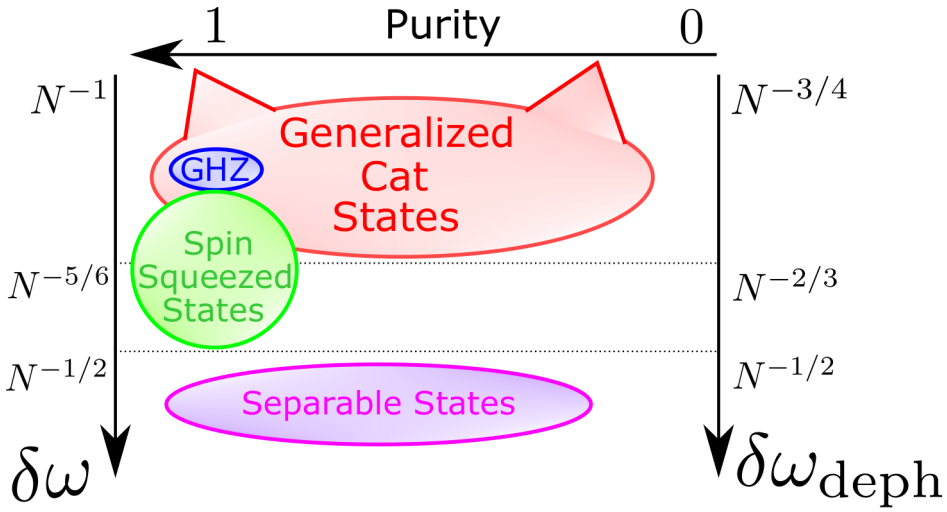

Figure 5.2: Schematic of the relationship between the scaling of the uncertainty and the purity of a given state in the Ramsey-type sensing. The ultimate scaling of the uncertainty without and with the dephasing is $\delta\omega = \Theta(N^{-1})$ and $\delta\omega_{\mathrm{deph}} = \Theta(N^{-3/4})$, respectively. The GHZ state is a pure state and achieves the ultimate scaling. One-axis and two-axis spin squeezed states [99] are pure states, and the former achieves $\delta\omega = \Theta(N^{-5/6})$, beating the SQL, and the latter achieves the Heisenberg scaling. The SQL is not beaten by separable states, whether pure or mixed. All the generalized cat states, including states with purity from one to exponentially small, achieve the ultimate scaling sensitivity.

5.3 Discussion on the intermediate scaling

Our calculation shows that the scaling of N^{-1} is obtained without dephasing, while $N^{-3/4}$ is obtained in the presence of dephasing. However, the reader may wonder whether or not an intermediate scaling such as $N^{-7/8}$ is obtainable in the case where the effect of the dephasing is present but extremely small. In this section, we consider the GHZ state and see why we do not obtain such an intermediate scaling in the standard Ramsey-type sensing and the presence of the dephasing with any amplitude makes a jump in the scaling from N^{-1} to $N^{-3/4}$. The proof for other general cases is yet to be done, but we believe the logic should be qualitatively the same.

The protocol for estimating ω of $\hat{H} = \sum_{j=1}^{N} \frac{\omega}{2}\hat{\sigma}_z^{(j)}$ with the GHZ state, $\frac{1}{\sqrt{2}}(|\uparrow\rangle^{\otimes N} + |\downarrow\rangle^{\otimes N})$, is the same as the one explained in the previous chapters in this thesis. We let the GHZ state evolve for time t_{int}, read out, and repeat for T/t_{int} times. Note that we freely fix the total measurement time T at some finite value. Hence we consider the behavior of $\delta\omega\sqrt{T}$ in the following. For the

GHZ state,

$$\hat{\rho}(t) = \frac{1}{2}|\uparrow\rangle^{\otimes N}\langle\uparrow|^{\otimes N} + \frac{\exp(-i\omega N t_{\rm int} - 2\lambda^2 N t_{\rm int}^2)}{2}|\uparrow\rangle^{\otimes N}\langle\downarrow|^{\otimes N} + \frac{\exp(i\omega N t_{\rm int} - 2\lambda^2 N t_{\rm int}^2)}{2}|\downarrow\rangle^{\otimes N}\langle\uparrow|^{\otimes N} + \frac{1}{2}|\downarrow\rangle^{\otimes N}\langle\downarrow|^{\otimes N} \tag{5.46}$$

and by assuming $\omega N t_{\rm int} \ll 1$ we have

$$P = \frac{1+\exp(-2\lambda^2 t_{\rm int}^2 N)\sin\omega N t_{\rm int}}{2} \tag{5.47}$$

$$\simeq \frac{1+\exp(-2\lambda^2 t_{\rm int}^2 N)\omega N t_{\rm int}}{2}. \tag{5.48}$$

Then $\delta\omega\sqrt{T}$ is as follows.

$$\delta\omega\sqrt{T} = \frac{\sqrt{P(1-P)}}{\left|\frac{dP}{d\omega}\right|\sqrt{1/t_{\rm int}}} \tag{5.49}$$

$$\simeq \frac{e^{\frac{N t_{\rm int}^2}{(T_2^*)^2}}}{N\sqrt{t_{\rm int}}} \tag{5.50}$$

Note that $T_2^* = 1/2\lambda$ is the coherence time of a single spin.

When T_2^* is finite, i.e., there is dephasing, the minimum of $\delta\omega\sqrt{T}$ is $\frac{\sqrt{2}\exp(1/4)}{N^{3/4}\sqrt{T_2^*}}$ at $t_{\rm int} = T_2^*/2\sqrt{N}$. The value of $\frac{\sqrt{2}\exp(1/4)}{N^{3/4}\sqrt{T_2^*}}$ depends on the coherence time T_2^*, and the minimum point moves to the right as T_2^* increases, i.e., the amplitude of noise decreases (Fig. 5.3). When there is no noise, i.e., $T_2^* \to \infty$, there is no minimum point anymore, and $\delta\omega$ which scales as N^{-1} keeps decreasing with the increase of $t_{\rm int}$. This is the reason why the optimal scaling jumps from N^{-1} to $N^{-3/4}$ with the emergence of noise. The formula (5.50) has already been known, but our work was the first and only to explicitly discuss why there are only two scalings, providing an intuitive original figure.

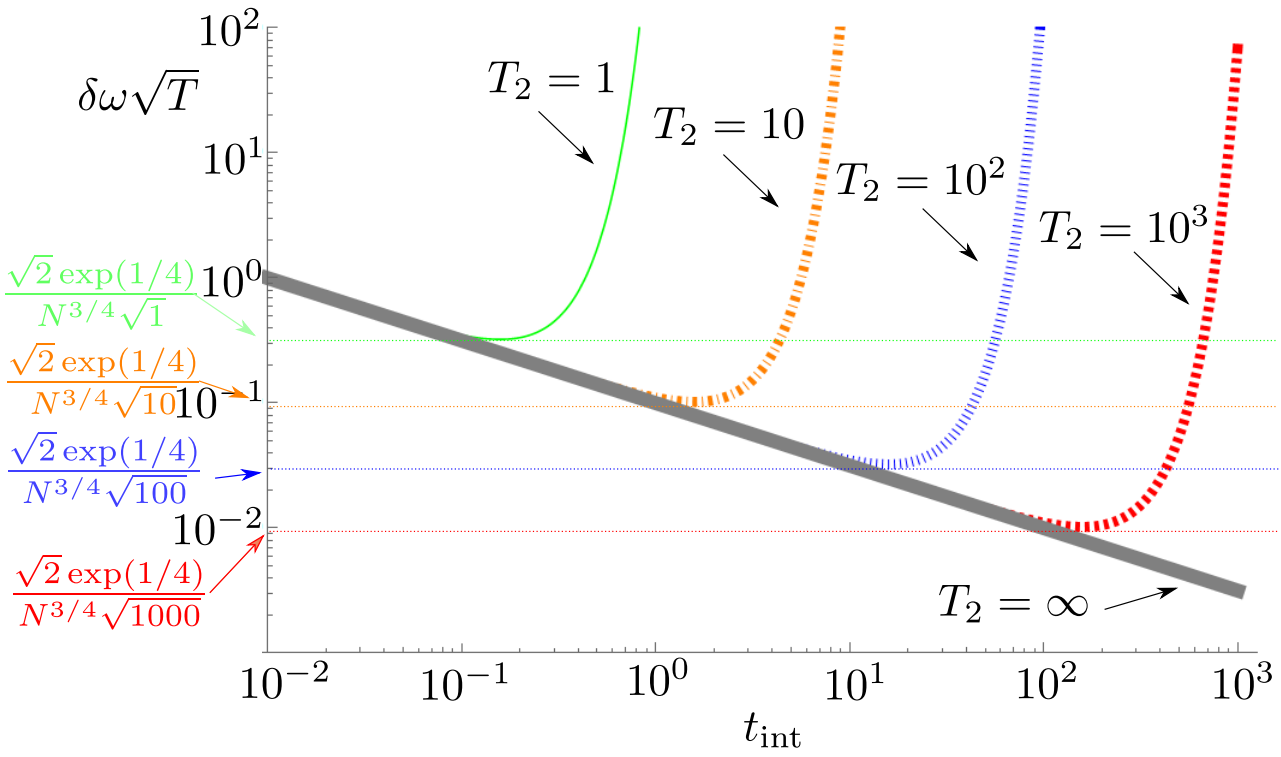

Figure 5.3: Log-log plots of $\delta\omega\sqrt{T}$ for different T_2^*s against $t_{\rm int}$ for $N = 10$. From the left, green, orange, blue, and red curves correspond to $T_2^* = 1$, $T_2^* = 10$, $T_2^* = 10^2$, $T_2^* = 10^3$, respectively. The gray line corresponds to $T_2^* \to \infty$. The minimum value moves to the right as T_2^* increases, but always scales as $N^{-3/4}$ for finite T_2^*. However, when $T_2^* \to \infty$, $\delta\omega\sqrt{T} \propto 1/N\sqrt{t_{\rm int}}$ has no minimum point, giving another scaling N^{-1} for the optimal uncertainty.

Intuitively, the minimum value appears because of the competing two factors: phase accumulation and the change of the amplitude of the useful generalized cat state. With a larger $t_{\rm int}$, the sensor state can acquire more phase, i.e., more information, of the target field. However, under the effect of dephasing, the longer the sensor state evolves, the less the amplitude of the state with useful coherence for sensing becomes. In the absence of noise, this latter factor does not yield, hence there is no minimum point. The uncertainty scales as N^{-1} for any $t_{\rm int}$.

5.4 Comparison with the QFI, revisited

Let us comment another advantage of q compared to the QFI. As depicted in Fig. 5.4, the dynamical aspects in the presence of noise are not clear enough for the QFI because in the Cramer-Rao inequality the QFI is of the state *after* the noisy time evolution, which is not directly related to the QFI of the initial state. By contrast, we have obtained the upper bound of $\delta\omega$ in terms of q of the

initial generalized cat state. Such a practical bound is derived because q is directly connected to the equation of motion.

Hence, our results reveal different aspect of the quantum metrology that the QFI cannot provide.

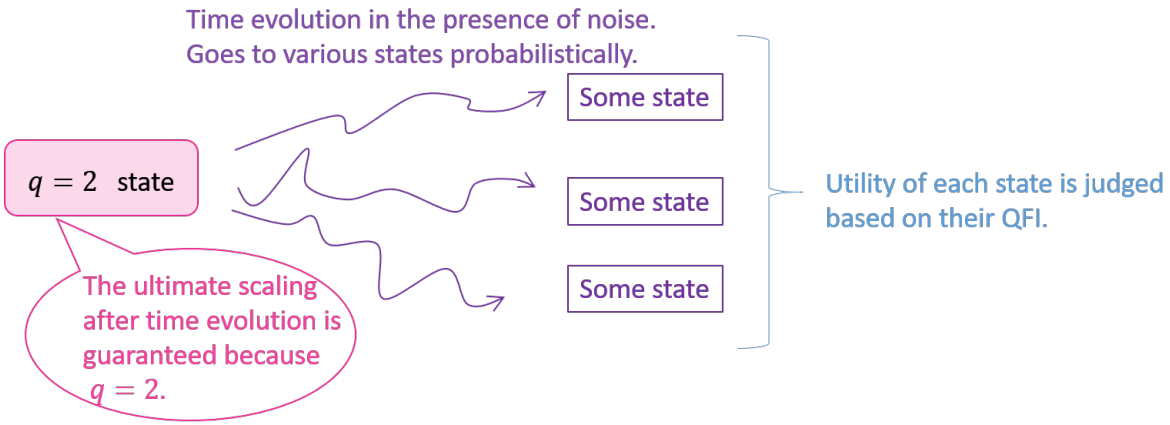

Figure 5.4: Schematic of the comparison between QFI and q. If we have a state with $q = 2$, we immediately know it achieves the ultimate scaling even in the presence of dephasing. On the other hand, when we try to judge whether a given state is useful or not using the QFI, we must see the QFI of the final state after the time evolution.

Chapter 6

Example: generalized cat state with a small purity

In this chapter, we show one example of a nontrivial generalized cat state. It is generated from a thermal equilibrium state at finite temperature, being a mixture of exponentially large number of states. First we introduce the recipe for generating this state and discuss the condition for successfully obtaining the state with high probability. We then see the purity of the state is exponentially low. After generalizing the recipe by loosening the condition on the initial state that is to be converted into a generalized cat state, we discuss the sensitivity if realized in a silicon substrate. In the following we call this example state generated by the recipe in section 6.1 as "Mamineko", implying maximally mixed neko (cat) state.

6.1 Recipe

The recipe to create Mamineko is simple. As depicted in Fig. 6.1,

1. Prepare N spins
2. Apply magnetic field along z axis
3. Let the system equilibrate
4. Measure the magnetization along x axis

Then the post-measurement state is a generalized cat state.

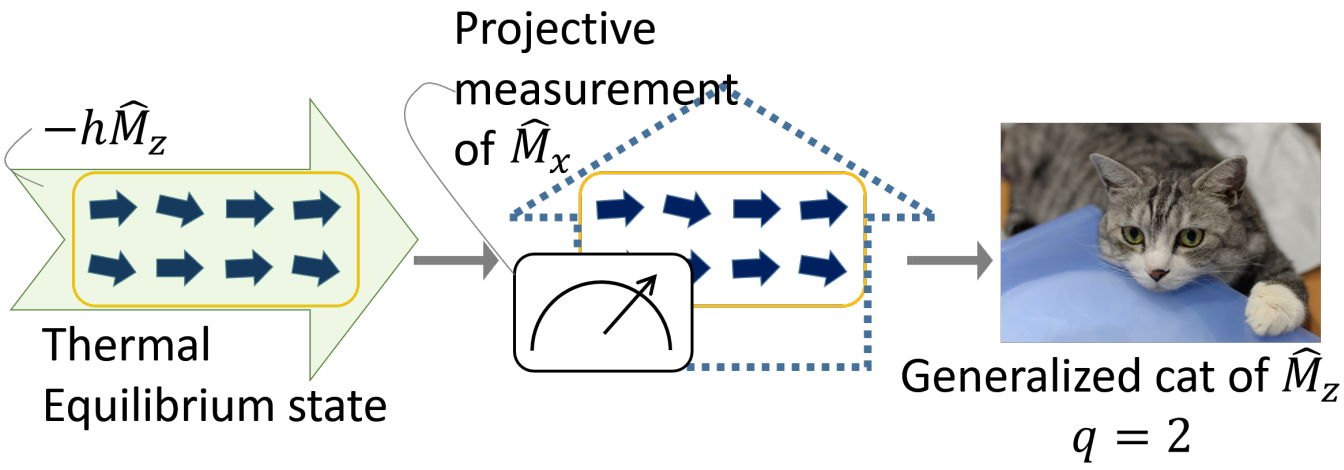

Table 6.1: Schematic of the recipe of generating Mamineko. (Left) External magnetic field, depicted with a bright green arrow, polarizes the spins, the small navy arrows, at finite temperature. (Middle) Projective measurement of the magnetization perpendicular to the external magnetic field. (Right) Generalized cat state satisfying $\|[\hat{M}_z,[\hat{M}_z,\hat{\rho}]]\|_1 = \Theta(N^2)$ is generated. The photo is taken by Professor Shimizu.

Let us follow the recipe with a specific model. We assume that the external field is $-h\hat{M}_z$ and the inverse temperature is β. For simplicity, we assume there is no interaction between spins, i.e,

$$\hat{H}^0 = -h\hat{M}_z \tag{6.1}$$

although generalized cat states are obtainable even when there are interactions. Then the pre-measurement state $\hat{\rho}_{\rm eq}$ is

$$\hat{\rho}_{\rm eq} := \frac{\exp(\beta h\hat{M}_z)}{{\rm Tr}(\exp(\beta h\hat{M}_z))}. \tag{6.2}$$

To this state, we perform a projective measurement $\hat{\eta}_x$ onto $\hat{M}_x = M$ subspace. The post-measurement state $\hat{\rho}_M$ is

$$\hat{\rho}_M := \frac{\hat{\eta}_x \exp(\beta h\hat{M}_z)\hat{\eta}_x}{{\rm Tr}(\exp(\beta h\hat{M}_z)\hat{\eta}_x)}. \tag{6.3}$$

This state is a generalized cat state. Recall that if there exists an additive observable $\hat{A}$ and a projection operator $\hat{\eta}$ such that

$${\rm Tr}(\hat{\rho}[\hat{A},[\hat{A},\hat{\eta}]]) = \Theta(N^2), \tag{6.4}$$

then $\hat{\rho}$ is a generalized cat state. For the case of Mamineko, we find $\hat{M}_z$ is a good candidate for $\hat{A}$ because of the uncertainty relation. The projective measurement $\hat{\eta}_x$ greatly reduced the uncertainty of $\hat{M}_x$, so $\hat{M}_z$ should have a large fluctuation. However, we cannot distinguish whether the cause of the large fluctuation is a superposition or a classical mixture, hence we need to calculate $\mathrm{Tr}(\hat{\rho}[\hat{A},[\hat{A},\hat{\eta}]])$. For the choice of $\hat{\eta}$, we try with $\hat{\eta}=\hat{\eta}_x$. We find that it maximizes $\mathrm{Tr}(\hat{\rho}_M(\hat{M}_z^2\hat{\eta}_x))$ and makes $\mathrm{Tr}(\hat{\rho}_M(\hat{M}_z\hat{\eta}\hat{M}_z))=0$ simultaneously. Then we have

$$\begin{aligned}\mathrm{Tr}(\hat{\rho}_M[\hat{M}_z,[\hat{M}_z,\hat{\eta}_x]]) &= \mathrm{Tr}(\hat{\rho}_M(\hat{M}_z^2\hat{\eta}_x+\hat{\eta}_x\hat{M}_z^2-2\hat{M}_z\hat{\eta}_x\hat{M}_z)) &(6.5)\\ &= \mathrm{Tr}(\hat{\eta}_x\hat{\rho}_{\mathrm{eq}}\hat{\eta}_x(\hat{M}_z^2\hat{\eta}_x+\hat{\eta}_x\hat{M}_z^2-2\hat{M}_z\hat{\eta}_x\hat{M}_z)) &(6.6)\\ &= 2\mathrm{Tr}(\hat{\rho}_M\hat{M}_z^2) &(6.7)\\ &= 2N+(N^2-M^2)\tanh^2(\beta h). &(6.8)\end{aligned}$$

This is $\Theta(N^2)$ if $M\neq\pm N+o(N)$. The probability of obtaining such M is

$$\Pr\left[\hat{M}_x=M\neq\pm N+o(N)\right]=1-N^{o(N)}/(o(N))!2^N. \tag{6.9}$$

Therefore, we obtain Mamineko with high probability.

6.2 Resolution of the projection

We have assumed $\hat{\eta}_x$ is a projection onto the $\hat{M}_x=M$ subspace, which means the resolution of the projective measurement is 1, i.e., being able to distinguish the change of the total magnetization caused by the change of the magnetization of a single spin. With such a measurement, Mamineko is obtained with high probability. However, it is a challenging task to realize, so we also consider whether Mamineko is obtainable when a projection onto a broader subspace is done. We consider a projection onto the $M_-\leq\hat{M}_x\leq M_+$ subspace and how the success probability differs for different M_+-M_-.

Through some algebra, it was proven in [2] that it is possible to obtain Mamineko with high probability when $M_+-M_-=\Theta(1)$ with $M_\pm\neq\pm N+o(N)$. Regarding the projection onto a broader subspace, it was proven that Mamineko is obtainable with any $M_+-M_->\Theta(1)$ such as $M_+-M_-=\Theta(\sqrt{N})$, only when a severe condition below is satisfied. When $M_+-M_->\Theta(1)$, we need $M_-=\Theta(N)$ for $M_->0$ (or, $M_+=-\Theta(N)$ for $M_+<0$), meaning that the measurement outcome must be $\pm\Theta(N)$. Probability of obtaining such an outcome is exponentially small.

$$\Pr\left[\Theta(N)=M_-\leq\hat{M}_z\leq M_+\right]=Z'^0_{\mathrm{post}}/Z^0_{\mathrm{eq}}=e^{-\Theta(N)} \tag{6.10}$$

Therefore, there is a trade-off between success probability of obtaining Mamineko and the resolution of a measurement (Table 6.2). When applying in experiments, one should consider this fact.

Success probability	Resolution	Difficulty
High	$\Theta(N^0)$	Difficult
Low	$\Theta(\sqrt{N})$	Easy

Table 6.2: Trade-off relation between the success probability of obtaining Mamineko and the resolution of the projection for generating it.

6.3 Purity of Mamineko

One peculiar feature about Mamineko is that its purity is $\exp(-\Theta(N))$. This is because of two factors. One is that Mamineko is created from a Gibbs state at finite temperature, which is a mixture of an exponentially large number of states. Another is that the projective measurement is a projection onto an exponentially large subspace. Let us check it with free spins. The post-measurement state is expressed as

$$\hat{\rho}^0_{\rm post} = \frac{\hat{\eta}_x \hat{\rho}^{\rm eq}_0 \hat{\eta}_x}{{\rm Tr}[\hat{\eta}_x \hat{\rho}^{\rm eq}_0 \hat{\eta}_x]} = \frac{\hat{\eta}_x \hat{e}^{-\beta \hat{H}_0} \hat{\eta}_x}{Z^0_{\rm post}(\beta h)}. \tag{6.11}$$

The purity of this state is evaluated as

$$\begin{aligned} {\rm Tr}[(\hat{\rho}^0_{\rm post})^2] &= \frac{{\rm Tr}[\hat{\eta}_x \hat{e}^{-\beta \hat{H}_0} \hat{\eta}_x \hat{e}^{-\beta \hat{H}_0} \hat{\eta}_x]}{(Z^0_{\rm post}(\beta h))^2} && (6.12)\\ &\leq \frac{{\rm Tr}[\hat{\eta}_x (\hat{e}^{-\beta \hat{H}_0})^2 \hat{\eta}_x]}{(Z^0_{\rm post}(\beta h))^2} && (6.13)\\ &= \frac{Z^0_{\rm post}(2\beta h)}{Z^0_{\rm post}(\beta h)^2}. && (6.14) \end{aligned}$$

Using

$$Z^0_{\rm post}(\beta h) = \binom{N}{(N+M)/2} \cosh^N(\beta h), \tag{6.15}$$

we can calculate (6.14) as

$$2^N \frac{(e^{2\beta h}+e^{-2\beta h})^N}{\binom{N}{(N+M)/2}(e^{\beta h}+e^{-\beta h})^{2N}}$$
$$= \frac{2^N}{\binom{N}{(N+M)/2}(1+2/(e^{2\beta h}+e^{-2\beta h}))^N} \tag{6.16}$$
$$= \frac{2^N}{\binom{N}{(N+M)/2}(1+1/\cosh(\beta h))^N}. \tag{6.17}$$

The binomial can be simplified by using the Stirling formula, and $\frac{2^N}{\binom{N}{(N+M)/2}} \simeq \sqrt{\frac{\pi N}{2}}\exp(M^2/2N)$ is obtained when $|M| \lesssim \sqrt{N}$. Hence when $|M| \lesssim \sqrt{N}$, which occurs with high probability, and $\beta h = \Theta(N^0)$,

$$\mathrm{Tr}[(\hat{\rho}^0_{\mathrm{post}})^2] \leq \frac{1}{e^{\Theta(N)}}. \tag{6.18}$$

Thus we can see that the post-measurement state is a mixture of $e^{\Theta(N)}$ states. This is because the pre-measurement state $\hat{\rho}^{\mathrm{eq}}_0$ is a mixture of $e^{\Theta(N)}$ states with its entropy $-\mathrm{Tr}[\hat{\rho}^{\mathrm{eq}}_0 \ln \rho^{\mathrm{eq}}_0]$ is $\Theta(N)$ when $T > 0$, and $\hat{\eta}_x$ is a projection onto an $e^{\Theta(N)}$ dimensional space:

$$\mathrm{Tr}[\hat{\eta}_x] = \binom{N}{(N+M)/2} \sim 2^N \tag{6.19}$$

for $M \sim 0$.

When $\beta h \to \infty$, i.e., at zero temperature, on the other hand, the pre-measurement state is a ground state, i.e. a pure state. In this case, the post-measurement state is also a pure state.

Hence, at finite temperature, Mamineko is a mixture of an exponentially large number of states.

6.3.1 Time evolution

How does Mamineko evolve with time after it is generated? For free spins (6.1) or other systems where $\hat{M}_z$ commutes with the Hamiltonian, i.e., $\hat{M}_z$ is conserved, the state actually keeps being a generalized cat state. In fact, after Mamineko is generated at time $t = 0$, the system evolves with time as

$$\hat{\rho}_{\mathrm{post}}(t) := \hat{U}_t \hat{\rho}_{\mathrm{post}} \hat{U}_t^\dagger, \tag{6.20}$$

where $\hat{U}_t := e^{-i\hat{H}^0 t}$. Mamineko $\hat{\rho}_{\mathrm{post}}$ satisfies

$$\mathrm{Tr}\left[\hat{\rho}_{\mathrm{post}} \hat{C}_{\hat{M}_a \hat{P}}\right]. = \Theta(N^2), \tag{6.21}$$

Since $[\hat{U}_t, \hat{M}_z] = 0$, we insert $\hat{U}_t\hat{U}_t^\dagger$ and obtain

$$\Theta(N^2) = \mathrm{Tr}\big[\hat{U}_t\hat{\rho}_{\mathrm{post}}\hat{U}_t^\dagger(\hat{M}_z^2\hat{U}_t\hat{P}\hat{U}_t^\dagger - 2\hat{M}_z\hat{U}_t\hat{P}\hat{U}_t^\dagger\hat{M}_z + \hat{U}_t\hat{P}\hat{U}_t^\dagger\hat{M}_z^2)\big] = \mathrm{Tr}\big[\hat{\rho}_{\mathrm{post}}(t)\hat{C}_{\hat{M}_a\hat{P}(t)}\big], \quad (6.22)$$

where we denoted $\hat{P}(t) = \hat{U}_t\hat{P}\hat{U}_t^\dagger$. Since $\hat{P}(t)^2 = \hat{P}(t)$, i.e., $\hat{P}(t)$ is a projection operator, $\hat{\rho}_{\mathrm{post}}(t)$ indeed satisfies the condition of being a generalized cat state of $\hat{M}_z$. Therefore, during time evolution, Mamineko moves around the Hilbert space while keeps being a generalized cat state.

6.4 General condition

Up to this point in this chapter, we considered the system without interactions between spins. However, we can prove that Mamineko is obtainable even in the systems with spin-spin interactions. In fact, the Hamiltonian itself does not matter. The only condition required to be satisfied is $\langle\hat{M}_z\rangle_{\mathrm{pre}} = \Theta(N)$. Let us denote the probability of obtaining $\hat{M}_x = M$ as the outcome, or, in other words, the probability of the projection $\hat{\eta}_x$ occurring, as

$$\Pr(M) := \mathrm{Tr}[\hat{\eta}_x\hat{\rho}_{\mathrm{pre}}\hat{\eta}_x] \quad (6.23)$$

$$=: \langle\hat{\eta}_x\rangle_{\mathrm{pre}} \quad (6.24)$$

With such an outcome, the post-measurement state is expressed as

$$\frac{\hat{\eta}_x\hat{\rho}_{\mathrm{pre}}\hat{\eta}_x}{\Pr(M)}. \quad (6.25)$$

Quite obviously,

$$\hat{\eta}_x\hat{M}_z\hat{\eta}_x = \hat{\eta}_x\hat{M}_y\hat{\eta}_x = 0, \quad (6.26)$$

$$\therefore \langle\hat{M}_z\rangle_{\mathrm{post}} = \langle\hat{M}_y\rangle_{\mathrm{post}} = 0. \quad (6.27)$$

Hence $2\langle C_{\hat{M}_z,\hat{\eta}_x}\rangle_{\mathrm{post}} = \langle\hat{M}_z^2\rangle_{\mathrm{post}}$. The quantity $\langle\hat{M}_z^2\rangle_{\mathrm{post}}$ itself is hard to relate to $\langle\hat{M}_z\rangle_{\mathrm{pre}}$, so we think of taking an average over the outcome M.

$$\sum_M \Pr(M)\langle\hat{M}_z^2\rangle_{\mathrm{post}} = \sum_M \mathrm{Tr}[\hat{\eta}_x\hat{\rho}_{\mathrm{pre}}\hat{\eta}_x\hat{M}_z^2] \quad (6.28)$$

Since the sum $\hat{M}_z^2 + \hat{M}_y^2$ commutes with $\hat{\eta}_x$, $\langle \hat{M}_z^2 + \hat{M}_y^2 \rangle_{\text{post}}$ is easier to evaluate.

$$\sum_M \Pr(M) \langle \hat{M}_x^2 + \hat{M}_y^2 \rangle_{\text{post}} = \sum_M \text{Tr}[\hat{\eta}_x \hat{\rho}_{\text{pre}} \hat{\eta}_x (\hat{M}_z^2 + \hat{M}_y^2)] \tag{6.29}$$

$$= \sum_M \text{Tr}[\hat{\eta}_x \hat{\rho}_{\text{pre}} (\hat{M}_z^2 + \hat{M}_y^2)] \tag{6.30}$$

$$= \langle \hat{M}_z^2 + \hat{M}_y^2 \rangle_{\text{pre}} \tag{6.31}$$

$$\geq \langle \hat{M}_z^2 \rangle_{\text{pre}} \tag{6.32}$$

$$\geq (\langle \hat{M}_z \rangle_{\text{pre}})^2 \tag{6.33}$$

$$= \Theta(N^2). \tag{6.34}$$

This shows that a generalized cat is obtained with non-vanishing probability.

For example, the initial state can be $\hat{\rho}_{M_z} = \hat{P}_z / \text{Tr}(\hat{P}_z)$, where

$$\hat{P}_z := \sum_\xi |M_z, \nu\rangle \langle M_z, \nu| \tag{6.35}$$

is a projection onto $\hat{M}_z = M_z = \Theta(N)$ subspace. Since it has macroscopic magnetization, a generalized cat state is obtainable by applying the projection

$$\hat{\eta}_x := \sum_\xi |M_x, \xi\rangle \langle M_x, \xi| \tag{6.36}$$

onto the $\hat{M}_x = M_x$ subspace. Note that ν and ξ label the degeneracy. The post-measurement state is

$$\hat{\rho}_{M_x} := \frac{\hat{\eta}_x \hat{P}_z \hat{\eta}_x}{\text{Tr}\left[\hat{\eta}_x \hat{P}_z \hat{\eta}_x\right]}. \tag{6.37}$$

We can prove this state is a generalized cat state by calculating $\langle \hat{C}_{\hat{M}_z, \hat{\eta}_x} \rangle$.

$$\langle \hat{C}_{\hat{M}_z, \hat{\eta}_x} \rangle = 2N + \frac{4 \sum_\xi \sum_{|M_z, \xi\rangle'} \langle M_z, \xi | \hat{P}_z | M_z, \xi \rangle'}{\text{Tr}\left[\hat{\eta}_x \hat{P}_z \hat{\eta}_x\right]}, \tag{6.38}$$

where $|M_z, \xi\rangle'$ is a state that differs from $|M_z, \xi\rangle$ by one $|+\rangle := (|\uparrow\rangle + |\downarrow\rangle)/\sqrt{2}$ and one $|-\rangle := (|\uparrow\rangle - |\downarrow\rangle)/\sqrt{2}$ being flipped. After some algebra (see Appendix B), we obtain

$$\langle \hat{C}_{\hat{M}_z, \hat{\eta}_x} \rangle = 2N + (N^2 - M_x^2) \left(1 - \frac{N^2 - M_z^2}{N(N-1)}\right) \tag{6.39}$$

$$= 2N + (N^2 - M_x^2) \frac{M_z^2 - N}{N(N-1)}. \tag{6.40}$$

Since we assumed $M_z = \Theta(N)$, $\hat{\rho}_{M_x}$ is a generalized cat state when $(N^2 - M_x^2) = \Theta(N^2)$.

The only condition needed is a macroscopic magnetization in the pre-measurement state. So, this method is also applicable in systems with disorder such as NV centers in diamond.

Interaction between spins

It may sound nontrivial that we do not need interactions between spins, in spite of the resulting Mamineko has the spins correlated to each other. The thing is, correlation is generated through the measurement. The key is that the probe system that reads out the total magnetization is connected to all the spins.

6.5 Mamineko as a sensor

Since we have shown all the generalized cat states achieve the ultimate scaling in magnetic field sensing, Mamineko achieves the ultimate scaling as well. In this section we numerically study how well Mamineko works as a sensor if created in a silicon substrate. Note that in the following we discuss the sensitivity of Mamineko for sensing $\hat{M}_z$ through the Ramsey-type measurement with the readout projection $\hat{\eta}_x = \hat{P}_z$.

6.5.1 Upper bound formula

Up to here, we mainly considered of the scaling of the uncertainty. However, when $\hat{\rho}$ is specifically given, we can obtain the value of the upper bound of $\delta\omega_{\rm deph}\sqrt{T}$. To do that, one should calculate $\mathrm{Tr}(\hat{\rho}[\hat{M}_z,\hat{\eta}_x])$ and $\mathrm{Tr}(\hat{\rho}[\hat{M}_z,[\hat{M}_z,\hat{\eta}_x]])$, and then tune $t_{\rm int}$ to minimize

$$(N\sqrt{t_{\rm int}})^{-1}\Big[U\Big(\frac{1+e^{-2\lambda^2 t_{\rm int}^2}}{2}\Big)^N - 2e^{2\omega t_{\rm int}\|\hat{M}_z\|}\Big(1-\Big(\frac{1+e^{-2\lambda^2 t_{\rm int}^2}}{2}\Big)^N\Big)\Big]^{-1}, \tag{6.41}$$

where

$$U := \left|\frac{\big|\omega t_{\rm int}\mathrm{Tr}(\hat{\rho}[\hat{M}_z,[\hat{M}_z,\hat{\eta}_x]])\big|}{N} - \frac{\big|i\mathrm{Tr}(\hat{\rho}[\hat{M}_z,\hat{\eta}_x])\big|}{N}\right| - 2\frac{\|\hat{M}_z\|}{N}(e^{2\omega t_{\rm int}\|\hat{M}_z\|} - 1 - 2\omega t_{\rm int}\|\hat{M}_z\|). \tag{6.42}$$

In the following we use this formula to see Mamineko is advantageous in metrology not only in the sense of scaling but also in the numerical sense.

6.5.2 Sensitivity with Si substrate

As a stage of creating Mamineko, consider phosphorus donor electron spins in a ^{28}Si substrate. An electron in this system is known to have a very long coherence time around 10s [100], being suitable for generation of a generalized cat state. Typically, the density of the electron spins is

$\sim 10^{15}\text{cm}^{-3}$. Les us take the size of the substrate as 32μ m $\times 32\mu$ m$\times 1\mu$m, which makes the number of electron spins in the substrate approximately $N = 10^6$. To create Mamineko, we need an external magnetic field. We assume it to be 10mT. Also, we assume the temperature of the system is 10mK, meaning "finite temperature" because the thermal energy ($k_B T/2\pi \simeq 208$ MHz) is comparable with the Zeeman splitting ($g\mu_b B/2\pi \simeq 280$ MHz) and thus the spins are not fully polarized.

A projective measurement of the total magnetization generates the generalized cat state with $q = 2$. Using the parameters above and the formula (6.41), we numerically optimize the interaction time and find that the uncertainty takes its minimum $\delta\omega_{\text{deph}}\sqrt{T} = 5.2 \times 10^{-5}/\sqrt{\text{Hz}}$ at $t_{\text{int}} = 5.4$ms, which corresponds to $\delta B\sqrt{T} = 0.30\text{fT}/\sqrt{\text{Hz}}$. The interaction time $t_{\text{int}} = 5.4$ms agrees with our theoretical prediction that to obtain the optimal uncertainty t_{int} should be taken comparable with the coherence time divided by $\sqrt{N}$.

To see how good $\delta\omega_{\text{deph}}\sqrt{T} = 5.2 \times 10^{-5}/\sqrt{\text{Hz}}$ is, we compare with a thermal equilibrium state(Fig. 6.1). Spins in the same substrate in a thermal equilibrium state in the same temperature and same magnetic field, i.e., the pre-measurement state that is before begin converted into Mamineko, has the uncertainty $\delta\omega_{\text{deph}}\sqrt{T} = 9.8 \times 10^{-4}/\sqrt{\text{Hz}}$. As can be seen, there is almost twenty times advantage when a thermal equilibrium state is converted into a generalized cat state. With Mamineko being a mixture of exponentially large number of states, it is promising that other generalized cat states are even more useful.

To further see the advantage, let us compare with other known theoretical results (Fig. 6.1). The spins in the following are also considered to be in the same substrate. If a fully polarized separable state, i.e., in zero temperature with the same magnetic field, is used, $\delta\omega_{\text{deph}}\sqrt{T} = 8.1 \times 10^{-4}/\sqrt{\text{Hz}}$ is estimated [27]. In [27], they also investigate the uncertainty of the squeezed state prepared by one-axis twisting, i.e., a nonlinear interaction that suppresses the fluctuation of $\hat{M}_z$ down to $\Theta(N^0)$, to the fully polarized state. This squeezed state is not a generalized cat state. The uncertainty of this squeezed state is estimate to be $\delta\omega_{\text{deph}}\sqrt{T} = 7.1 \times 10^{-5}/\sqrt{\text{Hz}}$, somewhat comparable to our results. An important remark is that to implement these proposals, a perfect initialization of the electron spins is necessary. The initialization may be difficult because of the small Zeeman energy of the electron spins. Compared to this fact, Mamineko seems to be easier to prepare in the silicon substrate because the polarization the spins initially have in the given temperature and magnetic field is merely ~ 0.6, more feasible to prepare than a state with polarization 1. We can see the advantage of Mamineko when used in metrology.

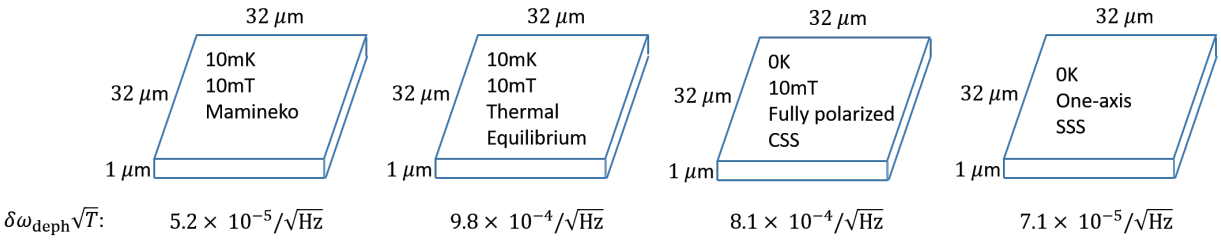

Figure 6.1: Comparison of the uncertainty $\delta\omega\sqrt{T}$ for different states in the same substrate.

The spatial resolution of the sensor is $\sim 10\mu$m, according to the size of the substrate. The records of the experimentally realized sensors with similar spatial resolution are the following. A superconducting flux qubit, a SQUID, and an ensemble of NV centers showed sensitivities of $3.3\mathrm{pT}/\sqrt{\mathrm{Hz}}$ with 5μm resolution [37], $1.4\mathrm{pT}/\sqrt{\mathrm{Hz}}$ with 100μm resolution [101], and $150\mathrm{fT}/\sqrt{\mathrm{Hz}}$ with 100μm resolution [39, 102], respectively. They all use separable states for sensing, leaving the possibility of further improvement by using generalized cat states.

Chapter 7

Attempt to creating Mamineko through repetitive measurements

In the previous chapter, we discussed the utility and the protocol to generate Mamineko. There are interesting things about the recipe such as we can do it at finite temperature, and so the generalized cat state may be a highly mixed state, and we have been successful in showing that generalized cat states, (not only this one, but all of them) can achieve the Heisenberg scaling sensitivity if used as a sensor. In this chapter, we specify physical systems, and discuss a concrete method to realize the recipe and thus create Mamineko with a realistic setup. The recipe of Mamineko assumed a very powerful projection measurement; a projection with a high resolution that can distinguish the change of the total magnetization caused by the change of the magnetization of a few spins. Fortunately, a superconducting flux qubit is considered to have a potential to realize the projection with single spin detection level. A single measurement of the flux qubit coupled to the spin ensembles just provides us with a binary information, which is not useful enough to estimate the total magnetization from the spin. However, the accuracy of the measurement of the magnetization from the spins is increased via the repetitive measurements. Therefore in this chapter, we consider a more realistic strategy to generate Mamineko via the repetitive measurements of the spin magnetization. We numerically observe the emergence of metrologically useful state.

7.1 Idea

To follow the theoretical recipe for generating Mamineko, we must read out the spins' magnetization along the axis that is perpendicular to the external magnetic field which polarizes the spins macroscopically. Since the single projection measurement with high resolution is harder to realize,

we consider replacing it with low resolution repetitive measurements. To read out, we consider using the flux qubit. We consider creating Mamineko in NV diamond, since the interaction between the flux qubit and NV centers is experimentally realized [103].

7.1.1 NV center

Systems with longer coherence times are preferable in creating a generalized cat state. As reviewed in Sec. 2.4, an NV center is a defect in diamond, and it has effectively spin $1/2$. Its coherence time is quite long, about 0.6 second at 77K [104]. This is a suitable system for Mamineko.

7.1.2 Superconducting flux qubit

A flux qubit [105] is a superconducting loop with several (normally three) Josephson junctions, and it can be regarded as a spin $1/2$ system by considering the state with clock-wise current as $|\uparrow\rangle$ state and the state with counter clock-wise current as $|\downarrow\rangle$ state. It can be used as a very sensitive magnetic field sensor. In Fig. (7.1), we illustrate the magnetometry using a flux qubit.

A flux qubit normally has Hamiltonian

$$\hat{H}_{\mathrm{FQ}} = \varepsilon\hat{\sigma}_3 + \Delta\hat{\sigma}_1 \simeq \varepsilon\hat{\sigma}_3. \tag{7.1}$$

To do the Ramsey-type magnetometry, we assume $\Delta \ll \varepsilon$. Note that for the flux qubit, $\hat{\sigma}_3$ means the population difference between the clockwise current and the counter-clockwise current. The sensor state $|+\rangle$ is a superposition of the states with these currents. It can be prepared by applying $\pi/2$ pulse. The readout of the flux qubit is done by DC SQUID by projecting to the $\hat{\sigma}_2$ basis. One readout only gives either $+1$ or -1 as a result, with a probability encoded with the B field. By repeating this procedure, we can find out the probability more accurately, meaning the improvement of the sensitivity. From the central limit theorem, the uncertainty improves by the square root of the number of repetition m:

$$\delta\omega \propto \frac{1}{\sqrt{m}}. \tag{7.2}$$

Hence, rapid repetitive measurements may become a substitute of a powerful single projection.

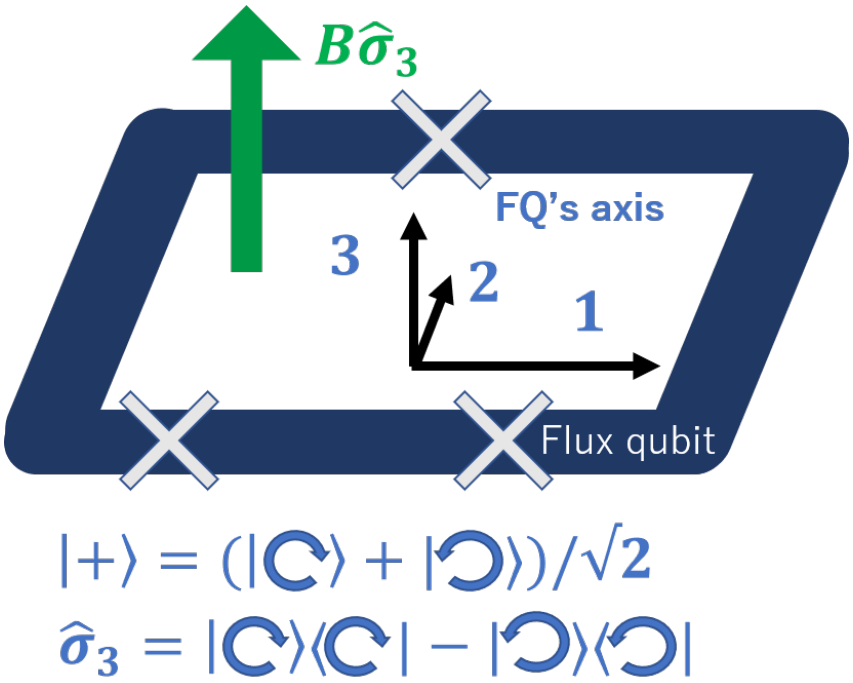

Figure 7.1: Schematic of magnetic field (green arrow) sensing using a flux qubit(navy loop). Note that $\hat{\sigma}_3$ is a population difference between clockwise and counter-clockwise currents. Three gray crosses represent Josephson junctions.

7.1.3 Hybrid system of NV center and flux qubit

We assume the following setup. On the same plane as the flux qubit, we set a diamond containing NV centers. We take the NV's quantization axis, that, is, NV's z axis, to be parallel to the plane. To realize that, we apply magnetic field as indicated in Fig.7.2. For simplicity, we assume NVs are all identical and apart from each other so that they do not interact with each other, and also we drop some irrelevant terms such as strain effect in the Hamiltonian.

$$\hat{H}_{\mathrm{NV}} = \frac{\omega_{\mathrm{NV}}}{2}\hat{S}_z = \frac{\omega_{\mathrm{NV}}}{2}\sum_{j=1}^{N}\hat{\sigma}_z^{\mathrm{NV}}(j) \tag{7.3}$$

The flux qubit creates a magnetic field perpendicular to the plane, and NVs couple to it.

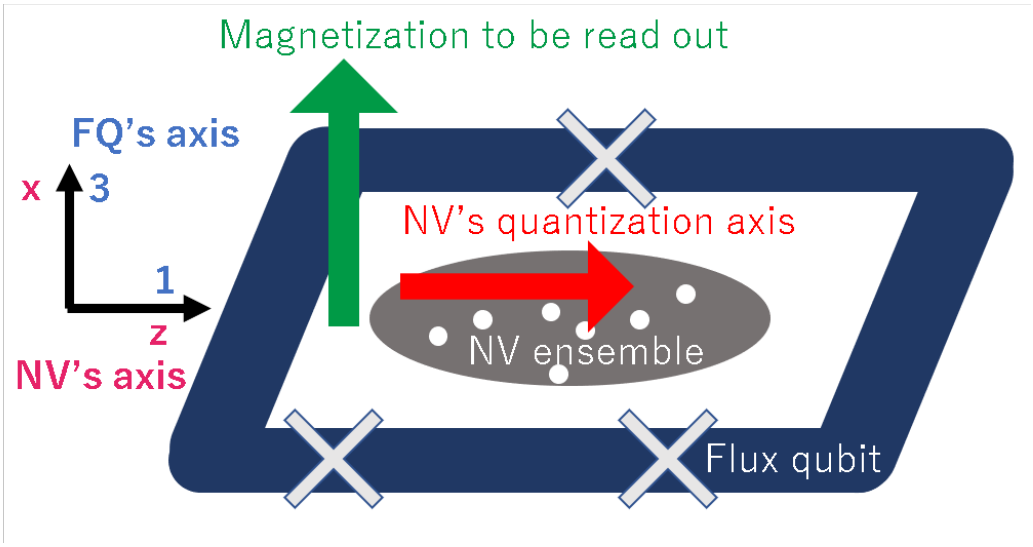

Figure 7.2: Schematic of the NV diamond and the flux qubit. The NV spins (white dots) are in the diamond sample (gray oval) placed in the loop of the flux qubit. NV's x axis is parallel to the flux qubit's 3rd axis.

The interaction Hamiltonian is

$$\hat{H}_{\text{int}} = g(t)\hat{S}_x \otimes \hat{\sigma}_3 \tag{7.4}$$

The total is the Hamiltonian we consider for creating Mamineko.

$$\hat{H} = \hat{H}_{\text{FQ}} + \hat{H}_{\text{NV}} + \hat{H}_{\text{int}}. \tag{7.5}$$

It might give the impression that we are now ready to read out $\hat{S}_x$ of NVs by the flux qubit. However, if $g(t)$ is a constant, the interaction term will disappear once we go to the rotating frame of $\hat{V} = e^{-i\frac{\omega_{\text{NV}}t}{2}\hat{S}_z}$ and apply rotating frame approximation.

$$\hat{H}_{R1} = \hat{H}_{\text{FQ}} + g\frac{\hat{S}_+ e^{i\omega_{\text{NV}}t} + \hat{S}_- e^{-i\omega_{\text{NV}}t}}{2} \otimes \hat{\sigma}_3 \simeq \hat{H}_{\text{FQ}} \tag{7.6}$$

To overcome this problem, we propose to consider a situation where this interaction strength oscillates in such a way that $g(t) = g\cos(\omega_{\text{NV}}t)$, as depicted in Fig. 7.3. Then with the rotating wave approximation, the Hamiltonian can be simplified to

$$\hat{H}_{R2} \simeq \frac{g}{2}\hat{S}_x \otimes \hat{\sigma}_3. \tag{7.7}$$

Now, $\hat{S}_x$ of NVs can be read out by the flux qubit. We assume the coupling strength is zero during initialization and readout, and oscillates during interaction.

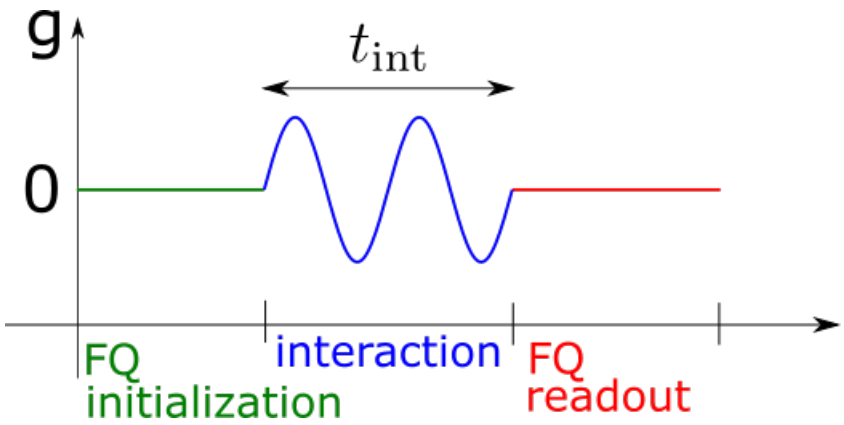

Figure 7.3: Schematic of the time dependence of $g(t)$. Only during the interaction for sensing $g(t)$ is set to oscillate.

One measurement by the flux qubit changes the density operator of NVs as

$$\hat{\rho}_{\mathrm{NV}}(m) \mapsto \hat{\rho}_{\mathrm{NV}}(m+1), \tag{7.8}$$

where $\hat{\rho}_{\mathrm{NV}}(m+1)$ is either

$$\frac{(e^{-i\frac{g}{2}\hat{S}_x t_{\mathrm{int}}} - ie^{i\frac{g}{2}\hat{S}_x t_{\mathrm{int}}})\hat{\rho}_{\mathrm{NV}}(m)(e^{-i\frac{g}{2}\hat{S}_x t_{\mathrm{int}}} + ie^{i\frac{g}{2}\hat{S}_x t_{\mathrm{int}}})}{4\mathrm{Prob}[\hat{\sigma}_2 = +1]} \tag{7.9}$$

or

$$\frac{(e^{-i\frac{g}{2}\hat{S}_x t_{\mathrm{int}}} + ie^{i\frac{g}{2}\hat{S}_x t_{\mathrm{int}}})\hat{\rho}_{\mathrm{NV}}(m)(e^{-i\frac{g}{2}\hat{S}_x t_{\mathrm{int}}} - ie^{i\frac{g}{2}\hat{S}_x t_{\mathrm{int}}})}{4\mathrm{Prob}[\hat{\sigma}_2 = -1]},$$

depending on the outcome of the readout. By repeating the measurement, the state of NV gradually changes. Since we are expecting the emergence of a generalized cat state of $\hat{S}_z$, we can numerically see how Mamineko emerges step by step by calculating the catness $\frac{1}{2}\|[\hat{S}_z,[\hat{S}_z,\hat{\rho}_{\mathrm{NV}}(m)]]\|_1 =: \frac{1}{2}\|\hat{C}_{\hat{S}_z}\|_1$ at each m.

7.2 Simulation result

Here we show the result of the numerical simulation. Since we are interested in how our idea works in principle, we restrict the temperature of the initial state to be zero. Then what we do is to consider spin $N/2$ system and apply ladder operators to see the dynamics. The parameters are taken as follows.

- $gt = 10^{-3}$ because the realized interaction strength between NV centers and the flux qubit is about $2\pi \times 1.5$kHz, and the flux qubit's coherence time is about 200ns [106].
- $T = 10$mK because the characteristic energy, the zero field splitting, of a NV center is about 2.87GHz, hence the temperature 10mK$= 2\pi \times 0.20$GHz is reasonable.

First let us examine the 1-run simulation data for 7 spins. In Fig. 7.4, the horizontal axis represents the number of repetition, i.e., readout by the flux qubit, and the vertical axis represents the "catness" $\frac{1}{2}\|\hat{C}_{\hat{S}_z}\|_1$, the quantity used in defining the index q. Since each measurement yields probabilistic output, the value of catness hops up and down. However, we can see its gradual increase. That means, we can indeed see the state drastically changes with the repetitive measurement.

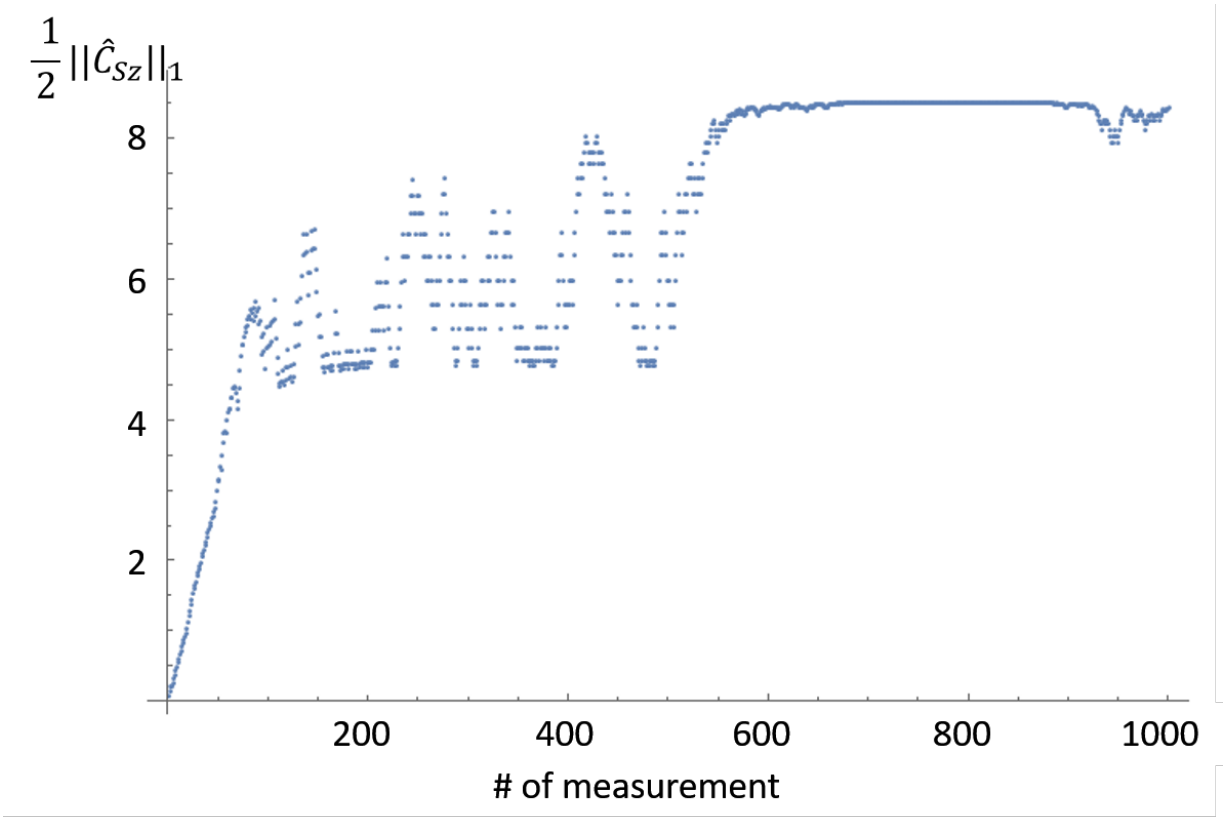

Figure 7.4: The plot of m (number of measurements) dependence of $\|\hat{C}_{\hat{S}_z}\|_1$ (catness) for a single run with $N = 7$. Each measurement gives probabilistic result, hence the value hops up and down.

Next, let us take a look at the average. Fig. 7.5 is the 3000 average of $N = 7$ case. We can see the quick increase in the beginning and slow increase for large m. This promises a drastic change of the state. However, we cannot tell if this is a cat or not yet. To check the existence of a cat, we must see how the catness $\frac{1}{2}\|\hat{C}_{\hat{S}_z}\|_1$ scales with N.

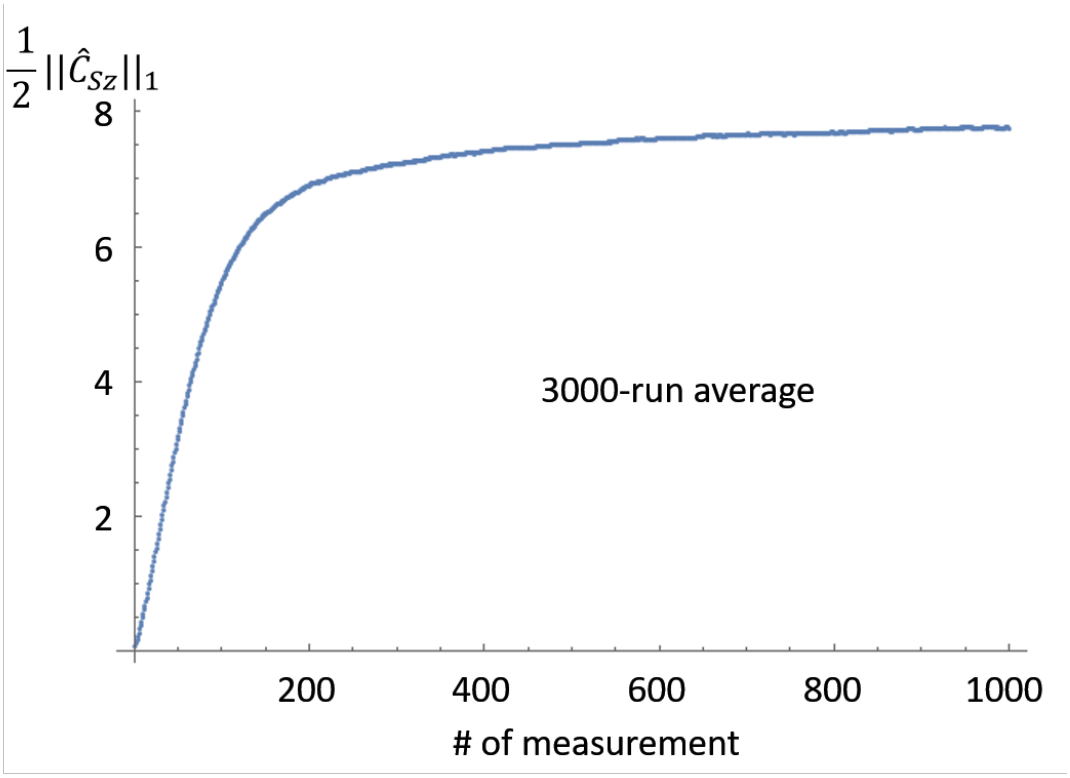

Figure 7.5: The plot of m dependence of $\|\hat{C}_{\hat{S}_z}\|_1$ for the average over 3000 runs with $N = 7$. We can see the gradual increase.

To see the gradual increase of q, we examine the value of $\|\hat{C}_{\hat{S}_z}\|_1$ of different N for each m. We slice the average curve (Fig. 7.6) at $m = 10$, 50, 100 and 600.

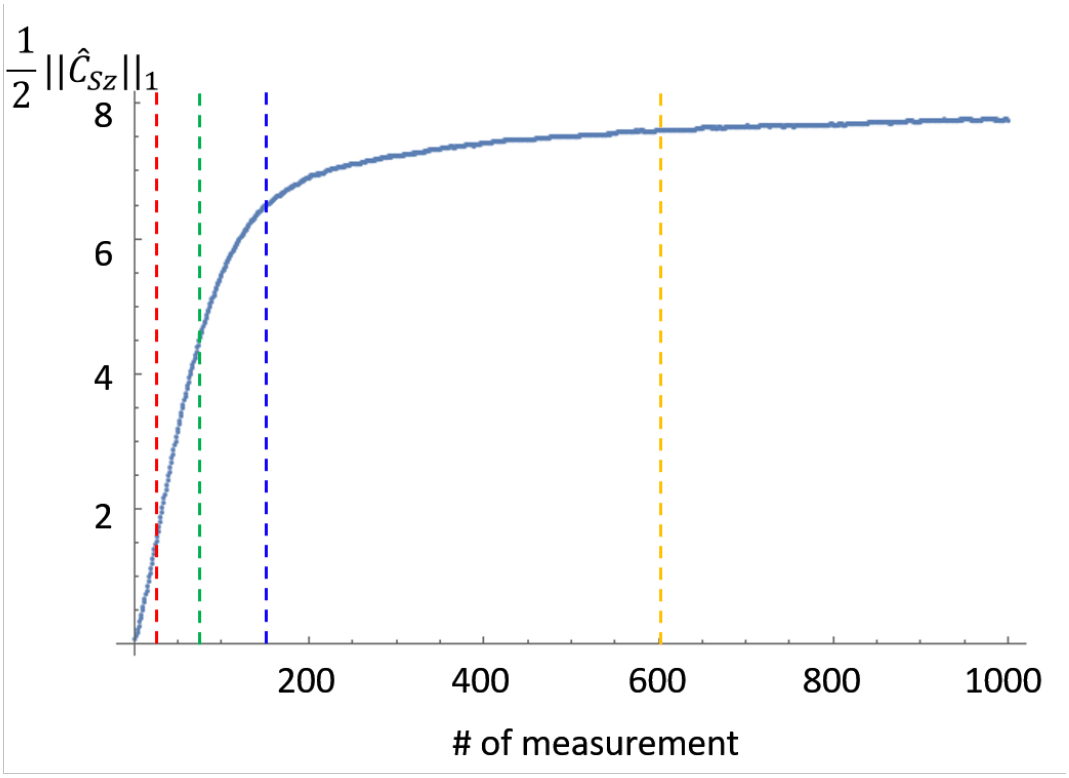

Figure 7.6: Reference of how to slice the data. Below we discuss q of $m = 10$(red), $m = 50$(green), $m = 100$(blue), and $m = 600$(yellow).

In Fig. 7.7, we take the horizontal axis to be the number of spins N, and the vertical axis to be $\frac{1}{2}\|\hat{C}_{\hat{S}_z}\|_1$. For different N, we consider the repetition measurement and obtain the value of $\|\hat{C}_{\hat{S}_z}\|_1$. We plot the value of q for different number of m, the number of repetition to see how the scaling of $\frac{1}{2}\|\hat{C}_{\hat{S}_z}\|_1$ changes.

From this, we see that it is relatively easy to obtain q up to ~ 1.8; 100 repetition is sufficient. We also see that, it seems to be a long way to obtain exactly $q = 2$, although we do expect that for more repetition, the value of q will asymptotically become 2.

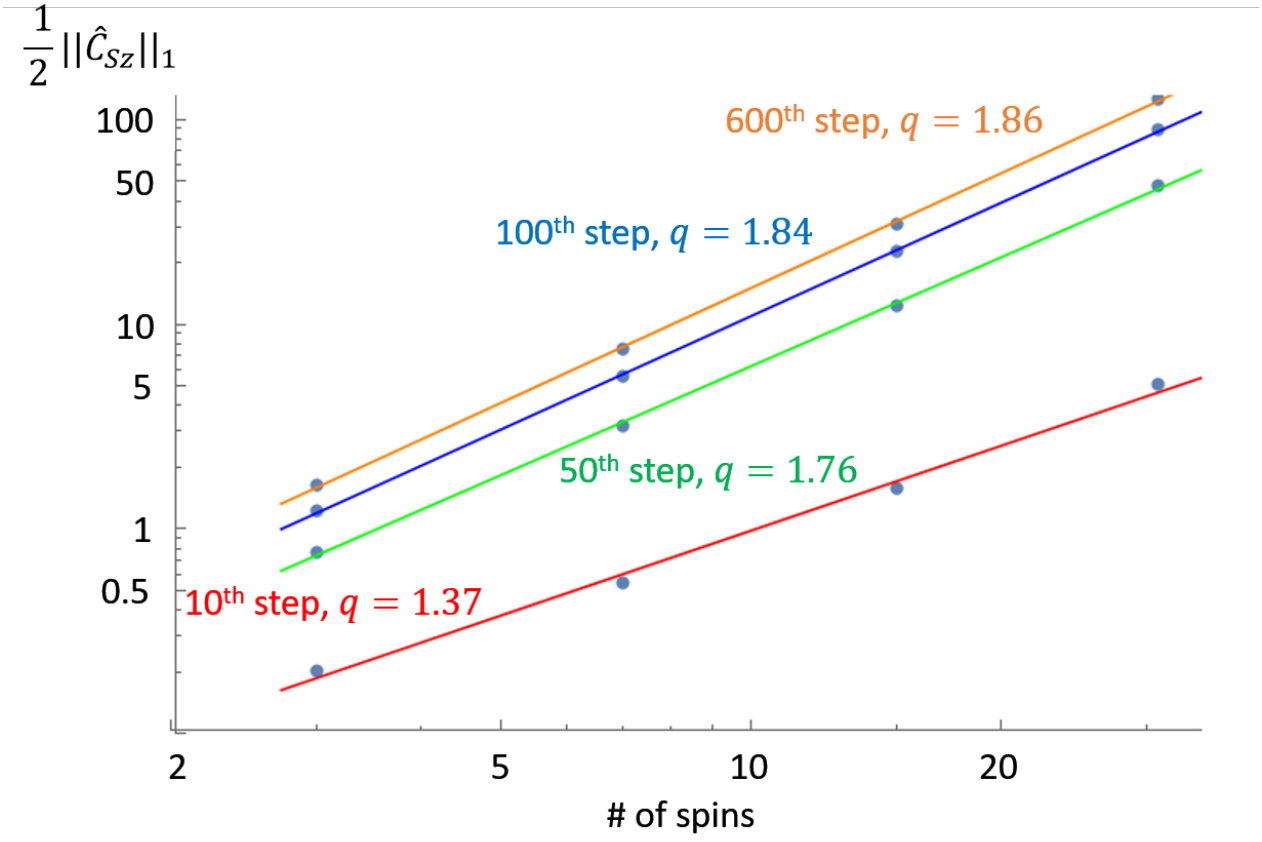

Figure 7.7: Plots of $\frac{1}{2}\|\hat{C}_{\hat{S}_z}\|_1$ against N for different number of measurements. From the slope we find $q = 1.37$, 1.76, 1.84, and 1.86 for $m = 10$, 50, 100, and 600, respectively.

The good thing is, $q = 1.8$ can provide the scaling better than the SQL. Recall that $\delta\omega \leq \Theta(N^{-1})$ is guaranteed by the term $|\omega t_{\rm int}^2 {\rm Tr}(\hat{\rho}[\hat{A},[\hat{A},\hat{\eta}]])|$, and that we assume $\omega t_{\rm int} N = \Theta(N^0)$. It means for $1 \leq q < 2$, the scaling of the upper bound is roughly evaluated as

$$\delta\omega \lesssim |\omega t_{\rm int}^2 \Theta(N^q)|^{-1} \tag{7.10}$$

$$= |\Theta(N^0) t_{\rm int} \Theta(N^{q-1})|^{-1} \tag{7.11}$$

$$= \frac{1}{\Theta(N^{q-1})}. \tag{7.12}$$

By "rough," we mean that there is a possibility of a better sensitivity. We do not know if there is $k > 2$ such that ${\rm Tr}(\hat{\rho}[\hat{A},\hat{\eta}]_k) = \Theta(N^{q'+k-2})$ with $q' > q$, and if there is, then we have $\delta\omega \leq \Theta(N^{-(q'-1)})$, which bounds $\delta\omega$ more tightly than q and thus guarantees a better sensitivity.

Note that this is merely an upper bound, not something that clarifies the limit of the given state. The bound is sometimes discouragingly loose and sometimes encouraging. For example, the

uncertainty of a separable state with $q = 1$ is bounded as

$$\delta\omega \leq \Theta(N^0), \tag{7.13}$$

although it can ultimately reach $\delta\omega = \Theta(N^{-1/2})$. As can be seen, the upper bound we give is loose when q is small. The encouraging part is, a state with $q > 1.5$ are all guaranteed to beat the SQL because $q - 1 > 0.5$. Therefore, the created state with $q \simeq 1.8$ is guaranteed to achieve the sensitivity $\delta\omega \leq \frac{1}{\Theta(N^{0.8})}$, beating the SQL by the scaling $N^{0.3}$.

We have seen the step-by-step drastic change of the state and its approach to a generalized cat state through repetitive measurements by a qubit sensor. Though the achievement up to $q = 2$ was not observed, the obtained state shows better scaling than a separable state.

Chapter 8

Summary and outlook

In this thesis, we have looked into the application of superpositions of macroscopically distinct states in quantum metrology. We have shown that every generalized cat state, a superposition state of macroscopically distinct states characterized by the index q, achieves the ultimate scaling sensitivity if used as a magnetic field sensor through the standard Ramsey-type sensing protocol. Various states can be identified as a generalized cat state, thus our result is widely applicable. As an example, we discussed a generalized cat state that is a mixture of $\exp(\Theta(N))$ states. We propose a recipe to generate such a state, and showed that its usage in quantum metrology is indeed advantageous. We also discussed a realistic system to implement the recipe with NV centers and superconducting flux qubit to obtain a metrologically useful state. Below we summarize each chapter.

In Chapter 1, the overview of the thesis was given, and the significance of the results in this thesis is clarified.

In Chapter 2, we have first reviewed the standard Ramsey-type sensing protocol, in which state preparation, time evolution in the presence of the target magnetic field, readout, and the repetition of them are done. The two bounds of the uncertainty, i.e., the standard quantum limit $\delta\omega \propto N^{-1/2}$ and the Heisenberg limit $\delta\omega \propto N^{-1}$ were also reviewed, and how $\delta\omega$ depends on the initial state was also summarised. Implementation of the sensing protocol with NV centers was also explained along with a brief review of other two major magnetometers, SQUID and SERF.

In Chapter 3, we reviewed the indices p and q for characterizing superposition of macroscopically distinct states, and the term generalized cat states was introduced. For pure states, $p = 2$ corresponds to the maximal fluctuation of an additive observable, meaning the existence of superposition of macroscopically distinct states. For mixed states, we need the condition $q = 2$ to

know there is superposition of macroscopically distinct states, for we cannot distinguish the superposition and classical mixture just by looking at the fluctuation. The index q is associated with a quantity that we call "catness", i.e., $\mathrm{Tr}(\hat{\rho}[\hat{A},[\hat{A},\hat{\eta}]])$, which quantifies the coherence between macroscopically distinct states. Generalized cat states are states with $q=2$, regardless the purity.

In Chapter 4, we proved that all the generalized cat states can achieve the Heisenberg scaling sensitivity if used as a magnetic field sensor in the absence of noise. We also showed how to calculate the catness when we are given a sensor state and the observable associated with the target parameter. We also clarified how to construct the projection operator for realizing the sensing that achieves the Heisenberg scaling uncertainty. The relationship between $q=2$ state and the quantum Fisher information is discussed as well.

In Chapter 5, realistic independent dephasing is considered. We prove that in the presence of non-Markovian dephasing, generalized cat states achieves the ultimate scaling sensitivity, i.e., $\delta\omega=\Theta(N^{-3/4})$. This scaling is known to be the ultimate in the presence of dephasing, beating the SQL. The key was to consider the regime where the decay of the metrologically useful coherence is slow. Such a technique is not possible for Markovian dephasing. By non-Markovian, we mean that the correlation time τ_c of the environment is sufficiently large so that we can take the phase accumulation time t_{int} smaller than the correlation time. In the regime $t_{\mathrm{int}}\ll\tau_c$, the decay of the signal is slower than the case for Markovian dephasing which has $\tau_c\to 0$. We also discussed why only two scalings, i.e., $\Theta(N^{-1})$ and $\Theta(N^{-3/4})$ appeared. Chapters 4 and 5 are based on [1].

In Chapter 6, Mamineko, maximally mixed neko (cat), and its recipe were introduced. By measuring $\hat{M}_x$ of a state with a macroscopic value of $\hat{M}_z$, we obtain Mamineko, a generalized cat state of $\hat{M}_z$. We discussed the conditions and the success probability of generating Mamineko, and also several features were described. Then we estimated how Mamineko is useful if used as a magnetic field sensor, assuming Mamineko is realized in a silicon substrate, by using realistic parameters. There indeed was an advantage, about 20 times improvement, than a separable state sensor in the same setup. This chapter is mainly based on [2].

Encouraged by the numerical estimate that Mamineko could be useful in reality, we discussed implementation of the recipe of Mamineko in a realistic setup in Chapter 7. By considering the setup in which repetitive readout of the NV ensemble's $\hat{S}_x$ is done by a superconducting flux qubit, we numerically observed that after each measurement the state of the NV ensemble becomes closer to Mamineko, and obtained up to $q=1.86$ state. We also discussed that even though states with $1.5<q<2$ does not show the scaling as good as $q=2$ state, could also be metrologically useful,

beating the SQL.

As a future work, application of $q = 2$ state to other quantum information processing tasks is appealing. The GHZ state, having $q = 2$, is known to be useful in quantum computation [79–87] and quantum teleportation [107–110]. If other generalized cat states are proven to be as well useful, possibility of quantum enhanced application will be greatly expanded.

Another possible future work that is fundamentally interesting is the further clarification of the relation between the QFI and q. In this thesis we have seen $q = 2$ states have QFI$= \Theta(N^2)$, and it seems promising that the inverse is true, for both of them characterizing the macroscopic quantum phenomena.

Also, the experimental realization of the magnetic field sensor with Mamineko is attractive and seems somewhat feasible according to this thesis.

Appendix A

proof of $q \leq 1.5$ for pure states with $p = 1$

For $|\psi\rangle$ such that

$$\max_{\hat{A}} \langle\psi|(\Delta\hat{A})^2|\psi\rangle = \Theta(N^1), \tag{A.1}$$

we prove

$$\max_{\hat{A}} \|[\hat{A},[\hat{A},|\psi\rangle\langle\psi|]]\|_1 \leq \Theta(N^{1.5}). \tag{A.2}$$

We consider some fixed $\hat{A}$. Let us denote the eigenvalues and eigenstates of $[\hat{A},[\hat{A},|\psi\rangle\langle\psi|]]$ as n and $|e_n\rangle$, i.e.,

$$[\hat{A},[\hat{A},|\psi\rangle\langle\psi|]]|e_n\rangle = n|e_n\rangle.$$

Since $\|[\hat{A},[\hat{A},|\psi\rangle\langle\psi|]]\|_1$ is the sum of positive n's,

$$\|[\hat{A},[\hat{A},|\psi\rangle\langle\psi|]]\|_1 = \sum_{n>0} \langle e_n|[\hat{A},[\hat{A},|\psi\rangle\langle\psi|]]|e_n\rangle \tag{A.3}$$

$$= \sum_{n>0} \mathrm{Tr}(|e_n\rangle\langle e_n|\,[\hat{A},[\hat{A},|\psi\rangle\langle\psi|]]) \tag{A.4}$$

$$= \sum_{n>0} \mathrm{Tr}([|e_n\rangle\langle e_n|,\hat{A}]^\dagger[|\psi\rangle\langle\psi|,\hat{A}]). \tag{A.5}$$

Maximizing with $\hat{A}$ and using the Cauchy-Schwartz inequality, we have

$$\max_{\hat{A}} \sum_{n>0} \mathrm{Tr}([|e_n\rangle\langle e_n|, \hat{A}]^\dagger [|\psi\rangle\langle\psi|, \hat{A}]) \tag{A.6}$$

$$\leq \sum_{n>0} \left(\max_{\hat{A}} \mathrm{Tr}([|e_n\rangle\langle e_n|, \hat{A}]^\dagger [|e_n\rangle\langle e_n|, \hat{A}]) \right)^{1/2} \left(\max \hat{A}' \mathrm{Tr}([|\psi\rangle\langle\psi|, \hat{A}']^\dagger [|\psi\rangle\langle\psi|, \hat{A}']) \right)^{1/2} \tag{A.7}$$

$$= \sum_{n>0} \left(\max_{\hat{A}} \mathrm{Tr}(2\hat{A}^2 |e_n\rangle\langle e_n| - 2\hat{A}|e_n\rangle\langle e_n|\hat{A}|e_n\rangle\langle e_n|) \right)^{1/2}$$

$$\times \left(\max_{\hat{A}'} \mathrm{Tr}(2\hat{A}'^2 |\psi\rangle\langle\psi| - 2\hat{A}'|\psi\rangle\langle\psi|\hat{A}'|\psi\rangle\langle\psi|) \right)^{1/2} \tag{A.8}$$

$$= 2 \sum_{n>0} \left(\max_{\hat{A}} \langle e_n|(\Delta\hat{A})^2|e_n\rangle \right)^{1/2} \left(\max_{\hat{A}'} \langle\psi|(\Delta\hat{A}')^2|\psi\rangle \right)^{1/2} \tag{A.9}$$

$$= 2 \sum_{n>0} \left(\max_{\hat{A}} \langle e_n|(\Delta\hat{A})^2|e_n\rangle \right)^{1/2} \Theta(N^{1/2}) \tag{A.10}$$

$$\leq \Theta(N^{1.5}) \tag{A.11}$$

Therefore, pure states with $p = 1$ has $q \leq 1.5$.

Appendix B

Derivation of (6.40)

We denote the eigenstates of $\hat{\sigma}_x$ and $\hat{\sigma}_z$ as

$$\hat{\sigma}_x |+\rangle = |+\rangle , \tag{B.1}$$

$$\hat{\sigma}_x |-\rangle = -|-\rangle , \tag{B.2}$$

$$\hat{\sigma}_z |\uparrow\rangle = |\uparrow\rangle , \tag{B.3}$$

$$\hat{\sigma}_z |\downarrow\rangle = -|\downarrow\rangle . \tag{B.4}$$

Thus,

$$|+\rangle = \frac{|\uparrow\rangle + |\downarrow\rangle}{\sqrt{2}}, \quad |-\rangle = \frac{|\uparrow\rangle - |\downarrow\rangle}{\sqrt{2}}. \tag{B.5}$$

We calculate

$$\mathrm{Tr}\left[\hat{\rho}_{M_x} \hat{C}_{\hat{M}_z \hat{P}_x}\right] = 2N + \frac{4 \sum_{\xi} \sum_{|M_x, \xi\rangle'} \langle M_x, \xi | \hat{P}_z | M_x, \xi \rangle'}{\mathrm{Tr}\left[\hat{P}_x \hat{P}_z \hat{P}_x\right]}, \tag{B.6}$$

where $|M_x, \xi\rangle'$ is a state that differs from $|M_x, \xi\rangle$ by one $|+\rangle$ and one $|-\rangle$ being flipped. Since

- $|M_x, \xi\rangle$ is a product state of $|+\rangle$ and $|-\rangle$
- $|M_z, \nu\rangle$ is a product state of $|\uparrow\rangle$ and $|\downarrow\rangle$
- $\langle +|\uparrow\rangle\langle\uparrow|+\rangle = \frac{1}{\sqrt{2}}\frac{1}{\sqrt{2}} = \frac{1}{2}$, $\langle +|\downarrow\rangle\langle\downarrow|+\rangle = \frac{1}{\sqrt{2}}\frac{1}{\sqrt{2}} = \frac{1}{2}$, $\langle -|\uparrow\rangle\langle\uparrow|-\rangle = \frac{1}{\sqrt{2}}\frac{1}{\sqrt{2}} = \frac{1}{2}$, $\langle -|\downarrow\rangle\langle\downarrow|-\rangle = \left(-\frac{1}{\sqrt{2}}\right)\left(-\frac{1}{\sqrt{2}}\right) = \frac{1}{2}$

the denominator of the second term is

$$\mathrm{Tr}\left[\hat{P}_x \hat{P}_z \hat{P}_x\right] = \sum_{\xi} \langle M_x, \xi | \left(\sum_{\nu} |M_z, \nu\rangle \langle M_z, \nu| \right) |M_x, \xi\rangle \tag{B.7}$$

$$= \frac{1}{2^N} \binom{N}{\frac{N+M_z}{2}} \binom{N}{\frac{N+M_x}{2}}. \tag{B.8}$$

Next we consider the numerator of the second term of (6.38). Since

$$\langle +|\downarrow\rangle\langle\downarrow|-\rangle = -\frac{1}{2} \tag{B.9}$$

$$\langle -|\downarrow\rangle\langle\downarrow|+\rangle = -\frac{1}{2}, \tag{B.10}$$

we must count the cases where (1) $|+\rangle$ of $\langle +|\downarrow\rangle\langle\downarrow|+\rangle$ is flipped and $|-\rangle$ of $\langle -|\uparrow\rangle\langle\uparrow|-\rangle$ is flipped, (2) $|-\rangle$ of $\langle -|\downarrow\rangle\langle\downarrow|-\rangle$ is flipped and $|+\rangle$ of $\langle +|\uparrow\rangle\langle\uparrow|+\rangle$ is flipped. Then,

$$\begin{aligned}
&\sum_{\xi}\sum_{|M_x,\xi\rangle'}\langle M_x,\xi|\hat{P}_z|M_x,\xi\rangle' \\
&=\sum_{\xi}\sum_{|M_x,\xi\rangle'}\langle M_x,\xi|\left(\sum_{\nu}|M_z,\nu\rangle\langle M_z,\nu|\right)|M_x,\xi\rangle' && \text{(B.11)}\\
&=\frac{1}{2^N}\left(\binom{N}{\frac{N+M_z}{2}}\binom{N}{\frac{N+M_x}{2}}\frac{N^2-M_x^2}{4}-2(\text{case}(1)+\text{case}(2))\right) && \text{(B.12)}\\
&=\frac{1}{2^N}\left(\binom{N}{\frac{N+M_z}{2}}\binom{N}{\frac{N+M_x}{2}}\frac{N^2-M_x^2}{4}-4N(N-1)\binom{N-2}{\frac{N+M_z}{2}-1}\binom{N-2}{\frac{N+M_x}{2}-1}\right) && \text{(B.13)}\\
&=\frac{1}{2^N}\binom{N}{\frac{N+M_z}{2}}\binom{N}{\frac{N+M_x}{2}}\frac{N^2-M_x^2}{4}\left(1-\frac{N^2-M_z^2}{N(N-1)}\right) && \text{(B.14)}
\end{aligned}$$

since

$$\binom{N-2}{\frac{N+M_z}{2}-1} = \frac{N^2-M_z^2}{4N(N-1)}\binom{N}{\frac{N+M_z}{2}} \tag{B.15}$$

$$\binom{N-2}{\frac{N+M_x}{2}-1} = \frac{N^2-M_x^2}{4N(N-1)}\binom{N}{\frac{N+M_x}{2}}. \tag{B.16}$$

Summing up,

$$\begin{aligned}
\langle\hat{C}\rangle &= 2N+(N^2-M_x^2)\left(1-\frac{N^2-M_z^2}{N(N-1)}\right) && \text{(B.17)}\\
&= 2N+(N^2-M_x^2)\frac{M_z^2-N}{N(N-1)}. && \text{(B.18)}
\end{aligned}$$

Thus $\hat{\rho}_{M_x}$ is a generalized cat state when $(N^2-M_x^2)=\Theta(N^2)$ and $M_z=\Theta(N)$.

Bibliography

[1] Mamiko Tatsuta, Yuichiro Matsuzaki, and Akira Shimizu. Quantum metrology with generalized cat states. *Physical Review A*, 100(3):032318, 2019.

[2] Mamiko Tatsuta and Akira Shimizu. Conversion of thermal equilibrium states into superpositions of macroscopically distinct states. *Physical Review A*, 97(1):012124, 2018.

[3] Carl W Helstrom. Detection theory and quantum mechanics. *Information and Control*, 10(3):254–291, 1967.

[4] Carl Wilhelm Helstrom. *Quantum detection and estimation theory*. Academic press, 1976.

[5] Alexander S Holevo. *Probabilistic and statistical aspects of quantum theory*, volume 1. Springer Science & Business Media, 2011.

[6] Florian Dolde, Helmut Fedder, Marcus W Doherty, Tobias Nöbauer, Florian Rempp, Gopalakrishnan Balasubramanian, Thomas Wolf, Friedemann Reinhard, Lloyd CL Hollenberg, Fedor Jelezko, et al. Electric-field sensing using single diamond spins. *Nature Physics*, 7(6):459, 2011.

[7] Kan Hayashi, Yuichiro Matsuzaki, Takashi Taniguchi, Takaaki Shimo-Oka, Ippei Nakamura, Shinobu Onoda, Takeshi Ohshima, Hiroki Morishita, Masanori Fujiwara, Shiro Saito, and Norikazu Mizuochi. Optimization of temperature sensitivity using the optically detected magnetic-resonance spectrum of a nitrogen-vacancy center ensemble. *Phys. Rev. Applied*, 10:034009, Sep 2018.

[8] M Buchner, K Höfler, B Henne, V Ney, and A Ney. Tutorial: Basic principles, limits of detection, and pitfalls of highly sensitive squid magnetometry for nanomagnetism and spintronics. *Journal of Applied Physics*, 124(16):161101, 2018.

[9] Riitta Hari and Riitta Salmelin. Magnetoencephalography: from squids to neuroscience: neuroimage 20th anniversary special edition. *Neuroimage*, 61(2):386–396, 2012.

[10] Lisa Tauxe. *Paleomagnetic principles and practice*, volume 17. Springer Science & Business Media, 2006.

[11] Vittorio Giovannetti, Seth Lloyd, and Lorenzo Maccone. Quantum-enhanced measurements: beating the standard quantum limit. *Science*, 306(5700):1330–1336, 2004.

[12] Vittorio Giovannetti, Seth Lloyd, and Lorenzo Maccone. Advances in quantum metrology. *Nature photonics*, 5(4):222–229, 2011.

[13] Matteo GA Paris. Quantum estimation for quantum technology. *International Journal of Quantum Information*, 7(supp01):125–137, 2009.

[14] Alex W Chin, Susana F Huelga, and Martin B Plenio. Quantum metrology in non-markovian environments. *Physical review letters*, 109(23):233601, 2012.

[15] R Chaves, JB Brask, Marcin Markiewicz, J Kołodyński, and A Acín. Noisy metrology beyond the standard quantum limit. *Physical review letters*, 111(12):120401, 2013.

[16] Jonathan A. Jones, Steven D. Karlen, Joseph Fitzsimons, Arzhang Ardavan, Simon C. Benjamin, G. Andrew D. Briggs, and John J. L. Morton. Magnetic field sensing beyond the standard quantum limit using 10-spin noon states. *Science*, 324(5931):1166–1168, 2009.

[17] Susanna F Huelga, Chiara Macchiavello, Thomas Pellizzari, Artur K Ekert, Martin Bodo Plenio, and J Ignacio Cirac. Improvement of frequency standards with quantum entanglement. *Physical Review Letters*, 79(20):3865, 1997.

[18] A Kuzmich, NP Bigelow, and L Mandel. Atomic quantum non-demolition measurements and squeezing. *EPL (Europhysics Letters)*, 42(5):481, 1998.

[19] M Fleischhauer, A B Matsko, and M O Scully. Quantum limit of optical magnetometry in the presence of ac stark shifts. *Physical Review A*, 62(1):013808, 2000.

[20] J M Geremia, John K Stockton, Andrew C Doherty, and Hideo Mabuchi. Quantum kalman filtering and the heisenberg limit in atomic magnetometry. *Physical review letters*, 91(25):250801, 2003.

[21] D Leibfried, Murray D Barrett, T Schaetz, J Britton, J Chiaverini, Wayne M Itano, John D Jost, Christopher Langer, and David J Wineland. Toward heisenberg-limited spectroscopy with multiparticle entangled states. *Science*, 304(5676):1476–1478, 2004.

[22] M Auzinsh, Dmitry Budker, D F Kimball, S M Rochester, J E Stalnaker, A O Sushkov, and V V Yashchuk. Can a quantum nondemolition measurement improve the sensitivity of an atomic magnetometer? *Physical review letters*, 93(17):173002, 2004.

[23] Jacob A Dunningham. Using quantum theory to improve measurement precision. *Contemporary Physics*, 47(5):257–267, 2006.

[24] Yuichiro Matsuzaki, Simon C Benjamin, and Joseph Fitzsimons. Magnetic field sensing beyond the standard quantum limit under the effect of decoherence. *Physical Review A*, 84(1):012103, 2011.

[25] Rafał Demkowicz-Dobrzański, Jan Kołodyński, and Mădălin Guţă. The elusive heisenberg limit in quantum-enhanced metrology. *Nature communications*, 3:1063, 2012.

[26] Justin G Bohnet, Kevin C Cox, Matthew A Norcia, Joshua M Weiner, Zilong Chen, and James K Thompson. Reduced spin measurement back-action for a phase sensitivity ten times beyond the standard quantum limit. *Nature Photonics*, 8(9):731, 2014.

[27] Tohru Tanaka, Paul Knott, Yuichiro Matsuzaki, Shane Dooley, Hiroshi Yamaguchi, William J Munro, and Shiro Saito. Proposed robust entanglement-based magnetic field sensor beyond the standard quantum limit. *Physical review letters*, 115(17):170801, 2015.

[28] Shane Dooley, Emi Yukawa, Yuichiro Matsuzaki, George C Knee, William J Munro, and Kae Nemoto. A hybrid-systems approach to spin squeezing using a highly dissipative ancillary system. *New Journal of Physics*, 18(5):053011, 2016.

[29] Emily Davis, Gregory Bentsen, and Monika Schleier-Smith. Approaching the heisenberg limit without single-particle detection. *Physical review letters*, 116(5):053601, 2016.

[30] Yuichiro Matsuzaki, Simon Benjamin, Shojun Nakayama, Shiro Saito, and William J Munro. Quantum metrology beyond the classical limit under the effect of dephasing. *Physical review letters*, 120(14):140501, 2018.

[31] Martin E Huber, Nicholas C Koshnick, Hendrik Bluhm, Leonard J Archuleta, Tommy Azua, Per G Björnsson, Brian W Gardner, Sean T Halloran, Erik A Lucero, and Kathryn A Moler. Gradiometric micro-squid susceptometer for scanning measurements of mesoscopic samples. *Review of Scientific Instruments*, 79(5):053704, 2008.

[32] Edward Ramsden. *Hall-effect Sensors: Theory and Application*. Elsevier, 2011.

[33] Martino Poggio and Christian L Degen. Force-detected nuclear magnetic resonance: recent advances and future challenges. *Nanotechnology*, 21(34):342001, 2010.

[34] W Happer and H Tang. Spin-exchange shift and narrowing of magnetic resonance lines in optically pumped alkali vapors. *Physical Review Letters*, 31(5):273, 1973.

[35] J C Allred, R N Lyman, T W Kornack, and M V Romalis. High-sensitivity atomic magnetometer unaffected by spin-exchange relaxation. *Physical Review Letters*, 89(13):130801, 2002.

[36] HB Dang, AC Maloof, and MV Romalis. Ultrahigh sensitivity magnetic field and magnetization measurements with an atomic magnetometer. *Applied Physics Letters*, 97(15):151110, 2010.

[37] Mustafa Bal, Chunqing Deng, Jean-Luc Orgiazzi, FR Ong, and Adrian Lupascu. Ultrasensitive magnetic field detection using a single artificial atom. *Nature communications*, 3:1324, 2012.

[38] Hiraku Toida, Yuichiro Matsuzaki, Kosuke Kakuyanagi, Xiaobo Zhu, William J Munro, Hiroshi Yamaguchi, and Shiro Saito. Electron paramagnetic resonance spectroscopy using a single artificial atom. *arXiv preprint arXiv:1711.10148*, 2017.

[39] V M Acosta, E Bauch, M P Ledbetter, C Santori, K-M C Fu, P E Barclay, R G Beausoleil, H Linget, J F Roch, F Treussart, et al. Diamonds with a high density of nitrogen-vacancy centers for magnetometry applications. *Physical Review B*, 80(11):115202, 2009.

[40] Gopalakrishnan Balasubramanian, Philipp Neumann, Daniel Twitchen, Matthew Markham, Roman Kolesov, Norikazu Mizuochi, Junichi Isoya, Jocelyn Achard, Johannes Beck, Julia Tissler, et al. Ultralong spin coherence time in isotopically engineered diamond. *Nature materials*, 8(5):383–387, 2009.

[41] Florian Dolde, Helmut Fedder, Marcus W Doherty, Tobias Nöbauer, Florian Rempp, Gopalakrishnan Balasubramanian, Thomas Wolf, Friedemann Reinhard, Lloyd CL Hollenberg, Fedor Jelezko, et al. Electric-field sensing using single diamond spins. *Nature Physics*, 7(6):459–463, 2011.

[42] Toyofumi Ishikawa, Kai-Mei C Fu, Charles Santori, Victor M Acosta, Raymond G Beausoleil, Hideyuki Watanabe, Shinichi Shikata, and Kohei M Itoh. Optical and spin coherence properties of nitrogen-vacancy centers placed in a 100 nm thick isotopically purified diamond layer. *Nano letters*, 12(4):2083–2087, 2012.

[43] Erwin Schrödinger. Die gegenwärtige situation in der quantenmechanik. *Naturwissenschaften*, 23(49):823–828, 1935.

[44] Anthony J Leggett. Macroscopic quantum systems and the quantum theory of measurement. *Progress of Theoretical Physics Supplement*, 69:80–100, 1980.

[45] Akira Shimizu and Takayuki Miyadera. Stability of quantum states of finite macroscopic systems against classical noises, perturbations from environments, and local measurements. *Phys. Rev. Lett.*, 89:270403, Dec 2002.

[46] Bernard Yurke and David Stoler. Generating quantum mechanical superpositions of macroscopically distinguishable states via amplitude dispersion. *Physical review letters*, 57(1):13, 1986.

[47] N David Mermin. Extreme quantum entanglement in a superposition of macroscopically distinct states. *Physical Review Letters*, 65(15):1838, 1990.

[48] SM Roy and Virendra Singh. Tests of signal locality and einstein-bell locality for multiparticle systems. *Physical Review Letters*, 67(20):2761, 1991.

[49] MS Kim and V Bužek. Schrödinger-cat states at finite temperature: influence of a finite-temperature heat bath on quantum interferences. *Physical Review A*, 46(7):4239, 1992.

[50] Akira Shimizu and Tomoyuki Morimae. Detection of macroscopic entanglement by correlation of local observables. *Physical Review Letters*, 95(9):090401, 2005.

[51] S Mancini, VI Man'ko, and P Tombesi. Ponderomotive control of quantum macroscopic coherence. *Physical Review A*, 55(4):3042, 1997.

[52] S Bose, K Jacobs, and PL Knight. Preparation of nonclassical states in cavities with a moving mirror. *Physical Review A*, 56(5):4175, 1997.

[53] Tomoyuki Morimae, Ayumu Sugita, and Akira Shimizu. Macroscopic entanglement of many-magnon states. *Physical Review A*, 71(3):032317, 2005.

[54] Wojciech Hubert Zurek. Decoherence, einselection, and the quantum origins of the classical. *Rev. Mod. Phys.*, 75:715–775, May 2003.

[55] Ayumu Sugita and Akira Shimizu. Correlations of observables in chaotic states of macroscopic quantum systems. *Journal of the Physical Society of Japan*, 74(7):1883–1886, 2005.

[56] Mauro Paternostro. Engineering nonclassicality in a mechanical system through photon subtraction. *Physical Review Letters*, 106(18):183601, 2011.

[57] Florian Fröwis and Wolfgang Dür. Measures of macroscopicity for quantum spin systems. *New Journal of Physics*, 14(9):093039, 2012.

[58] Ryotaro Inoue, Shin-Ichi-Ro Tanaka, Ryo Namiki, Takahiro Sagawa, and Yoshiro Takahashi. Unconditional quantum-noise suppression via measurement-based quantum feedback. *Phys. Rev. Lett.*, 110:163602, Apr 2013.

[59] Tomoyuki Morimae and Akira Shimizu. Visualization of superposition of macroscopically distinct states. *Phys. Rev. A*, 74:052111, Nov 2006.

[60] Uzma Akram, Warwick P Bowen, and Gerard J Milburn. Entangled mechanical cat states via conditional single photon optomechanics. *New Journal of Physics*, 15(9):093007, 2013.

[61] MR Vanner, M Aspelmeyer, and MS Kim. Quantum state orthogonalization and a toolset for quantum optomechanical phonon control. *Physical Review Letters*, 110(1):010504, 2013.

[62] Markus Arndt and Klaus Hornberger. Testing the limits of quantum mechanical superpositions. *Nature Physics*, 10:271–277, 2014.

[63] R Ghobadi, S Kumar, B Pepper, D Bouwmeester, AI Lvovsky, and C Simon. Optomechanical micro-macro entanglement. *Physical Review Letters*, 112(8):080503, 2014.

[64] Tomoyuki Morimae. Superposition of macroscopically distinct states means large multipartite entanglement. *Physical Review A*, 81(1):010101(R), 2010.

[65] Géza Tóth and Iagoba Apellaniz. Quantum metrology from a quantum information science perspective. *Journal of Physics A: Mathematical and Theoretical*, 47(42):424006, 2014.

[66] Hyunseok Jeong, Minsu Kang, and Hyukjoon Kwon. Characterizations and quantifications of macroscopic quantumness and its implementations using optical fields. *Optics Communications*, 337:12–21, 2015.

[67] F Fröwis, N Sangouard, and N Gisin. Linking measures for macroscopic quantum states via photon–spin mapping. *Optics communications*, 337:2–11, 2015.

[68] Tahereh Abad and Vahid Karimipour. Scaling of macroscopic superpositions close to a quantum phase transition. *Phys. Rev. B*, 93:195127, May 2016.

[69] Neill Lambert, Kamanasish Debnath, Anton Frisk Kockum, George C. Knee, William J. Munro, and Franco Nori. Leggett-garg inequality violations with a large ensemble of qubits. *Phys. Rev. A*, 94:012105, Jul 2016.

[70] Ulrich B Hoff, Johann Kollath-Bönig, Jonas S Neergaard-Nielsen, and Ulrik L Andersen. Measurement-induced macroscopic superposition states in cavity optomechanics. *arXiv preprint arXiv:1601.01663*, 2016.

[71] Florian Fröwis, Pavel Sekatski, Wolfgang Dür, Nicolas Gisin, and Nicolas Sangouard. Macroscopic quantum states: Measures, fragility, and implementations. *Reviews of Modern Physics*, 90(2):025004, 2018.

[72] Wolfgang Dür, Christoph Simon, and J Ignacio Cirac. Effective size of certain macroscopic quantum superpositions. *Physical review letters*, 89(21):210402, 2002.

[73] Chae-Yeun Park, Minsu Kang, Chang-Woo Lee, Jeongho Bang, Seung-Woo Lee, and Hyunseok Jeong. Quantum macroscopicity measure for arbitrary spin systems and its application to quantum phase transitions. *Physical Review A*, 94(5):052105, 2016.

[74] Hyukjoon Kwon, Chae-Yeun Park, Kok Chuan Tan, and Hyunseok Jeong. Disturbance-based measure of macroscopic coherence. *New Journal of Physics*, 19(4):043024, 2017.

[75] Sergio Boixo, Steven T Flammia, Carlton M Caves, and John M Geremia. Generalized limits for single-parameter quantum estimation. *Physical review letters*, 98(9):090401, 2007.

[76] Marcin Zwierz, Carlos A Pérez-Delgado, and Pieter Kok. General optimality of the heisenberg limit for quantum metrology. *Physical review letters*, 105(18):180402, 2010.

[77] DD Awschalom, JR Rozen, MB Ketchen, WJ Gallagher, AW Kleinsasser, RL Sandstrom, and B Bumble. Low-noise modular microsusceptometer using nearly quantum limited dc squids. *Applied physics letters*, 53(21):2108–2110, 1988.

[78] IM Savukov and MV Romalis. Effects of spin-exchange collisions in a high-density alkali-metal vapor in low magnetic fields. *Physical Review A*, 71(2):023405, 2005.

[79] Paul T Cochrane, Gerard J Milburn, and William J Munro. Macroscopically distinct quantum-superposition states as a bosonic code for amplitude damping. *Physical Review A*, 59(4):2631, 1999.

[80] H Jeong and Myung Shik Kim. Efficient quantum computation using coherent states. *Physical Review A*, 65(4):042305, 2002.

[81] Timothy C Ralph, Alexei Gilchrist, Gerard J Milburn, William J Munro, and Scott Glancy. Quantum computation with optical coherent states. *Physical Review A*, 68(4):042319, 2003.

[82] Akihisa Ukena and Akira Shimizu. Appearance and stability of anomalously fluctuating states in shor ' s factoring algorithm. *Physical Review A*, 69(2):022301, 2004.

[83] Nicolas J Cerf, Gerd Leuchs, and Eugene S Polzik. *Quantum information with continuous variables of atoms and light*. Imperial College Press, 2007.

[84] AP Lund, TC Ralph, and HL Haselgrove. Fault-tolerant linear optical quantum computing with small-amplitude coherent states. *Physical review letters*, 100(3):030503, 2008.

[85] Akira Shimizu, Yuichiro Matsuzaki, and Akihisa Ukena. Necessity of superposition of macroscopically distinct states for quantum computational speedup. *Journal of the Physical Society of Japan*, 82(5):054801, 2013.

[86] Reinier W Heeres, Philip Reinhold, Nissim Ofek, Luigi Frunzio, Liang Jiang, Michel H Devoret, and Robert J Schoelkopf. Implementing a universal gate set on a logical qubit encoded in an oscillator. *arXiv preprint arXiv:1608.02430*, 2016.

[87] Wolfgang Pfaff, Christopher J Axline, Luke D Burkhart, Uri Vool, Philip Reinhold, Luigi Frunzio, Liang Jiang, Michel H Devoret, and Robert J Schoelkopf. Schrodinger's catapult: Launching multiphoton quantum states from a microwave cavity memory. *arXiv preprint arXiv:1612.05238*, 2016.

[88] TC Ralph. Coherent superposition states as quantum rulers. *Physical Review A*, 65(4):042313, 2002.

[89] Christopher C Gerry, Adil Benmoussa, and RA Campos. Nonlinear interferometer as a resource for maximally entangled photonic states: Application to interferometry. *Physical Review A*, 66(1):013804, 2002.

[90] William J Munro, Kae Nemoto, Gerard J Milburn, and Sam L Braunstein. Weak-force detection with superposed coherent states. *Physical Review A*, 66(2):023819, 2002.

[91] Jaewoo Joo, William J Munro, and Timothy P Spiller. Quantum metrology with entangled coherent states. *Physical review letters*, 107(8):083601, 2011.

[92] Adrien Facon, Eva-Katharina Dietsche, Dorian Grosso, Serge Haroche, Jean-Michel Raimond, Michel Brune, and Sébastien Gleyzes. A sensitive electrometer based on a rydberg atom in a schrödinger-cat state. *Nature*, 535(7611):262–265, 2016.

[93] Chao Song, Kai Xu, Hekang Li, Yuran Zhang, Xu Zhang, Wuxin Liu, Qiujiang Guo, Zhen Wang, Wenhui Ren, Jie Hao, et al. Observation of multi-component atomic schr\" odinger cat states of up to 20 qubits. *arXiv preprint arXiv:1905.00320*, 2019.

[94] Akira Shimizu. 熱力学の基礎. 東京大学出版会, 2007.

[95] G Massimo Palma, Kalle-Antti Suominen, and Artur Ekert. Quantum computers and dissipation. *Proc. R. Soc. Lond. A*, 452(1946):567–584, 1996.

[96] Andrea Smirne, Jan Kołodyński, Susana F Huelga, and Rafał Demkowicz-Dobrzański. Ultimate precision limits for noisy frequency estimation. *Physical review letters*, 116(12):120801, 2016.

[97] Katarzyna Macieszczak. Zeno limit in frequency estimation with non-markovian environments. *Physical Review A*, 92(1):010102(R), 2015.

[98] G De Lange, ZH Wang, D Riste, VV Dobrovitski, and R Hanson. Universal dynamical decoupling of a single solid-state spin from a spin bath. *Science*, 330(6000):60–63, 2010.

[99] Masahiro Kitagawa and Masahito Ueda. Squeezed spin states. *Physical Review A*, 47(6):5138, 1993.

[100] Alexei M. Tyryshkin, Shinichi Tojo, John J L Morton, Helge Riemann, Nikolai V. Abrosimov, Peter Becker, Hans Joachim Pohl, Thomas Schenkel, Michael L W Thewalt, Kohei M. Itoh, and S. A. Lyon. Electron spin coherence exceeding seconds in high-purity silicon. *Nature Materials*, 11(2):143–147, 2 2012.

[101] F Baudenbacher, LE Fong, JR Holzer, and M Radparvar. Monolithic low-transition-temperature superconducting magnetometers for high resolution imaging magnetic fields of room temperature samples. *Applied Physics Letters*, 82(20):3487–3489, 2003.

[102] D Le Sage, K Arai, DR Glenn, SJ DeVience, LM Pham, L Rahn-Lee, MD Lukin, A Yacoby, A Komeili, and RL Walsworth. Optical magnetic imaging of living cells. *Nature*, 496(7446):486, 2013.

[103] Xiaobo Zhu, Shiro Saito, Alexander Kemp, Kosuke Kakuyanagi, Shin-ichi Karimoto, Hayato Nakano, William J Munro, Yasuhiro Tokura, Mark S Everitt, Kae Nemoto, et al. Coherent coupling of a superconducting flux qubit to an electron spin ensemble in diamond. *Nature*, 478(7368):221, 2011.

[104] Nir Bar-Gill, Linh M Pham, Andrejs Jarmola, Dmitry Budker, and Ronald L Walsworth. Solid-state electronic spin coherence time approaching one second. *Nature communications*, 4:1743, 2013.

[105] Jonas Bylander, Simon Gustavsson, Fei Yan, Fumiki Yoshihara, Khalil Harrabi, George Fitch, David G Cory, Yasunobu Nakamura, Jaw-Shen Tsai, and William D Oliver. Noise spectroscopy through dynamical decoupling with a superconducting flux qubit. *Nature Physics*, 7(7):565, 2011.

[106] I Chiorescu, Y Nakamura, CJP Ma Harmans, and JE Mooij. Coherent quantum dynamics of a superconducting flux qubit. *Science*, 299(5614):1869–1871, 2003.

[107] Danilo Boschi, Salvatore Branca, Francesco De Martini, Lucien Hardy, and Sandu Popescu. Experimental realization of teleporting an unknown pure quantum state via dual classical and einstein-podolsky-rosen channels. *Physical Review Letters*, 80(6):1121, 1998.

[108] SJ Van Enk and O Hirota. Entangled coherent states: Teleportation and decoherence. *Physical Review A*, 64(2):022313, 2001.

[109] H Jeong, MS Kim, and Jinhyoung Lee. Quantum-information processing for a coherent superposition state via a mixedentangled coherent channel. *Physical Review A*, 64(5):052308, 2001.

[110] Jonas S Neergaard-Nielsen, Yujiro Eto, Chang-Woo Lee, Hyunseok Jeong, and Masahide Sasaki. Quantum tele-amplification with a continuous-variable superposition state. *Nature Photonics*, 7(6):439–443, 2013.